International
WOCE
Newsletter

Number 25 February 1997

IN THIS ISSUE

Published by WOCE International Project Office at Southampton Oceanography Centre, UK

Happy New Year!

W. John Gould and Roberta Boscolo, WOCE IPO

First I should apologise for the delay in circulating Newsletter Number 24. Although it was datelined October and had a banner in a nice autumnal colour, production delays meant that most of you received it right at the end of the year. However, we enter 1997 with another full issue and hope that interest in the Newsletter as a means of rapidly disseminating WOCE results will continue. The deadlines and likely topics for the next issues are listed below.

We have started detailed planning for the 1998 WOCE Conference and the panel on page 25 can be regarded as the first formal announcement. It will be followed by a much wider mail-shot and the establishment of a Conference WWW page later in the spring. The next task for the organising committees is to identify the detailed topics for the plenary sessions and to approach the speakers. Obtaining financial sponsorship will be another task.

Meetings

I promised to report on the 23rd meeting of the WOCE Scientific Steering Group. We touched again on the means of identifying the achievements of WOCE and of assessing the progress that has been made towards WOCE's objectives. These topics are going to be used as the framework around which the WOCE Conference will be structured. We also discussed at some length the proposal to carry out an Ocean Modelling Intercomparison Project (OMIP). The SSG concluded that an intercomparison of models alone would not be realistic and instead have suggested that the WOCE Synthesis and Modelling Working Group together with the CLIVAR Numerical Experimentation Group work towards carrying out an Ocean Model and Data Intercomparison Project (OMDIP). The SSG also decided that it would be inappropriate to hold the next scheduled meeting of the Intergovernmental WOCE Panel (IWP) in 1997 since the resolutions passed at the previous meeting in 1995 (concerning access to EEZs, resources for the AIMS phase and submission of data) were still valid.

Perhaps the SSG decision of most immediate significance is that the papers stemming from last year's Pacific regional workshop will be published in JGR (Oceans) and later be bound together to produce a nice compact but comprehensive summary. Eric Lindstrom will be the principal guest editor. The report of the SSG meeting is being published as WOCE Report No. 148/97.

The report of the first two meetings of the Synthesis and Modelling Working Group has just been published by the IPO (WOCE Report No. 144/96) and we expect to publish the international strategy document on WOCE Synthesis and Assimilation by March.

WHPO - A message of thanks

You will see on page 43 an announcement from Jim Swift about the new location and work programme for the WOCE Hydrographic Programme Office. We wish Jim and his staff well in taking on this task but an equally important and pleasant duty is to publicly express WOCE's gratitude to Terry Joyce and to all the staff who have worked in Woods Hole over the past 7 years to establish the WHPO, to set-up the comprehensive WHP data base and to make such an effective start on the difficult task of obtaining data sets from PIs and then carrying out the data quality evaluation. Well done all of you!

A message from Roberta Boscolo, the Newsletter editor

As the new editor of the WOCE Newsletter I have been delighted by the positive responses and the cooperation I have received from potential contributors: It makes my job much easier and I hope this will continue in the future.

I must thank my predecessor, Andrea Frische, for having left the Newsletter in such good shape. I hope to prove a worthy successor.

A big "Thank you" to all who have returned the card asking to continue to receive the Newsletter. However we have (mid-January) received replies from only about 30% of the present list. Our mailing list is being updated accordingly and from Newsletter 27 onwards we will start to use the new list. Therefore if you haven't returned the card yet please do so otherwise you won't receive the WOCE Newsletter in the future!

For 1997 the issues of WOCE Newsletter have been scheduled as follows:

No.	Deadline	Theme
26	30 January	Atmospheric-ocean coupled models
27	14 April	General science topics
28	30 June	South Atlantic
29	15 September	Southern Ocean
30	30 November	Experience with Instrumentation in WOCE

If you have some new and good results in any of these subject areas please let me know.

The Large-Scale, Wind-Driven Response of the North Pacific

Dudley B. Chelton, College of Oceanic and Atmospheric Sciences, Oregon State University; and Alberto M. Mestas-Nunez, NOAA/AOML, Miami, USA.
dud@osuvax.oce.orst.edu

Observational evidence from tide gauge measurements across Tokara Strait (Blaha and Reed, 1982) and from hydrographic sections across the Kuroshio (Sekine *et al.*, 1991; see also Sekine and Kutsuwada, 1994) suggest that the poleward transport of the Kuroshio is maximum in summer and minimum in winter. To the extent that Kuroshio transport variations are indicative of basin-scale variability, fluctuations on interannual and shorter time scales must be primarily barotropic since the baroclinic adjustment time for the midlatitude North Pacific is longer than a decade. The observed seasonal variability of the Kuroshio has been reproduced by Greatbatch and Goulding (1989; 1990) from a linear, barotropic model of the North Pacific circulation. These observational and modelling results are rather surprising since a summertime maximum is 180° out of phase with an equilibrium Sverdrup response to seasonally varying wind stress forcing.

Sekine and Kutsuwada (1994) have recently investigated the circulation of the North Pacific from a 2-layer, nonlinear, primitive equation model. They find a seasonal variation of the Kuroshio that is in very close agreement with an equilibrium Sverdrup balance. They argue that the dramatic difference between their results and the earlier modelling studies by Greatbatch and Goulding (1989; 1990) is due to the effects of nonlinearities, mean flow and baroclinic adjustment that are not accounted for in the simple Greatbatch and Goulding model. Sekine and Kutsuwada suggest that the barotropic flow of the Kuroshio shifts to the east of Tokara Strait during the wintertime maximum and is therefore not detected by the tide gauge measurements. They attribute the lack of a wintertime maximum in the hydrographic data to a large volume transport in the deep water that is not detected in the geostrophic transport estimates.

In this note, we present the results of an investigation of the validity of the time-varying Sverdrup balance in the North Pacific based on analysis of three years of: (1) a simple flat-bottom Sverdrup model; (2) the primitive equation global ocean circulation model developed by the Parallel Ocean Program (POP) at the Los Alamos National Laboratory; and (3) observations of sea surface height (SSH) by the TOPEX/POSEIDON (T/P) altimeter. The 3-year period considered here is October 1992 through November 1995.

Data processing

The T/P altimeter data analyzed here were processed by applying standard corrections and editing criteria. The large-scale, low-frequency variability in SSH fields constructed from T/P data are relatively insensitive to the details of this processing. For the seasonal and longer time scales of interest here, the T/P data were filtered in time to attenuate signals with scales shorter than 6° and 40 days (Greenslade *et al.*, 1997), which is analogous to the filtering properties of 3.5° and 25 day block averages. The filter transfer function of the loess smoother used here has much better characteristics (sharper band-edge rolloff and smaller side lobes) than the simple block average smoother (Schlax and Chelton, 1992).

For the Sverdrup model considered here, twice-daily ECMWF winds at 10 m were converted to wind stress using the Large and Pond (1982) drag coefficient. These ECMWF wind fields were smoothed with a loess smoother to retain the same 6° and 40 day scales as the T/P SSH fields described above. The wind stress curl required for the Sverdrup model was computed from the smoothed wind stress fields by simple centred first differences.

ECMWF wind fields were also used to force the POP model. A description of an earlier version of this model is given by Dukowicz and Smith (1994). For the version of the POP model analyzed here (referred to as Run 11), the wind forcing consisted of 3-day averages of the twice-daily ECMWF wind stress fields. The horizontal resolution of the model is approximately 0.25°. The analysis here considers fields of the barotropic streamfunction at 1-day intervals. These fields were smoothed to retain the same 6° and 40 day scales as the T/P SSH fields and the ECMWF wind stress fields described above.

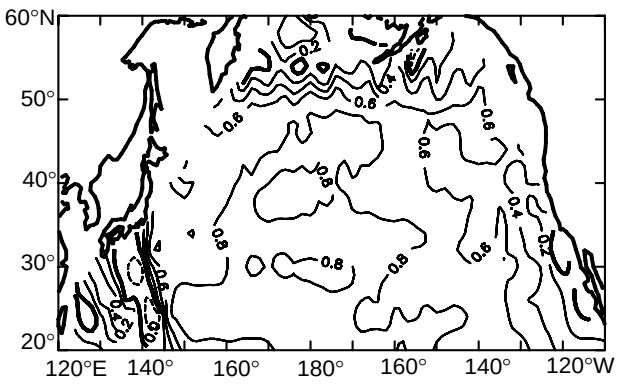

Figure 1. The cross correlation at zero lag between the flat-bottom Sverdrup transport streamfunction forced by ECMWF winds and the smoothed barotropic streamfunction of Run 11 of the Los Alamos POP model.

Sverdrup and POP model simulations

The dynamical basis for a time-varying Sverdrup balance is that the basin-scale barotropic adjustment time for the midlatitude North Pacific is less than a month. The circulation is therefore able to equilibrate with the wind forcing on seasonal and longer time scales. The large-scale bathymetry of the North Pacific is relatively simple. Contours of the ambient potential vorticity f/H are approximately zonal over most of the basin (Koblinsky, 1990). Moreover, Anderson and Killworth (1977) showed that the baroclinic adjustment of the circulation tends to diminish the effects of topography on the barotropic response. To first order, then, a flat-bottom approximation can be considered for a Sverdrup model of the North Pacific circulation.

A map of the correlation between the Sverdrup streamfunction fields and the smoothed POP barotropic streamfunction fields is shown in Fig. 1. The results are quite remarkable. The correlation is low in the eastern basin, increasing from about 0.2 near the eastern boundary to about 0.6 at 140°W. Farther west, the correlation is about 0.8 over the entire central and western North Pacific. The correlation drops abruptly north of the Aleutian Islands and west of the Izu Ridge near 140°E, indicating that topographic effects cannot be neglected in the Sverdrup model in these regions. It can be concluded that the POP simulation of the large-scale, low-frequency variability over most of the North Pacific is dominated by a simple time-varying Sverdrup response to wind forcing.

The seasonal to interannual variations of the subtropical and subpolar western boundary currents (WBCs) and the Kuroshio Extension are of particular interest. The

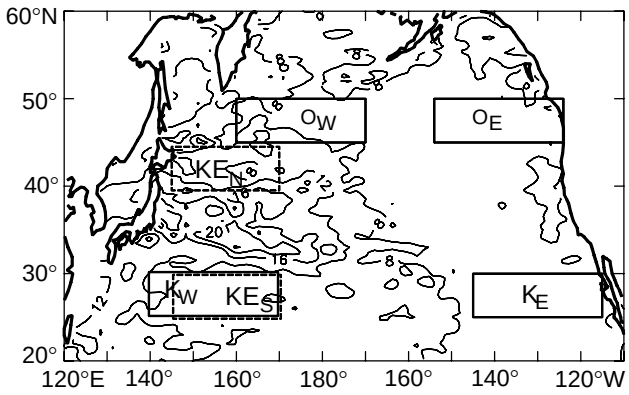

Figure 2. The standard deviation of SSH in cm measured by the T/P altimeter. The boxes with solid borders correspond to the western (subscript W) and eastern (subscript E) areal averages used to estimate the transport variations of the Oyashio and Kuroshio western boundary currents. The boxes with the dashed borders correspond to the northern (subscript N) and southern (subscript S) areal averages used to estimate the transport variations of the Kuroshio Extension. The southern box used for Kuroshio Extension transport estimate has been shifted slightly to distinguish it from the western box used for the Kuroshio transport estimate.

total vertically integrated transport between any two locations is just the difference between the barotropic streamfunction values at the two locations. Since the streamfunction is zero along the western boundary, the streamfunction value at a location east of the boundary current provides a direct estimate of the transport of the WBC. If the location is far enough east, then the transport estimate represents the net transport of the WBC minus any recirculation east of the WBC.

In anticipation of the method required below to estimate transport from SSH fields constructed from T/P data, the WBC transport can alternatively be estimated indirectly from the difference between the barotropic streamfunction values averaged over boxes in the western and eastern basin. In order to conserve mass, the meridional transport between the western and eastern locations must be balanced by a net meridional transport of the opposite sign in the WBC.

The boxes over which the streamfunction fields were averaged to obtain indirect estimates of Oyashio and Kuroshio transports are shown in Fig. 2. The sizes of the boxes are dictated by the T/P analysis described below. The locations of the boxes were chosen to be coincident with the maximum variability of the subpolar and subtropical Sverdrup streamfunction field near the western boundary. The resulting indirect estimates of WBC transport were found to be very highly correlated (typically about 0.9) with the direct estimates described above. The indirect estimates are smaller than those of the direct estimates. The magnitudes of the differences depend on the sizes of the boxes over which indirect indices of transport are obtained. For the box sizes shown in Fig. 2, the indirect estimates are approximately 30% smaller than the direct estimates.

The indirect Sverdrup and POP estimates of Oyashio and Kuroshio transports are shown in the top two panels of Fig. 3. The maximum equatorward transport of the Oyashio and poleward transport of the Kuroshio both occur in winter and minimum transports occur in summer and fall. The cross correlations between these two model estimates of WBC transports at zero lag are 0.84 for the Oyashio and 0.82 for the Kuroshio. The Sverdrup transports are somewhat higher than the POP transports, especially for the Oyashio. For both WBCs, the correlations are slightly higher when the POP transports lag the Sverdrup transports by 10 days. This lag is consistent with the expected adjustment time required for barotropic Rossby waves to cross the basin and establish an equilibrium response to wind forcing in the POP model.

These results are all very consistent with those obtained from the 2-layer model developed by Sekine and Kutsuwada (1994). They found a maximum correlation in Kuroshio transports when their model lagged the Sverdrup model by 0.5 month. Their WBC transports were reduced when topography was added to the model, which may explain the discrepancies between the magnitudes of the POP and flat-bottom Sverdrup transport estimates in Fig. 3.

The sum of the Oyashio and Kuroshio transports shown in the third panel of Fig. 3 provide an indirect

estimate of the transport of the Kuroshio Extension. The correlation between the Sverdrup and POP indirect estimates of Kuroshio Extension transport is 0.90. The POP estimates are again smaller than the Sverdrup estimates and the correlation is slightly higher when the POP transports lag the Sverdrup transports by 10 days.

The Kuroshio Extension transport can also be estimated directly from streamfunction differences across the zonal jet. The direct estimates obtained by differencing the streamfunction fields averaged over the dashed boxes in Fig. 2 are shown in the bottom panel of Fig. 3. The correlation between the resulting Sverdrup and POP direct estimates of Kuroshio Extension transport are 0.91. The cross correlations between the direct and indirect indices of Kuroshio Extension transport are 0.87 for the Sverdrup model and 0.82 for the POP model. The variations in the transport of the Kuroshio Extension in both models are thus well accounted for by large-scale variations in the intensities of the subtropical and subpolar gyres of the North Pacific.

TOPEX/POSEIDON observations

T/P observations of SSH differ fundamentally in two important respects from the Sverdrup and POP barotropic streamfunction fields considered above. Firstly, SSH variability on seasonal and longer time scales is dominated by a steric response to heating and cooling that does not affect the Sverdrup fields at all and has only a minor affect on the POP barotropic streamfunction fields. Stammer (1997) has estimated the magnitude of the steric SSH variations from a simple 1-dimensional mixed layer model based on heat flux estimates from the ECMWF and NMC operational weather analyses. These steric signals were removed from the 6° and 40 day smoothed SSH fields analyzed here. The effects of any errors in the steric correction of the T/P data are further mitigated in the indirect WBC transport estimates constructed from the differences between residual SSH in the western and eastern basin.

The second major difference between the T/P data and the Sverdrup and POP barotropic streamfunction fields is the presence of energetic baroclinic Rossby wave signals in the SSH fields (Chelton and Schlax, 1996). There are no Rossby waves in the equilibrium Sverdrup model and the amplitudes of baroclinic Rossby wave signals are very much diminished in the POP barotropic streamfunction fields. The deleterious effects of the baroclinic Rossby wave signals on the correlations between T/P transport estimates and the Sverdrup and POP transport estimates can be reduced by averaging the SSH fields zonally over several wavelengths of the baroclinic Rossby waves. This defines the zonal dimensions of the boxes in Fig. 2 used to obtain estimates of the transports of the Oyashio, Kuroshio and Kuroshio Extension.

To the extent that the steric-corrected and zonally smoothed SSH is representative of barotropic variability, estimates of the barotropic streamfunction can be obtained by multiplying SSH by the scaling factor gH/f. Barotropic transport estimates obtained in this manner from T/P data thus vary linearly with the choice of H. An effective depth of H = 4000 m is used here.

It should be noted that, unlike the streamfunction fields in the Sverdrup and POP models, the barotropic streamfunction estimate obtained from SSH is not necessarily zero at the western boundary. T/P estimates of the WBC transports must therefore be estimated by the indirect method described above from basin-wide differences of spatially averaged T/P estimates of barotropic stream–function over the regions shown in Fig. 2.

The resulting T/P estimates of the transports of the Oyashio, Kuroshio and Kuroshio Extension are shown in

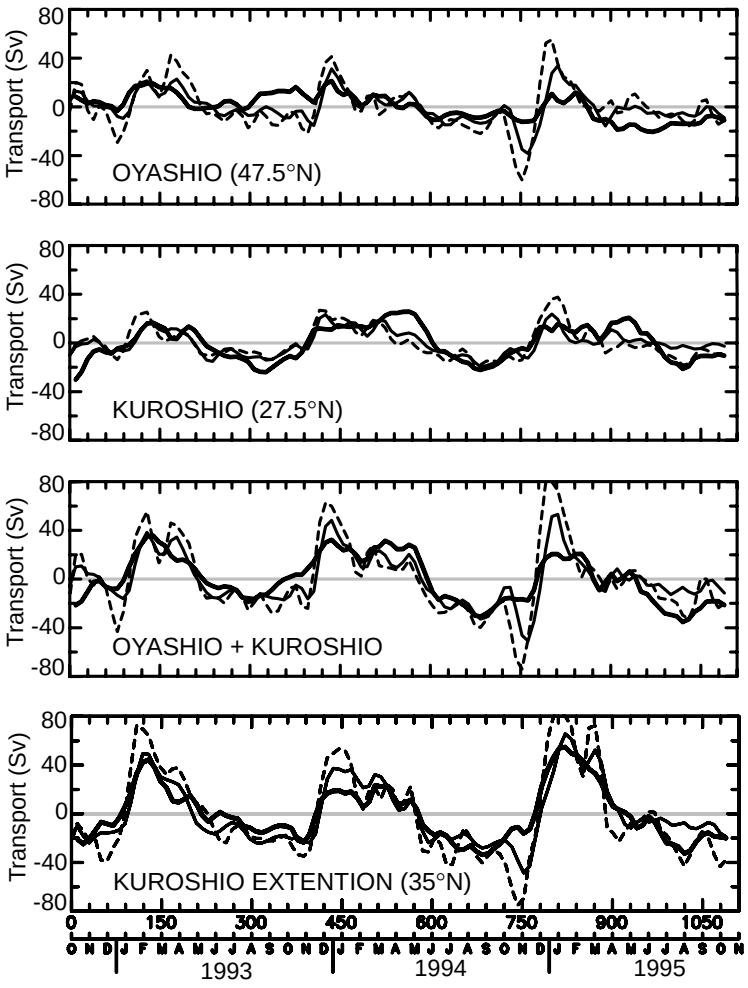

Figure 3. Transport time series estimated from the Sverdrup model (dashed lines), the POP model (thin solid lines) and T/P SSH (thick solid lines). The Oyashio and Kuroshio transports were estimated from differences of the spatially averaged streamfunctions over the solid boxes shown in Fig. 2. The third panel shows the sum of the Oyashio and Kuroshio transports and the bottom panel shows the Kuroshio Extension transport estimated from differences of the spatially averaged streamfunctions over the dashed boxes in Fig. 2.

Table 1. Cross correlations at zero lag between the Oyashio transports (upper right triangle of the table) and the Kuroshio transports (lower left triangle of the table) estimated from the flat-bottom Sverdrup model, the POP model and T/P data.

	Sverdrup	POP Run 11	T/P
Sverdrup	1.00	0.84	0.49
POP Run 11	0.82	1.00	0.59
T/P	0.64	0.77	1.00

Table 2. Cross correlations at zero lag between the sum of the Kuroshio and Oyashio transports (upper right triangle of the table) and the Kuroshio Extension transports (lower left triangle of the table) estimated from the flat-bottom Sverdrup model, of the POP model and T/P data.

	Sverdrup	POP Run 11	T/P
Sverdrup	1.00	0.90	0.74
POP Run 11	0.91	1.00	0.78
T/P	0.89	0.89	1.00

Fig. 3. As for the Sverdrup and POP models considered above, the sum of the T/P estimates of the transports of the Oyashio and the Kuroshio are highly correlated (0.81) with the direct estimate obtained from meridional differences of smoothed T/P data across the axis of the Kuroshio Extension. The correlations between T/P and Sverdrup estimates of the WBC transports are significantly lower than the correlations between the Sverdrup and POP transport (see Table 1). This is evidently indicative of inadequacies in the Sverdrup model. As shown in Table 1, the T/P transport estimates are more highly correlated with the POP transports (0.59 for the Oyashio and 0.77 for the Kuroshio). Thus, while the POP model appears to be very similar to the simple Sverdrup model on the large scales considered here, the added dynamics in the POP model substantially improve the comparison with T/P data.

The T/P, POP and Sverdrup estimates of Kuroshio Extension transport are all highly correlated, for both the indirect and the direct estimates (see Table 2). The agreements between the direct estimates are particularly impressive, with cross correlations of about 0.9 between all three estimates. It is not immediately apparent why the correlations between the T/P and Sverdrup estimates of Kuroshio Extension transport are so much higher than the correlations between T/P and Sverdrup estimates of the WBC transports.

Conclusions

We conclude from this analysis of Sverdrup, POP and T/P estimates of transport variations that much of the large-scale, low-frequency variability in the North Pacific can be accounted for by simple Sverdrup dynamics. The intensities of the subtropical and subpolar gyres of the North Pacific fluctuate seasonally in phase in response to the large-scale wind stress forcing. The Kuroshio Extension transport appears to be very simply related to the transports of the two WBCs of the North Pacific; the Oyashio and Kuroshio fluctuate in phase, summing to yield a Kuroshio Extension transport that is maximum during the winter and minimum in the summer and fall. The transition from minimum to maximum is much more abrupt than the transition back to minimum transport.

An intriguing characteristic can be noted from the transport variations in Fig. 3. From the limited view afforded by the 3-year records analyzed here, interannual variations appear to be very significant. For example, the maximum transport of the Kuroshio Extension occurred about two months later in the winter of 1992–93 than in the winters of 1993–94 and 1994–95. Furthermore, the transport magnitudes are different in all three years. A detailed understanding of the characteristics and dynamics of these interannual variations will develop as the T/P data and POP model simulation continue to accumulate.

Acknowledgements

We thank M. Freilich, R. Smith and D. Stammer, respectively, for providing the ECMWF wind fields, the barotropic streamfunction fields from the POP model and the steric SSH fields used in this analysis. This research was supported by the National Aeronautics and Space Administration.

References

Anderson, D.L.D., and P.D. Killworth, 1977: Spin-up of a stratified ocean, with topography. Deep-Sea Res., 24, 709–732.

Blaha, J., and R. Reed, 1982: Fluctuation of sea level in the western North Pacific and inferred flow of the Kuroshio. J. Phys. Oceanogr., 12, 669–678.

Chelton, D.B., and M.G. Schlax, 1996: Global observations of oceanic Rossby waves. Science, 272, 234–238

Dukowicz, J.K., and R.D. Smith, 1994: Implicit free-surface method for the Bryan-Cox-Semtner ocean model. J. Geophys. Res., 99, 7991–8014.

Greatbatch, R.J., and A. Goulding, 1989: Seasonal variations in a linear barotropic model of the North Pacific driven by the Hellerman and Rosenstein wind stress field. J. Geophys. Res., 94, 12,645–12,665.

Greatbatch, R.J., and A. Goulding, 1990: On the seasonal variation of transport through the Tokara Strait. J. Oceanogr. Soc. Japan, 46, 9–20.

Greenslade, D.G.M., D.B. Chelton, and M.G. Schlax, 1997: The resolution capability of sea level fields constructed from single and multiple altimeter datasets. J. Atmos. Oceanic Technol., in press.

Koblinsky, C.J., 1990: The global distribution of f/H and the barotropic response of the ocean. J. Geophys. Res., 95, 3213–3218.

Large, W.G., and S. Pond, 1982: Sensible and latent heat flux measurements over the ocean. J. Phys. Oceanogr., 12, 464–482.

Schlax, M.G., and D.B. Chelton, 1992: Frequency domain diagnostics for linear smoothers. J. Amer. Stat. Assoc., 87, 1070–1081.

Sekine, Y., and K. Kutsuwada, 1994: Seasonal variation in volume transport of the Kuroshio south of Japan. J. Phys. Oceanogr., 24, 261–272.

Sekine, Y., Y. Sato, H. Takamori, and I. Sakamoto, 1991: Observation on the volume transport of the Kuroshio south of Japan. Bull. Mie Univ., No. 6, 57–82.

Stammer, D., 1997: Steric and wind-induced changes in TOPEX/POSEIDON large-scale sea surface topography observations. J. Geophys. Res., in press.

Preliminary Estimates of North Pacific Circulation from Combined Altimetry, Acoustic Tomography, and a General Circulation Model

D. Menemenlis, D. Stammer, C. Wunsch, B.D. Dushaw, and the ATOC group,*
Massachusetts Institute of Technology, Cambridge, MA 02543, USA.
dimitri@gulf.mit.edu

A primary objective of WOCE is to obtain an understanding of the large-scale circulation of the world ocean, its variability, and its impact on climate. To meet this goal, all available data need to be employed jointly with our best knowledge about ocean dynamics as embodied in modern Ocean General Circulation Models (OGCMs), and consistent with both data and model uncertainties. All important aspects of the general circulation can subsequently be studied from the resulting ocean state estimates and their uncertainty. Here we illustrate the beginnings of a complete system for observing and studying the time-evolving general circulation of the ocean. The present focus is on the North Pacific, where two complementary large-scale observation systems, satellite altimetry and ocean acoustic tomography, are now in place. We show that these two systems, in combination with more traditional oceanographic data and with OGCMs, provide unprecedented information about the large-scale North Pacific circulation.

High-resolution altimetric observations of the sea surface elevation provide a dynamical surface boundary condition for the general circulation (Stammer and Wunsch, 1994; Wunsch, 1996a). In contrast acoustic tomography samples the interior ocean by transmitting sound pulses from sources to receivers along many paths (Munk *et al*., 1995). Variations in acoustic travel times are to first order a measure of temperature anomalies and to a much lesser degree they are also related to variations in current velocity and salinity. The combined power of these two technologies for the purpose of studying the ocean on basin to global scales was first discussed by Munk and Wunsch (1982), and was recently demonstrated in the Western Mediterranean by Menemenlis *et al*. (1996). The type of estimates made in the Mediterranean are repeated here for the entire North Pacific using TOPEX/POSEIDON altimeter data and a preliminary analysis of acoustic data from the Acoustic Thermometry of Ocean Climate (ATOC) project.

Fig.1 (page 21) displays the study area and the location of the ATOC array overlaid on a map of sea surface variability from the TOPEX/POSEIDON altimeter. The measured sea surface variability reflects primarily contributions from mesoscale eddy activity and from seasonal variations of local surface heat fluxes leading to dynamically passive steric height changes. It is clear

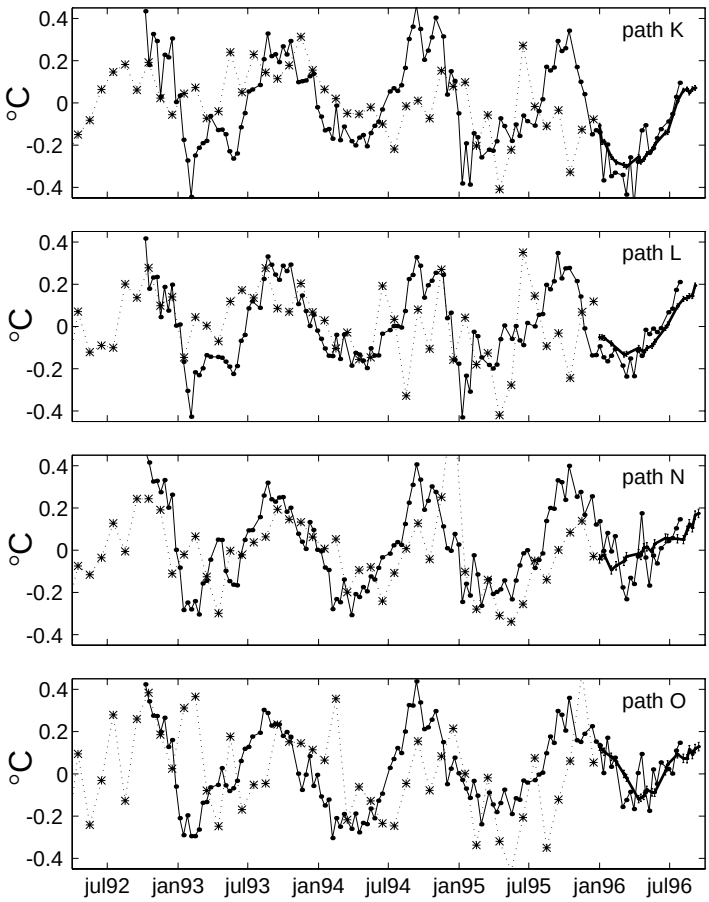

Figure 2. Comparison of depth (0–1000 m) averaged potential temperature along the paths marked by K, L, N, and O in Plate 1. The heavy solid lines with error bars are from a preliminary analysis of ATOC measurements. The dots represent temperature change inferred from TOPEX/POSEIDON altimeter data based on a conversion rate of 1°C distributed over the top 100 m depth per 2 cm height anomaly. The asterisks are estimates from mapped XBT data (XBT data courtesy of A. Leetmaa and M. Ji). The three types of measurements are complementary but also provide a certain amount of redundancy: the altimeter has excellent horizontal but poor vertical resolution, the acoustic measurements sample the ocean with moderate vertical resolution, both acoustic and altimetric data have good temporal resolution, and the XBT provide direct measurements of in-situ near-surface temperature. The data must be evaluated and employed jointly and in a manner consistent with the respective uncertainties.

*ATOC Group: A.B. Baggeroer, T.G. Birdsall, C. Clark, J.A. Colosi, B.D. Cornuelle, D. Costa, B.D. Dushaw, M. Dzieciuch, A.M.G. Forbes, B.M. Howe, D. Menemenlis, J.A. Mercer, K. Metzger, W.H. Munk, R.C. Spindel, P.F. Worcester, and C. Wunsch

from Fig. 1 that the acoustic measurements are obtained from and across dynamically distinct regions ranging from the "quiet" eastern basin to the energetic Kuroshio extension.

Here we use acoustic estimates of path-averaged temperature anomaly along paths K, L, N, and O (bold lines in Fig. 1). Fig. 2 displays the acoustic estimates and compares them with equivalent estimates from XBT and altimeter data. The dominant feature in all three measurement types is a seasonal heating and cooling cycle of order 0.5°C. Short-period fluctuations in the T/P estimates, whose magnitude is significantly larger than the uncertainties of the ATOC estimates, can be attributed to barotropic transports of mass and are enhanced during winter time when the atmospheric variability is maximum. Barotropic mass transports limit the accuracy of the altimeter data for measuring temperature anomalies but are to first order "invisible" in the acoustic measurements (although they can be detected using reciprocal measurements). We attribute the noisy appearance of the XBT time series to poor coverage and the aliasing of mesoscale energy. It is noteworthy that although acoustic path pairs (K, L) and (N, O) cross the North Pacific in adjacent regions, they nevertheless show striking differences in the inferred temperature changes. These discrepancies, at fairly short spatial separation, are indicative of natural space-time variability.

To recover an ocean state which is dynamically consistent with the observations, we use the OGCM developed by Marshall *et al*. (1996a, 1996b) as part of the ATOC program. The OGCM was run in a global configuration with realistic topography, 1° horizontal grid-spacing and 20 vertical levels. Surface wind stress and buoyancy forcing were specified from 12-hourly and daily National Centers for Environmental Prediction (NCEP) meteorological analyses, respectively. Vertical buoyancy instabilities were removed by a convective adjustment scheme, thereby permitting the formation of a buoyancy-driven mixed layer. However wind-driven surface mixing mechanisms are not included. The OGCM therefore produces a wind-driven circulation with realistic variability on the large scales (Stammer *et al*., 1996), but fails to accurately describe the seasonal cycle. The estimation scheme, described next, compensates in part for this and other OGCM deficiencies, as well as for shortcomings in the data.

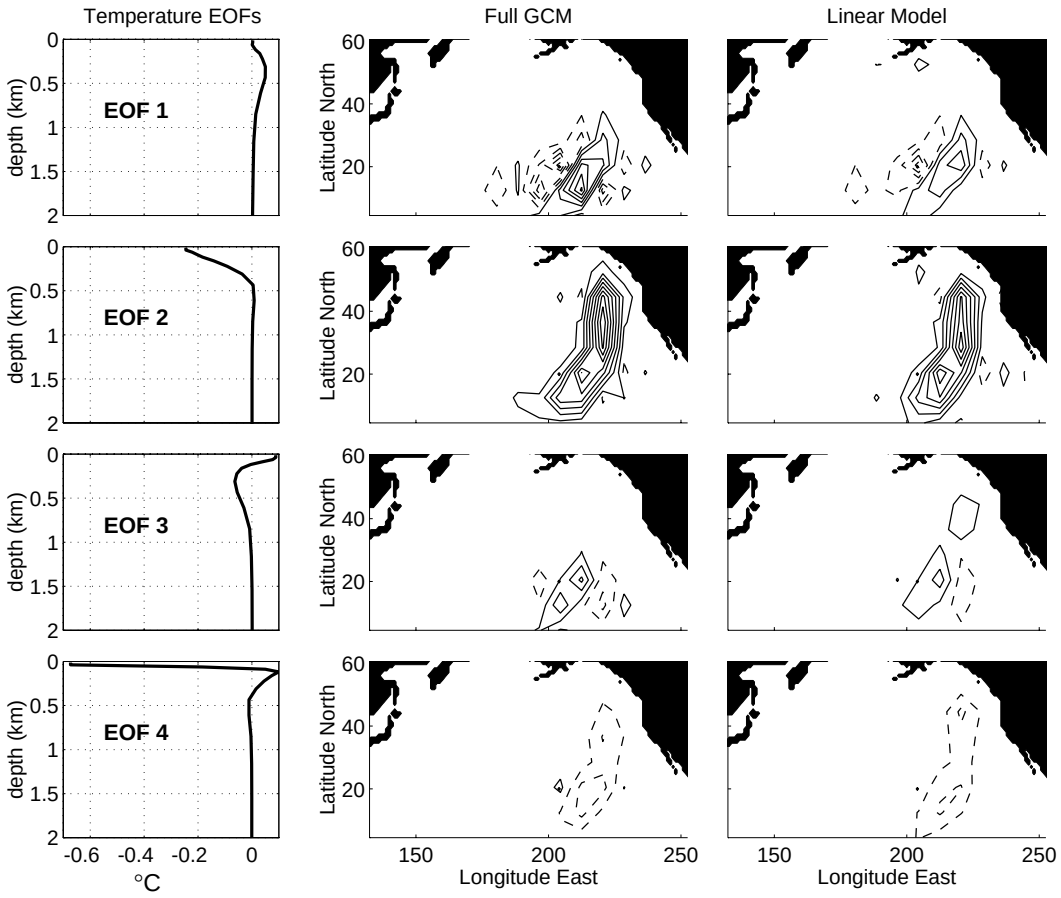

Figure 3. Response of the Marshall et al. (1996) Ocean General Circulation Model (OGCM) to a large scale meridional temperature perturbation: the first column displays four vertical temperature Empirical Orthogonal Functions (EOFs) used for state reduction in this study; the second column displays the exact OGCM response projected onto these four EOFs; and the third column is the response of a time-invariant reduced-state linear model to the same perturbation. The perturbation response shown here follows the initial temperature anomaly by a six-month interval and displays a characteristic Rossby-wave-like pattern, with the information propagating westward at an increasingly faster rate as one approaches the equator.

Observations and model forecasts are inevitably imperfect and the aim of estimation (or assimilation) procedures is to obtain an appropriately weighted average of observations and model forecasts that represents an improvement over either model or data alone. Many methods for forming such an average are known (*e.g.*, Wunsch, 1996b). Here we use a reduced-state linear perturbation approach (Stammer and Wunsch, 1996). The fundamental assumption of this approach is that the OGCM forecast is sufficiently skilful for the OGCM/data difference to be largely governed by linear dynamics. This assumption is tested *a posteriori*. The reduced state describes here the low-frequency (1-month time steps), large-scale (8° horizontal sampling and four vertical EOFs) temperature anomalies.

A time-invariant, reduced-state linear model is determined by systematically perturbing the OGCM and using the resulting anomalies to deduce a state transition matrix for the physics governing the perturbations (Menemenlis and Wunsch, 1996). The ability of the reduced-state linear model to adequately describe the perturbation response of the fully nonlinear OGCM is tested in Fig. 3 by comparing the OGCM response to a large-scale temperature perturbation with that of the linear model. A meridional perturbation is initially imposed at 225°E in EOF 2 and Fig. 3 displays the 6-month response. In both cases a characteristic Rossby wave pattern evolves and propagates westward. The leakage of energy from EOF 2 to adjacent EOFs (predicted by both the OGCM and the linear model) is to be expected since the EOFs are not dynamical modes, and mode coupling by spatially varying vertical stratification or bathymetry also results in EOF-to-EOF leakage.

The measurements and the linear model can be expressed as a set of simultaneous discrete linear equations,

$$y(t) = Ex(t) + n(t), \qquad (1)$$

$$x(t+1) = Ax(t) + q(t), \qquad (2)$$

where y(t) represents the measurements, x(t) is the reduced state vector, E is the observation matrix relating the state vector and the observations, and A is the linear model. (Note that in the present context, observations consist of model-data differences with time-means removed.) Vectors n(t) and q(t) represent errors in the observations and the linear model, respectively. We solve the estimation problem using the sequential Rauch-Tung-Striebel filter-smoother algorithm (Rauch et al., 1965) to minimize the quadratic function,

$$J = \sum_t \left[n^T(t) R^{-1}(t) n(t) + q^T(t) Q^{-1}(t) q(t) \right]. \qquad (3)$$

Here R(t) and Q(t) are weight matrices that control the relative size of data and model misfit. A major issue is that of specifying the prior statistics (the solution uncertainty variance will be minimized only when R and Q represent the prior covariance of data and model errors, respectively). We impose prior statistics in the form of stationary diagonal covariance matrices estimated from the observations

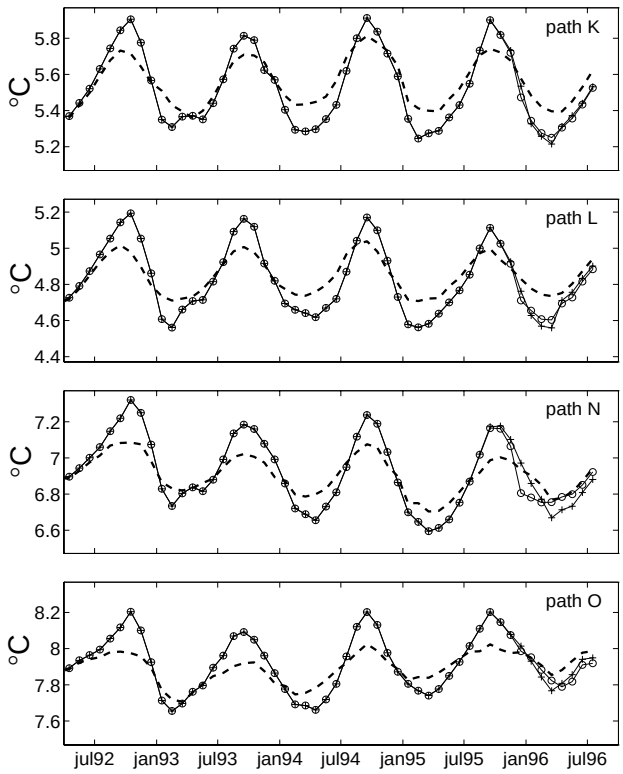

Figure 4. Estimates of depth (0–1000 m) and path-averaged potential temperature along the same paths as in Fig. 1. Dashed lines are from the OGCM, crosses are from an OGCM/altimeter combination, and circles are from an OGCM/altimeter/acoustic combination. The three estimates are at first coincident. The addition of the altimeter data, starting in September 1992, "corrects" the seasonal cycle of the OGCM by a factor of 2. Acoustic data, available starting in January 1996, further improve the heat content estimates.

themselves (*e.g.*, Fu and Fukumori, 1993); results are checked *a-posteriori* for consistency. As additional data becomes available, more realistic second order statistics can be obtained using adaptive filter theory (*e.g.*, Blanchet *et al.*, 1996).

To demonstrate the power of this type of data/model combinations for North Pacific studies, we provide two representative examples (Fig. 4 and Fig. 5 (page 22)). A detailed analysis of the estimation results will be presented elsewhere. Fig. 4 compares various estimates of path-averaged heat content in the top 1000 m: dashed lines are the OGCM estimates, crosses are from an OGCM/altimeter combination, and circles are from an OGCM/altimeter/acoustic combination. Although the OGCM is strikingly successful in simulating inter-annual variations in peak-to-peak seasonal heat content changes, it underestimates the strength of the seasonal cycle by a factor of 2 as compared to TOPEX/POSEIDON observations. This deficiency, present in almost all state-of-the-art ocean models, and represented in Q(t), results from missing mixed-layer physics and errors in the surface boundary conditions. The combined OGCM/altimeter estimates are in overall agreement with

the acoustic data along path K, but differ along the remaining paths. Accordingly, the combined OGCM/altimeter/acoustic estimates lead to further changes which reach about 0.1°C along path N.

Fig. 5 displays further results from the combined OGCM/altimeter/acoustic estimation, *i.e.*, the depth (0–1000 m) averaged temperature change from 16 January to 16 July 1996, and the corresponding temporal change in horizontal velocity below the Ekman layer. (This particular 6 month period represented the only overlap between acoustic, altimetric, and NCEP data at the time of writing of this note.) Remarkably, there are temporal temperature changes of up to 1°C present near the western boundary. Positive anomalies cover most of the North Pacific and reflect the seasonal heat uptake of the upper thermocline during early summer 1996. Deviations from this overall tendency are apparent in the tropical Pacific where wind induced changes of the equatorial current system produce a clear phase shift in the temperature changes consistent with the seasonal cycle in sea surface height observations (Stammer and Wunsch, 1994). Accordingly, changes in the current field reflect primarily seasonal fluctuations of the North Equatorial Current, and, to a lesser extent, the Equatorial Countercurrent at the southern domain boundary. At mid-latitudes large changes in the velocity field are found in the western boundary current region and along the California coast where the figure suggests a plume of cold water being advected southward by the California Current (compare with Strub *et al.*, 1987).

Estimates such as those of Figs. 4 and 5 can now be obtained on a weekly basis. The present results are preliminary and will be refined in many ways as more data become available, and as models and estimation procedures improve. In particular, the acoustic tomography time series is still too short to draw definitive conclusions. Nevertheless our results illustrate how the large-scale, low-frequency ocean variability can be monitored and understood on an ongoing basis with existing technology. We are now starting to use these combined estimates to study the time-evolving North Pacific circulation in detail. Envisioned applications are numerous – ranging from local predictions of temperature perturbations and basin-averaged heat content changes to potential vorticity flux estimates.

Acknowledgements

Work supported by the Strategic Environmental Research and Development Program through the Advanced Research Projects Agency, by the National Aeronautics and Space Administration, and by grants of High Performance Computer time from Project SCOUT at the Massachusetts Institute of Technology Laboratory for Computer Science.

References

Blanchet, I., C. Frankignoul and M.A. Cane, 1996: A Comparison of Adaptive Kalman Filters for a Tropical Pacific Ocean Model. Monthly Weather Review, in press.

Fu, L.-L., and I. Fukumori, 1993: Fitting dynamic models to the Geosat sea level observations in the tropical Pacific Ocean. part ii: A linear, wind-driven model. J. Phys. Oceanogr., 23:2162–2181.

Marshall, J., A. Adcroft, C. Hill, L. Perelman, and C. Heisey, 1996a: A finite-volume, incompressible navier-stokes model for studies of the ocean on parallel computers. J. Geophys. Res., in press.

Marshall, J., C. Hill, L. Perelman, and A. Adcroft, 1996b: Hydrostatic, quasi-hydrostatic and non-hydrostatic ocean modeling. J. Geophys. Res., in press.

Menemenlis, D., T. Webb, C. Wunsch, U. Send, and C. Hill, 1996: Demonstration in the Mediterranean Sea of a large-scale oceanic observation system. Submitted for publication.

Menemenlis, D., and C. Wunsch, 1996: Linearization of an oceanic circulation model for data assimilation and climate studies. J. Atmos. Oceanic Technol., in press.

Munk, W., P. Worcester, and C. Wunsch, 1995: Ocean Acoustic Tomography. Cambridge Monographs on Mechanics. Cambridge University Press, New York.

Munk, W., and C. Wunsch, 1982: Observing the Ocean in the 1990s. Phil. Trans. R. Soc. Lond., A307:439–464.

Rauch, H.E., F. Tung, and C.T. Striebel, 1965: Maximum likelihood estimates of linear dynamic systems. AIAA J., 3:1445–1450.

Stammer, D., R. Tokmakian, A. Semtner, and C. Wunsch, 1996: How well does a 1/4° global circulation model simulate large-scale oceanic observations? J. Geophys. Res., in press.

Stammer, D. and C. Wunsch, 1994: Preliminary assessment of the accuracy and precision of TOPEX/POSEIDON altimeter data with respect to the large-scale ocean circulation. J. Geophys. Res., 99(C12): 24,584–24,604.

Stammer, D. and C. Wunsch, 1996: The determination of the the large-scale circulation of the Pacific Ocean from satellite altimetry using model Green's functions. J. Geophys. Res., 101(C8):18,409–18,432.

Strub, P.T., J.S. Allen, A. Huyer, R.L. Smith, and R.C. Beardsley, 1987: Seasonal cycle of currents, temperatures, winds, and sea level over the northeast Pacific continental shelf: 35°N to 48°N. J. Geophys. Res., 95:1507–1526.

Wunsch, C., 1996a: The vertical partition of oceanic horizontal kinetic energy and the spectrum of global variability. Submitted for publication.

Wunsch C., 1996b: The Ocean Circulation Inverse Problem. Cambridge University Press, New York.

Drifter Data now available on the WWW

Surface drifter data sets have been supplied to the Marine Environmental Data Service (Canada) by the AOML laboratory of NOAA (Miami) and posted on the Internet. Drifter locations have been interpolated to 6 hourly positions and are grouped by year (1979–1995) and by Ocean Basin (Pacific, Atlantic, Indian and Arctic). The data packets are compressed, range in size from 20 Kb to 10 Mb, and their format is described. The address is

http://www.meds.dfo.ca/MEDS/e_svp.html

Congratulations to all parties concerned.

The Seasonal Heat Budget of the North Pacific: Net Heat Flux and Heat Storage Rates (1950–1990)

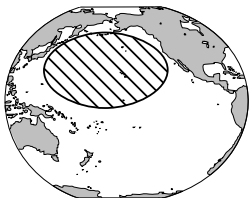

John R. Moisan and Pearn P. Niiler, Scripps Institution of Oceanography, University of California, La Jolla, CA 92093-0230, USA. moisan@drifter.ucsd.edu

The flux of heat across the ocean-atmosphere interface is an important link between the ocean and atmosphere systems. The current trend of ocean general circulation models (OGCMS) is to use estimates of these fluxes to seasonally force ocean system models. Recent model results from several tropical OGCMS showed too warm a sea surface temperature (SST) in the western Pacific which is believed to result from inaccuracies in the climatological heat flux estimates. Better estimates of these fluxes are needed if we are to accurately model, and thereby understand and potentially predict the interactions between the ocean and atmosphere systems. This article presents results from a new estimate of the heat budget for the North Pacific Ocean (Moisan and Niiler, submitted).

The net heat flux (NHF) and heat storage rates (HSR) were calculated for the North Pacific Ocean from 1950 to 1990 on a spatial resolution of 5° by 5°. The NHF was calculated using satellite remotely sensed solar irradiance (Bishop and Rossow, 1991) and ship marine weather reports from the Comprehensive Ocean Atmosphere Data Set (COADS; Slutz *et al.*, 1985), and the Liu *et al.* (1979) formulations for latent and sensible heat exchange. The HSR was calculated using temperature profiles from the National Ocean Data Center (NODC). Heat storage rates were calculated as the time rate of change of the heat content integrated from the surface down to the isotherm, which was 1°C below the coldest locally observed wintertime SST, defined as the locally observed wintertime ventilation isotherm. Integrating to a constant isotherm rather than a constant depth significantly improves the results. Integrating to a constant depth results in a highly variable seasonal HSR which correlates poorly to the NHF. However, by integrating to a constant isotherm the resulting HSR was predominantly seasonally variable and well correlated to the NHF.

The root mean square error in the difference between the NHF and HSR climatologies was $40\,\mathrm{W\,m^{-2}}$. The differences in the NHF and HSR for the northeast portion of the North Pacific had a semi-annual signal. This semi-annual variability may be caused by the seasonal fluctuations in the horizontal advection of heat which cannot be estimated at this present time. Ekman heat transport estimates did not account for the semi-annual signal in the differences. When the individual temperature profiles from the northeastern portion of the basin were normalized to the local 300 m mean temperature, removing some of the local seasonal changes caused by barotropic variability of water motion, the root mean square error in this region was reduced to $20\,\mathrm{W\,m^{-2}}$, and the large scale semi-annual periodicity observed in the differences was removed. The normalization process may also serve to remove some of the basin scale seasonal variability in the horizontal heat advection. The annual mean for the NHF estimates (Fig. 1) was calculated by averaging the seasonal climatology from each grid square that contained a full 12 month seasonal climatology. The mean of the seasonal climatology was used rather than the mean of the time series in order to remove any seasonal sampling bias in the data set. Oceanographic data density is generally larger in the summer months, especially at high latitudes. In the western region of the North Pacific, more than $100\,\mathrm{W\,m^{-2}}$ is lost to the atmosphere. A zero NHF contour line runs from the northern coast of Japan southeast to parallel along the coastline of Mexico. To the north of the zero contour line, heat is gained by the ocean at a rate of about $25\,\mathrm{W\,m^{-2}}$, and to the south heat is lost to the atmosphere at a rate of about $25\,\mathrm{W\,m^{-2}}$.

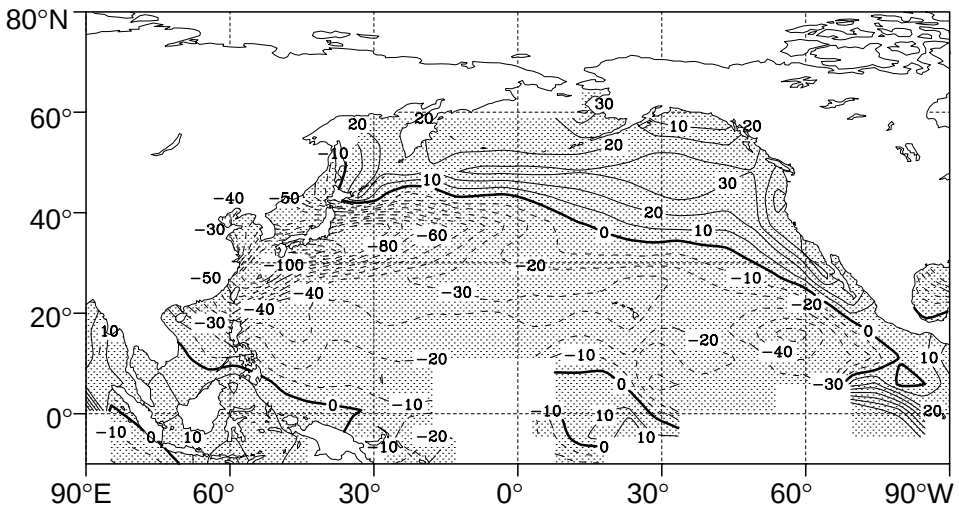

Figure 1. The annual mean net heat flux between 1950 to 1990. Contour interval is $10\,\mathrm{W\,m^{-2}}$. Positive contours: solid line, negative contours: dashed line. Shaded region indicates region where data were available.

Over decadal time scales the annual mean NHF is balanced by the annual mean horizontal advection and diffusion of heat. By assuming

that the flow of heat through the Bering Strait contributes little to the heat balance in the North Pacific, and the heat flux across the ocean-land boundary is insignificant, the annual mean NHF estimates from the northern part of the North Pacific basin to the equator can be spatially integrated to estimate the northward heat transport (NHT) as a function of latitude. Regions of missing data were assumed to have a zero net heat flux. The results of this calculation for this study and several previous heat flux estimates are shown in Fig. 2. The resulting NHT was closer to actual northward heat transport estimates made at 10, 24, 35, and 47°N, than previous ocean heat flux estimates. The NHT across the equator was estimated to be about 0.4 PW.

Previous comparisons between the estimates have been difficult because systematic errors from these calculations are cumulative and the resulting estimated envelope is large enough to encompass both the estimated and measured heat transport curves and latitude-specific estimates (Talley, 1984). However, because the errors associated with annual mean heat flux also affect the seasonal cycle, the difference between the seasonal cycles of the NHF and HSR was used as an estimate of the basin scale systematic error. The assumption here was that the seasonal cycle of the NHF was locally stored and that the effect of the seasonal horizontal heat transport was minimal. Because a bias was not anticipated in the HSR estimates, the error was calculated from the differences in the seasonal cycles of the NHF and HSR. This basin scale error was then used with the annual mean field of the NHF to integrate the error of the NHT estimate over the North Pacific. In practise, the basin-averaged bias was estimated using standard Principal Component Analysis (PCA) techniques with the climatologies from the NHF and HSR in the North Pacific. A bias of 7% in the annual mean net heat flux was observed. This bias was then used with the annual mean NHF and the calculated $38\,W\,m^{-2}$ RMS error in the difference between the seasonal NHF and HSR to calculate an error envelope for the annual mean NHT in the North Pacific.

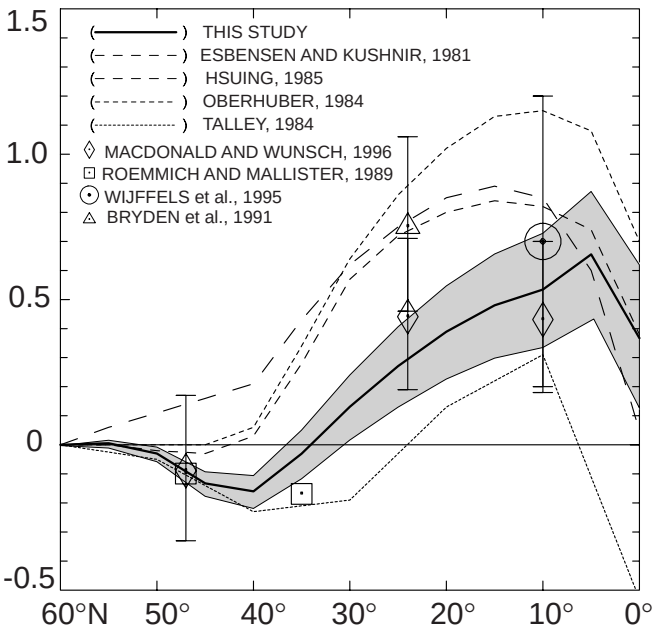

Figure 2. The annual mean northward heat transport (PW) for the North Pacific obtained by integrating the annual mean net heat flux estimates using data from this study (thick solid line), and the previous studies of Talley (1984) Oberhuber (1988), Hsuing (1985) and Esbensen and Kushnir (1981) (smallest to largest dashed lines, respectively). The error estimate from this study obtained from an estimated ± 20 W m^{-2} error and a 7% bias on the annual mean is shown with the thin solid line. The latitude specific estimates of northward heat transport from Roemmich and McCallister (1989) (47°N, -0.9 PW and 35°N, -0.31 PW), Bryden et al. (1991) (24°N, 0.75 ±0.3 PW) and Wijffels (1995) (10°N, 0.7 ±0.5 PW) are also shown.

A significant result from this new heat budget was that for most regions in the North Pacific the seasonal climatologies of the NHF and HSR were locally balanced. The greatest difference between the seasonal climatologies of the NHF and HSR occurred in the western boundary current region and is primarily attributed to the large meanders associated with the Kuroshio and Kuroshio extension, which meander into preferential patterns and thus cause error in the estimate of the HSR. The seasonal variability in the horizontal transport of heat may be another potential cause of the difference between the seasonal climatologies NHF and HSR. This source of error can affect the balance between the NHF and HSR in other regions of the Pacific.

This estimate of the annual mean northward heat transport agrees with five of the seven direct estimates available in the literature. However, the error in all these estimates is quite large. Because the comparison between the seasonal cycle of the NHF and HSR estimates demonstrated a bias of only 7%, the confidence in the heat transport estimate is greater since it has a much smaller error envelope than previous error estimates (Talley, 1984). However, because of the lack of data in the equatorial regions of the North Pacific, the estimates of the heat transport in that area may be too high. Presently, there are no direct estimates of the northward heat transport in this region with which to compare these results.

This study used data from the NODC archives to obtain temperature data and COADS to obtain the climate observations. There are other sources of data that are available to use in calculating the NHF and HSR. This study only focused on the COADS and NODC data. Results from this study can now be used in several areas of oceanography. The correct seasonal NHF can be used to force mixed layer models. The new cloud parameterization can be used to estimate the solar irradiance. And, because most of the regions on the North Pacific were shown to be seasonally balanced between the NHF and HSR, the implementation of 1-D models to these areas should be appropriate for studying the seasonal cycle of the mixed-layer.

References

Bishop, J.K B., and W.B. Rossow, 1991: Spatial and temporal variability of global surface solar irradiance. J. Geophys. Res., 96, 16,839–16858.

Bryden, H.L., D.H. Roemmich and J.A. Church, 1991: Ocean heat transport across 24°N in the Pacific. Deep-Sea Res., 38, 297–324.

Esbensen, S.K., and V. Kushnir, 1981: The heat budget of the global ocean: An atlas based on estimates from surface marine observations. Climate Research Institute, Rep. No. 29, Oregon State University, 27pp., 188 figs.

Hsiung, J., 1985: Estimates of global oceanic meridional heat transport. J. Phys. Oceanogr., 15, 1405–1413.

Liu, W.T., K.B. Katsaros, and J.A. Businger, 1979: Bulk parameterizations of air-sea exchanges of heat and water vapor including molecular constraints at the interface. J. Atmos. Sci., 36, 1722–1735.

Moisan, J.R., and P.P. Niiler: The seasonal heat budget of the North Pacific: Net heat flux and heat storage rates [1050-1990]. Submitted to J. Phys. Oceanogr.

Oberhuber, J.M., 1988: An atlas based on the 'COADS' data set: The budgets of heat, buoyancy and turbulent kinetic energy at the surface of the global ocean. Max-Planck-Institute for Meteorology, Report No. 15, 20pp.

Roemmich, D., and T. McCallister, 1989: Large scale circulation of the North Pacific Ocean. Prog. Oceanogr., 22, 171–204.

Slutz, R.J., S.J. Lubker, J.D. Woodruff, R.L. Jenne, D.H. Joseph, P.M. Steurer, and J.D. Elms, 1985: Comprehensive ocean-atmosphere data set: Release I. Boulder, NOAA Environmental Research Laboratories, Climate Research Program, 268pp.

Talley, L.D., 1984: Meridional heat transport in the Pacific Ocean. J. Phys. Oceanogr., 14, 231–241.

Wijffels, S.E., J.M. Toole, H.L. Bryden, R.A. Fine, W.J. Jenkins, and J.L. Bullister, 1995: The water masses and circulation at 10°N in the Pacific. Deep-Sea Res., 43, 501–544.

Mean Circulation in the North Western Pacific Mixed Layer from Drifter Data

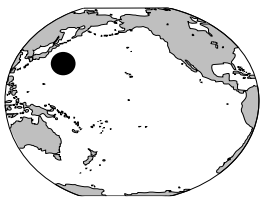

Nikolai Maximenko, P. Shirshov Institute of Oceanology, Moscow, Japan Marine Science Foundation, Tokyo; Pearn P. Niiler, Scripps Institution of Oceanography, USA; and Toshio Yamagata, University of Tokyo, Japan.
nikolai@ocean0.geoph.s.u-tokyo.ac.jp

We analyzed surface drifter data, edited and filtered by the Drifter Data Assembly Center, NOAA/AOML up to October 1996, in the area 20–60°N, 120–180°E. It contains 228 drogued (and 222 undrogued) drifter trajectories with about 32000 (32000) observational days of velocity and about 29000 (28000) days of temperature observations in the area of interest. The drifters were of standard TOGA/WOCE SVP configuration (Sybrandy and Niiler, 1991) with the drogue centred at 15 m depth and drag area ratio about 40 (Poulain *et al*., 1996). In this short note the mean velocity field on a $1°N \times 1°E$ grid is discussed. We are mostly interested in the relatively strong, stable currents and ignore the difference between the data from drogued and undrogued drifters except for cases when this influences our conclusions significantly. We also omit estimates of the accuracy of our statistics although we confess that it is weak in the Subpolar and central North Pacific.

A general impression of the drifter data distribution can be obtained from Fig. 2. The 1°-averaged mean velocity is represented in colour in Fig. 1 (page 22). Velocity vectors, superimposed on the zonal velocity component show: the eastward currents (red areas), in the Kuroshio, the Subtropical countercurrent around 22°N, in currents associated with Oyashio Front (OF) between 40°N, 148°E

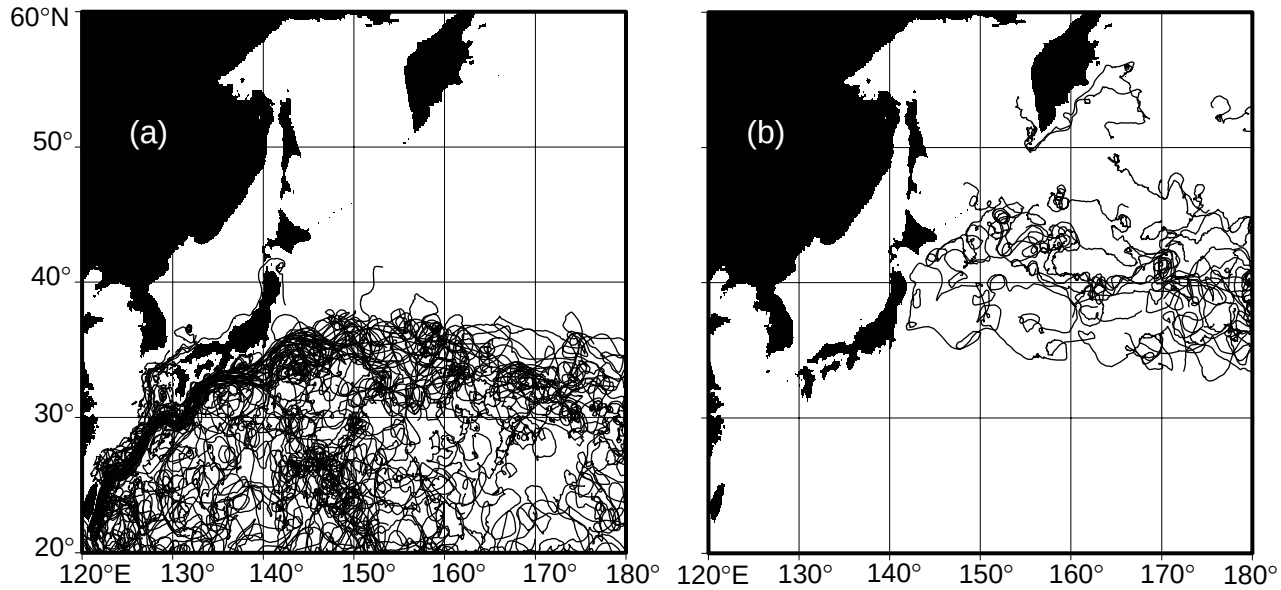

Figure 2. Trajectories of all drogued drifters in the domain deployed (a) south of 35°N, and (b) north of 35°N.

and 47°N, 162°E and in two quasi-zonal flows east of 150°E, centred around 32–35°N (the Kuroshio Extension – KE) and 38–43°N (probably, associated with the Subarctic Front – SF). Blue areas reveal the strong westward-flowing Kamchatka Current, Oyashio Current and Kuroshio recirculation with at least two intensive cells. In addition the Subtropical gyre and weak westward flows between the eastward OF current and SF jet around 40°N, as well as between the latter and KE are seen. Velocities of both SF and KE jets locally reach 40 cm/s and decrease slowly eastward. The origin of the SF jet can not be defined from the drifter data available. It could be either the result of Kuroshio branching or of the Oyashio Extension or even their superposition.

For a more detailed study of the kinematics of the SF-KE frontal area we split the drifters into two groups: "southern", *i.e.* launched south of 35°N and "northern", deployed further north. Fig. 2 shows that despite strong eddy activity and instability of both jets, no drogued drifter ever crossed both of them. Drifters from the Subarctic Pacific often entered the interfrontal zone, but never continued further south. In the same way drifters from the subtropical area arrived at the northern edge of Kuroshio Extension and showed rather chaotic motion there but never diffused further north.

At the same time, a few undrogued drifters (not displayed in this paper) crossed both fronts in both directions. This may be a demonstration of how a relatively weak influence of wind can affect the Lagrangian properties of a drifter and may change drastically its large-scale trajectory.

Fig. 3 shows the meridional distributions of various parameters calculated from the complete (drogued and undrogued) data set and averaged over 0.5°N and over 150–180°E, where zonal variability looks much weaker than meridional one. The thick line represents statistics calculated for all the drifters in the area, the thin line is only for the "southern" drifters and the dashed line is for the "northern" only. Two jets are seen at 35° and 41°N, respectively. Their maximum mean eastward velocities reach 20 and 12 cm/s, while meridional widths are about 4–5°N in average. Gap between them also shows eastward flow (about 2 cm/s in velocity) that can be due to actual non-zonality of the fronts, especially obvious in the vicinity of the Shatsky Rise. The strongest velocity variability is observed in the Kuroshio Extension around 34°N and magnitudes of velocity fluctuations are comparable with the mean velocities in both KE and SF jets. The value [VxdV/dt] can be easily calculated from Lagrangian data and is proportional both to the kinetic energy and angular velocity of the velocity vector rotation (roughly local angular velocity of the Lagrangian particle moving along the arc). It may characterize the relative role of eddies of different signs. From Fig. 3 we can conclude that cyclones prevail at the southern edge of KE, when anticyclonic motions are dominant at its northern edge and in the interfrontal zone. This is consistent with the important role of meandering KE in the region. In the SF jet and north of

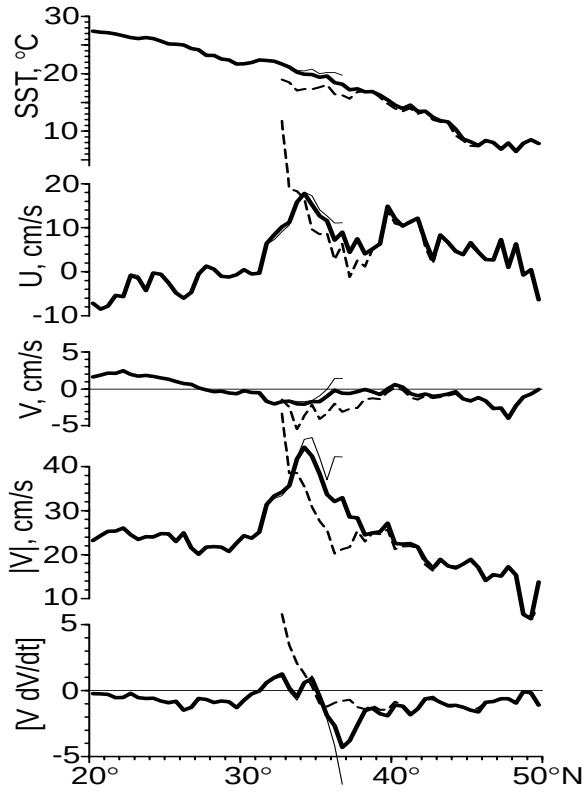

Figure 3. Meridional distribution of mean (averaged over all the drifters, 150–180°E and 0.5°N) sea surface temperature (SST), zonal (U), meridional (V) velocity components, its mean magnitude |V| (not magnitude of mean) and rotational parameter [VxdV/dt], as discussed in the text. The thick line represents statistics for all the drifters, the thin line is only for "southern" and the dashed line is only for "northern" drifters.

it we have found anticyclonic eddies to be more intensive.

Fig. 3 shows a rather big difference between "southern" and "northern" drifters in most of parameters (similar result was obtained for drogued drifters only). In the interfrontal zone northern drifters measured lower temperature, weaker eastward velocity, more tendency for southward drift, lower velocity variability and mainly cyclonic circulation. Qualitatively it is also consistent with their penetration from the north through the meanders of both jets.

It is remarkable that the drifters seem keeping most of their properties for rather long time along the trajectories that suggests an important role of Lagrangian processes in the world ocean at wide range of scales. We hope that currently increasing drifter family will provide our better understanding of the surface circulation.

References

Poulain, P.-M., A. Warn-Varnas, and P.P. Niiler, 1996: Near-surface circulation of the Nordic seas as measured by Lagrangian drifters. J. Geophys. Res., 101(C8), 18,237–18,258.

Sybrandy, A.L., P.P. Niiler, 1991: WOCE/TOGA Lagrangian drifter construction manual. SIO Ref. 91/6, WOCE Rep. 63, 58pp., Scripps Inst. of Oceanogr., La Jolla, CA.

Time Series of the Kuroshio Transport Derived from Field Observations and Altimetry Data

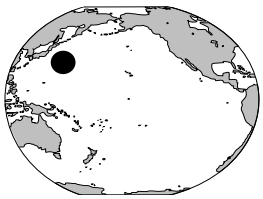

Shiro Imawaki and Hiroshi Uchida, Kyushu University, Fukuoka 816, Japan; Hiroshi Ichikawa, Kagoshima University, Kagoshima 890, Japan; Masao Fukasawa, Tokai University, Shizuoka 424, Japan; Shin-ichiro Umatani, Kyushu University, Fukuoka 816, Japan; and ASUKA Group. imawaki@riam.kyushu-u.ac.jp*

Introduction

The oceans are known to play an important role in the earth's poleward heat transport. For the North Pacific, the net meridional heat transport is believed to be controlled mostly by surface circulations including the subtropical gyre (Bryden *et al*., 1991). It is crucial to know the transport of those circulations accurately, especially, the transport of the western boundary current of the subtropical gyre, the Kuroshio.

The transport of the Kuroshio, however, has not yet been estimated accurately, because long-term direct current measurements in the Kuroshio cannot be easily carried out. Most information about the Kuroshio transport has been provided by geostrophic calculation under the assumption of no-motion at some abyssal depth; the transport thus estimated is a relative transport, which excludes the barotropic component. A few exceptions are pioneer studies including Takematsu *et al*. (1986), Mizuno *et al*. (1991) and Kaneko *et al*. (1992), in which direct current measurements were carried out to estimate the absolute transport of the Kuroshio. No previous studies, however, provided us with a long time series of the absolute transport on the basis of direct current measurements.

Recently, an effort was made to measure the Kuroshio and its recirculation south of Shikoku, Japan, and estimate their absolute volume and heat transports. A group called ASUKA carried out oceanographic surveys along a line crossing the Kuroshio, during 1993–1995. The line was chosen to coincide with a subsatellite track of TOPEX/POSEIDON, which has been measuring the sea surface height since 1992. The altimetry data combined with the field observation data give a fairly long continuous record about the Kuroshio transport. This effort was intended to be the western boundary current array PCM5 of WOCE, which is designed to be combined with trans-Pacific hydrographic data along 30°N (WHP line P2) in order to give an estimate of the net meridional heat transport of the mid-latitude North Pacific.

Field observations

A large number of scientists from Japan and USA were involved in the ASUKA surveys. In October 1993 they deployed nine moorings equipped with 33 current meters and two upward-looking Acoustic Doppler current profilers

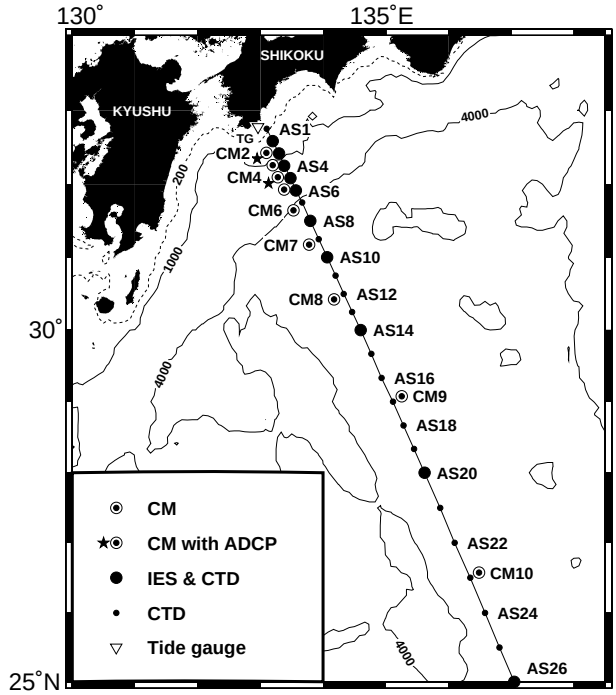

Figure. 1. The ASUKA Group Kuroshio observation line across the Kuroshio south of Shikoku, Japan. Moored current meter observations (CM), repeated hydrographic observations (CTD) and others (ADCP and IES) were carried out from October 1993 to November 1995. This line was chosen to coincide with a subsatellite track of TOPEX/POSEIDON.

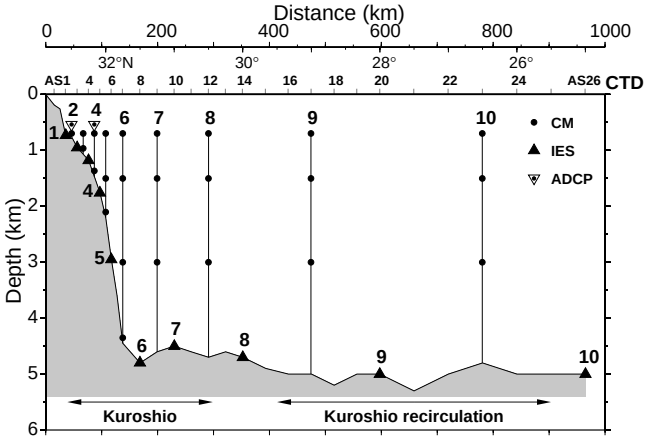

Figure 2. Vertical distribution of moored instruments including current meters (CM), upward-looking ADCPs and IESs. See the text for their recovery. Also shown are locations of nominal hydrographic stations (AS1–AS26).

*Affiliated Surveys of the Kuroshio off Cape Ashizuri

(ADCPs), and also 10 inverted echo sounders (IESs) to start the intensive survey. Figs. 1 and 2 show the location of the observation line and distribution of instruments. In September 1994 all those instruments except IESs were recovered and a similar array was redeployed. In November 1995 those instruments were recovered to finish the intensive survey. All instruments except three current meters at station CM8 for the second year mooring and an IES at station ES5 were successfully recovered.

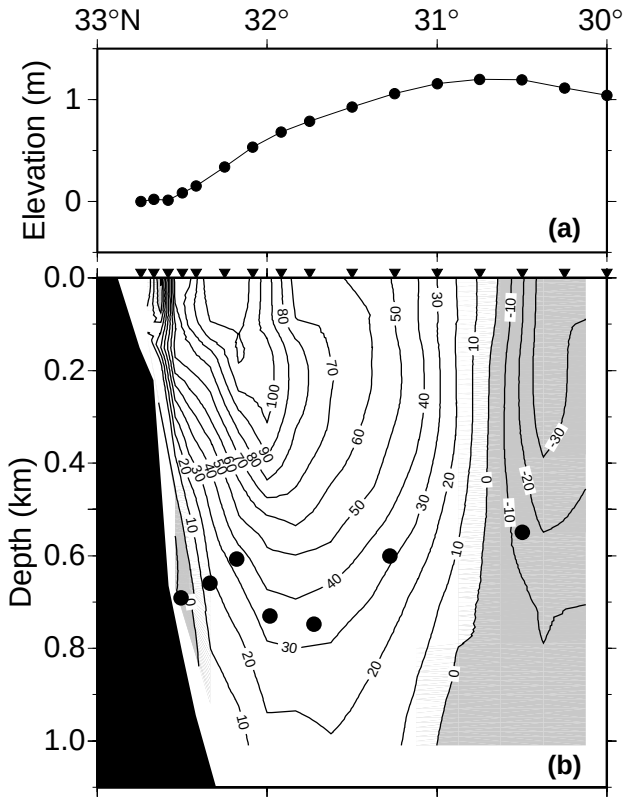

Figure 3. An example of the profile of SSDT and section of absolute geostrophic velocity (in cm/sec) of the Kuroshio in November 1993. The velocities are calculated from hydrographic data (obtained at stations indicated by triangles in Fig. 2) with reference to observed velocities at 550-750 m depths; dots show actual current meter locations at that time. Negative values are shaded. The profile of SSDT is estimated from surface geostrophic velocities thus obtained.

During this 2-year long intensive survey period, the ASUKA Group carried out repeated hydrographic surveys (CTD and/or XBT measurements) along the line, in order to estimate upper layer velocities, which cannot be measured adequately by the moored instruments. A total of 40 repeat sections were obtained for the Kuroshio region, or the northern part of the line. Towed-ADCP measurements from ships were also done twelve times during the period. Tide gauge measurements were maintained at Cape Ashizuri (see Fig. 1 for location) by the Japan Meteorological Agency.

Volume transport

The moored current meter data for the second year measurements data are being processed and hence only the first year data are used in this analysis. For the 1993–1994 annual mean field, the flow associated with the Kuroshio is directed to ENE, almost perpendicular to the ASUKA line. The vertical section of the mean velocity component normal to the observation line shows the maximum (30 cm/sec) at 700 m depth at CM4, indicating the core of the Kuroshio at this level. The section also shows that the Kuroshio reaches down to 2,000 m depth on the offshore side but does not reach to the bottom on the continental slope, where the component is almost zero or slightly negative.

Geostrophic velocities are calculated from the repeat hydrography, with reference to observed velocities at a nominal depth of 700 m; those velocities are called here absolute geostrophic velocities, in order to be distinguished from ordinary geostrophic velocities calculated with reference to assumed no-motion at some abyssal depths. Fig. 3b shows an example of the absolute geostrophic velocity section of the Kuroshio. Ten-day mean values are used for the reference velocities. In this example, velocities of up to 20 cm/sec are found at 1,000 m depth.

The volume transport of the Kuroshio is estimated from the absolute geostrophic velocities. The areal integral is made for the entire eastward flow representing the Kuroshio from the sea surface to 1,000 m depth. The 1,000 m depth is not satisfactorily deep to estimate the Kuroshio transport, but it is a compromise with the use of XBT data reaching only 800 m depth, which allow us to calculate dynamic depth anomalies down to 1,000 dbar using a very tight experimental relationship (Uchida and

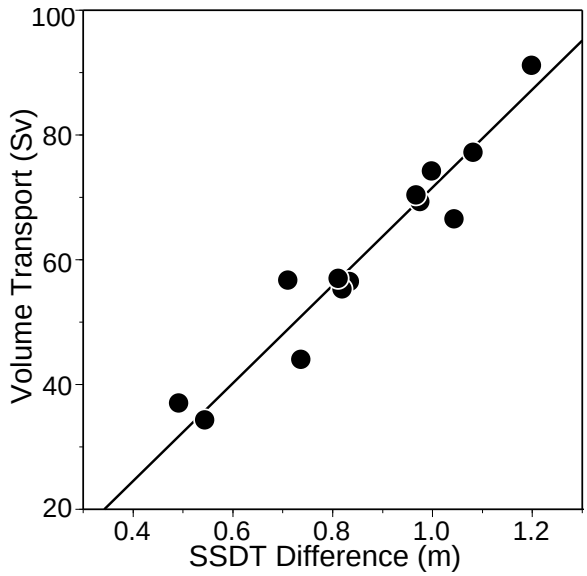

Figure 4. Scatter plot of the volume transport (Sv) of the Kuroshio and the SSDT difference (m) across the Kuroshio. Thirteen cases are shown. The correlation coefficient is 0.96 and the rms difference from the regression line (solid line) is 4.3 Sv.

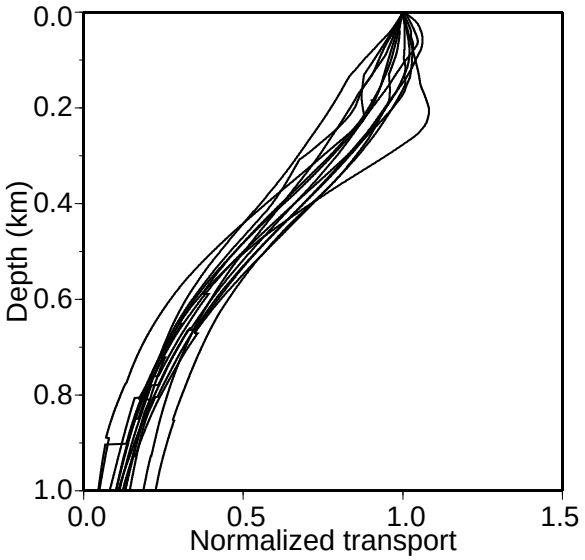

Figure 5. Vertical distributions of the Kuroshio transport per unit depth, normalized by the surface transport. Thirteen cases are shown.

Imawaki, 1996). As is shown below, the most transport is in the upper 1,000 m layer. The estimated transport is 91 Sv ($1\text{Sv}=10^6\ \text{m}^3/\text{sec}$) in the case shown in Fig. 3. The volume transport varies from 34 to 91 Sv for 13 repeat sections carried out during the first year mooring.

The profile of the sea surface dynamic topography (SSDT) is also estimated on the basis of the absolute geostrophic velocities at the sea surface. An example is shown in Fig. 3a.

A scatter plot of the volume transport and the SSDT difference across the Kuroshio is shown in Fig. 4 for those 13 cases. The figure shows that the volume transport of the Kuroshio has a very tight relationship with the SSDT difference across the Kuroshio; their correlation coefficient (0.96) is very high, and the rms (root-mean-square) difference (4.3 Sv) from the regression line is fairly small. This relationship indicates that if the SSDT difference across the Kuroshio is observed, the absolute volume transport of the Kuroshio can be estimated fairly accurately. A similar significantly linear relationship was also found for the Kuroshio east of Taiwan in a numerical model (Johns *et al*., 1995).

This very tight relationship can be understood by examining the vertical profile of transport of the Kuroshio per unit depth. Estimated profiles for 13 cases fluctuate very much, but if the transport is normalized by the transport at the sea surface, those profiles are almost the same as shown in Fig. 5. Therefore their integrals (*i.e*., normalized total transports) are almost constant. Therefore, the total transport is almost proportional to the surface transport, which is directly related with the SSDT difference across the Kuroshio. In other words, the increase (or decrease) of the total transport results from an increase (or decrease) in not just some limited layers but all the layers of the Kuroshio.

Time series of transport

Altimetry data from TOPEX/POSEIDON were processed for the first 116 repeat cycles (of a 10-day repeat period) beginning in September 1992. The presently available geoid model is not accurate enough to be used with the altimetry data in order to estimate the absolute SSDT (deviation of the sea surface from the geoid). Therefore only anomalies from the temporal mean are usable in the altimetry data. In the present analysis, the above-mentioned SSDT profiles estimated from *in situ* data along the ASUKA line are combined with SSDT anomalies from altimetry data to obtain the mean SSDT profile; see Imawaki and Uchida (1995) for details. The sum of the mean field thus obtained and the anomalies from the altimetry data gives us the absolute SSDT profiles. Tide gauge data at the Cape Ashizuri are used to improve the SSDT profiles near the coast (Uchida and Imawaki, 1996), where the altimeter cannot work well.

SSDT differences across the Kuroshio can be estimated from those absolute SSDT profiles, and combined with the above-mentioned relationship between the transport and the SSDT difference, to provide us with a time series of the Kuroshio transport, having a sufficiently fine resolution (10-day intervals) for a fairly long period as far as the satellite operates. Fig. 6 shows an example of such results, a 3-year long time series for 1992–1995. Altimeter-derived transports agree very well with transports estimated from in

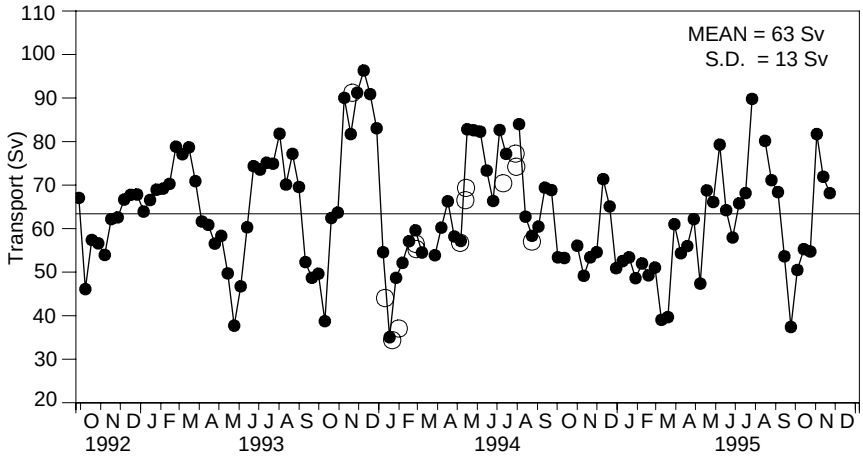

Figure 6. Time series of the absolute volume transport (solid line with dots; in Sv) of the Kuroshio through the ASUKA section during 1992–1995, estimated from TOPEX/POSEIDON altimetry data combined with the relationship (regression line in Fig. 4) between the transport and SSDT difference. The 3-year mean of the transport is estimated to be 63 Sv with a standard deviation of 13 Sv. Also shown are volume transports (circles) estimated from in situ data.

situ data. The volume transport of the Kuroshio fluctuates very much around an average of 63 Sv with a standard deviation of 13 Sv. An annual cycle (a seasonal cycle) is not apparent and fluctuations of shorter periods are dominant.

Discussions

The fluctuations of the Kuroshio transport estimated above may be associated with the fluctuations of the local stationary anticyclonic warm eddy located on the offshore side of the Kuroshio (Hasunuma and Yoshida, 1978). The present estimate of the Kuroshio transport obviously includes the eastward transport of the northern part of this eddy. Therefore the transport and its variability of the throughflow of the Kuroshio may be smaller than the transport estimated above. To observe this Kuroshio recirculation as well as the Kuroshio itself, the ASUKA line extends far beyond the Kuroshio (down to 25°N). Propagating cyclonic and anticyclonic mesoscale eddies are also very active in this region, and may introduce large fluctuations in the estimated transport. The transport of the Kuroshio recirculation (between the offshore edge of the Kuroshio and 26°N) is estimated tentatively in a similar way and subtracted from the above-estimated Kuroshio transport. The resulting time series of the transport of Kuroshio throughflow shows smaller fluctuations with no apparent seasonal signals. On the other hand, the recirculation transport due to occasional onshore-side cyclonic cold eddies has already been subtracted from the eastward transport including the Kuroshio.

Upward-looking ADCPs moored at CM2 and CM4 provided a very interesting record of flow field of the Kuroshio on the inshore edge; for example, very strong vertical shears of up to 10^{-2} sec^{-1} (100 cm/sec velocity difference in 100 m vertical interval) were observed. Those vertical shears will be compared carefully with geostrophic shears estimated from repeated hydrography data. Towed-ADCP observations provided vertical sections of upper layer velocity, describing fluctuations of the flow field of the strongest part of the Kuroshio. Most IESs provided good data, which are now under analysis. Those results will be published soon.

Acknowledgements

The repeat hydrography data were provided by K. Mimoto, K. Okuda, H. Yoritaka, H. Ichikawa, N. Yoshioka and M. Fukasawa. The TOPEX/POSEIDON altimetry data were provided by the Physical Oceanography Distributed Active Archive Center at the Jet Propulsion Laboratory, USA. This study is a part of activities of the International Cooperative Research Programme on Global Ocean Observing System sponsored by the Ministry of Education, Science, Sports and Culture, Japan.

References

Bryden, H.L., D.H. Roemmich, and J.A. Church, 1991: Ocean heat transport across 24°N in the Pacific. Deep-Sea Res., 38, 297–324.

Hasunuma, K., and K. Yoshida, 1978: Splitting of the subtropical gyre in the western North Pacific. J. Oceanogr. Soc. Japan, 34, 160–172.

Imawaki, S., and H. Uchida, 1995: Detecting sea level profiles across the Kuroshio by a satellite altimeter. Ann. Disaster Prevention Res. Inst., Kyoto Univ., 38B-2, 655–662 (in Japanese with English abstract).

Johns, W.E., T.N. Lee, C.-T. Liu, and D. Zhang, 1995: PCM-1 array monitors Kuroshio transport. WOCE Notes, 7(3), 10–13.

Kaneko, A., S. Mizuno, W. Koterayama, and R.L. Gordon, 1992: Cross-stream velocity structures and their downstream variation of the Kuroshio around Japan. Deep-Sea Res., 39, 1583–1594.

Mizuno, S., K. Kawatate, A. Kaneko, and T. Nagahama, 1991: Direct measurements of the Kuroshio in the East China Sea, Part 3. Bull. Res. Inst. for Applied Mechanics, Kyushu Univ., 71, 1–18 (in Japanese).

Takematsu, M., K. Kawatate, W. Koterayama, T. Suhara, and H. Mitsuyasu, 1986: Moored instrument observations in the Kuroshio south of Kyushu. J. Oceanogr. Soc. Japan, 42, 201–211.

Uchida, H., and S. Imawaki, 1996: Comparison of sea-level fluctuations off Shikoku derived from satellite altimeter and tide gauge. Bull. Res. Inst. for Applied Mechanics, Kyushu Univ., 80, 71–85 (in Japanese).

The Impact of Upper Ocean – Topographic Coupling on the Kuroshio Pathway South and East of Japan

Harley E. Hurlburt and E. Joseph Metzger, Naval Research Laboratory, Stennis Space Center; and Patrick J. Hogan, Sverdrup Technology, Inc., Stennis Space Center, USA.
hurlburt@nrlssc.navy.mil

Modelling the mean pathways of ocean currents has proven to be an exceptional challenge to ocean modellers in many cases, including the Kuroshio and the Gulf Stream. Simulating the pathways near the separation from the coast and their extensions into the ocean interior has been especially challenging. Here, we discuss the Kuroshio pathway using a set of simulations which have realistic coastline geometry and wind forcing, but which vary in nonlinearity, grid resolution and vertical structure.

Fig. 1 shows a whole domain snapshot of sea surface height (SSH) for 29 December 1995 from $\frac{1}{16}°$ Pacific simulation 16BT run using the Navy Layered Ocean Model (NLOM). The model is an isopycnal formulation with Lagrangian layers in the vertical, each with a prescribed constant density based on Levitus (1982). It is a descendent of the model by Hurlburt and Thompson (1980), but with expanded capability, including isopycnal outcropping and diapycnal mixing (Wallcraft, 1991). The model simulates the basic current systems and gyres. Eddies and meandering currents are ubiquitous. Compared to $\frac{1}{8}°$ counterparts, the $\frac{1}{16}°$ model shows the Kuroshio Extension (meandering along 32–37°N) and the subarctic front (40–46°N) as more sharply defined fronts that extend farther to the east. However, $\frac{1}{8}°$ resolution is sufficient for realistic simulation of the mean Kuroshio pathway south and east of Japan west of about 155°E (Hurlburt *et al.*, 1996).

Fig. 2 shows mean SSH in the NW Pacific from four simulations designed to demonstrate the impacts of nonlinearity, grid resolution and bottom topography. Fig. 2a shows results from linear simulation 4RGL, essentially a Munk (1950) solution done with realistic geometry and forced by the Hellerman and Rosenstein (1983) (HR) monthly wind stress climatology. The simulated Kuroshio Extension is associated with the winter time zero wind stress curl with maximum eastward flow along 33.5°N. However, the boundary between the subtropical and subarctic gyres is near 44°N at the western boundary, associated with the annual mean and April–September mean zero wind curl. Therefore, some of the western boundary current transport passes north of the Kuroshio Extension. In this simulation it does so in the form of flow through the Sea of Japan, which we constrained to reasonable values, and an unrealistic northward current along the east coast of Japan.

Simulations 4BT (Fig. 2b) and 8BT (Fig. 2c) are identical in design except for the horizontal grid resolution ($\frac{1}{4}°$ *vs* $\frac{1}{8}°$ for each variable) and the eddy viscosity, A. Simulations 8BT and 8FB (Fig. 2d) are identical except that 8FB has a flat bottom and 8BT has realistic bottom topography confined to the lowest layer. In all the simulations, flow is constrained to small values below the sill depth in straits. Comparing simulations 4BT and 8FB and focusing on the Kuroshio pathway south and east of Japan to about 150°E, where the simulations show a strong inertial character, one might arrive at the false conclusion that the bottom topography is

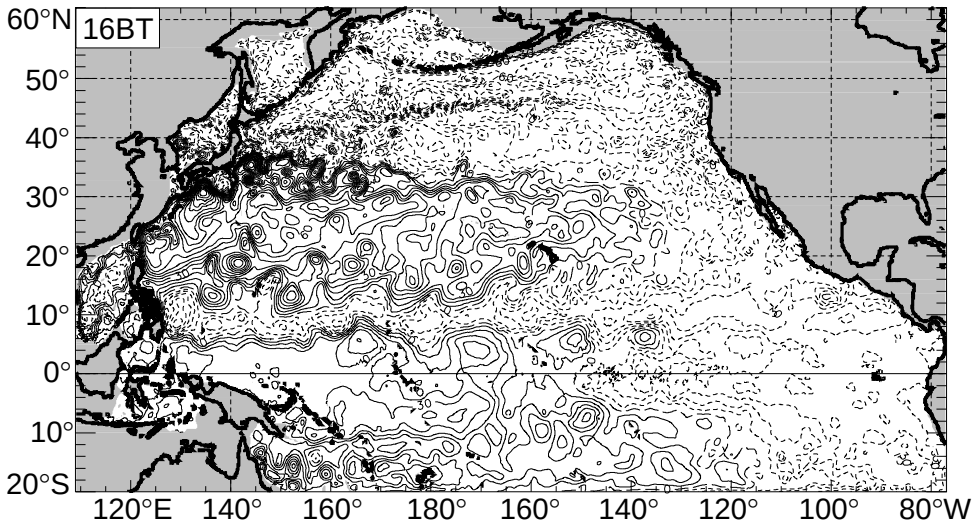

Figure 1. Whole domain snapshot of Sea Surface Height (SSH) for 29 December 1995 simulated by a Pacific Ocean model with $\frac{1}{16}°$ resolution for each variable ($\frac{1}{16}° \times \frac{45}{512}°$, lat. x long.), 6 layers, a free surface and realistic bottom topography. (Referred to as simulation 16BT here and as 16I2 by Hurlburt and Metzger, 1996). After spin-up to statistical equilibrium at progressively finer resolution using the Hellerman and Rosenstein (1983) (HR) monthly wind stress climatology, the model was run 1981–95 forced by 12 hourly European Centre for Medium-range Weather Forecasts (ECMWF) 1000 mb winds with the 1981–94 mean replaced by the annual mean from HR. The model boundary is the 200 m isobath except for a few shallow straits like those connecting to the Sea of Japan. The eddy viscosity is $A = 30\,m^2 s^{-1}$ The contour interval is 7.5 cm; long dashes mark the zero line and short-dashed contours are negative.

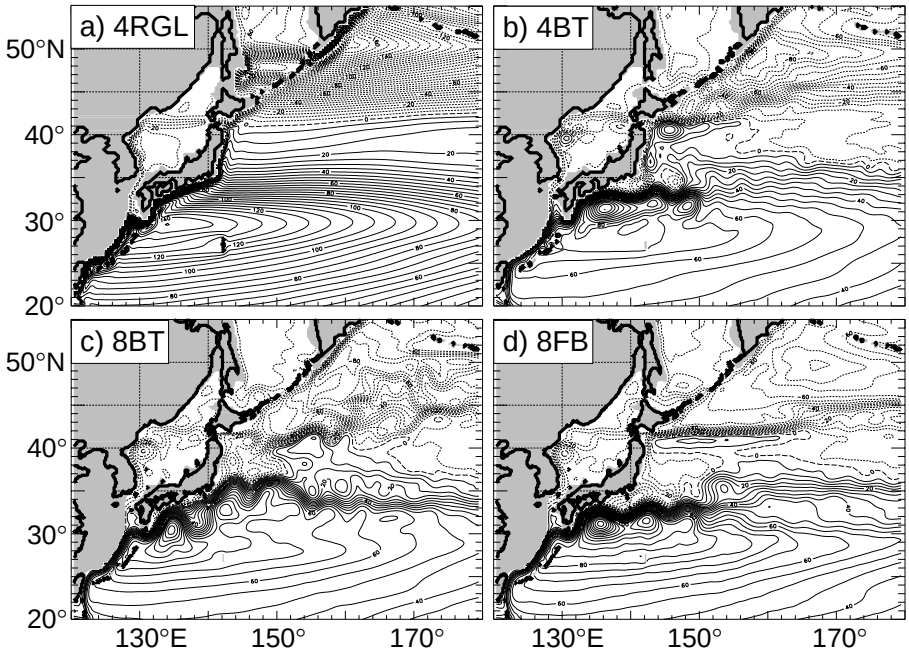

Figure 2. Mean SSH in the NW Pacific from 4 Pacific simulations north of 20°S. (a) ¼° 1.5 layer linear reduced gravity (lower layer infinitely deep and at rest), simulation 4RGL, (b) ¼° 6-layer nonlinear with realistic bottom topography, simulation 4BT, (c) ⅛° 6-layer nonlinear with realistic bottom topography, simulation 8BT and (d) ⅛° 6-layer nonlinear flat bottom, simulation 8FB. All were forced by the HR monthly wind stress climatology and all follow the design of simulation 16BT where appropriate. $A = 30\,m^2s^{-1}$ for the ¼° simulations and $100\,m^2s^{-1}$ for the ⅛° simulations. The contour interval is 5 cm. Simulations 4RGL, 8BT and 8FB are the same as simulations ¼° RG1.5f, BT6 and FB6, respectively in Hurlburt et al. (1996) and Fig. 2c is from that paper.

not important. In this region the simulated Kuroshio pathways are similar, including the latitude and the amplitudes and longitudes of the meander troughs and crests. In contrast, comparison of simulations 8BT and 8FB shows a large topographic impact with a 3° northward shift in the Kuroshio pathway east of Japan. This pathway is in much better agreement with the observations shown in Fig. 3.

Fig. 4 (page 23) is used to illustrate some of the dynamics of the topographic impact in the Kuroshio Extension region east of Japan. In essence, the Kuroshio Extension exhibits a mixed baroclinic-barotropic instability which transfers energy to the abyssal layer. The abyssal flow is constrained by the f/h (Coriolis parameter/depth) contours of the bottom topography (Fig. 4a). In turn, the abyssal flow can steer the upper ocean currents (Fig. 4b,c). Steering dynamics are discussed by Hurlburt *et al.* (1996). Even fairly small, low amplitude topographic features can show a substantial effect in steering the upper ocean currents (Fig. 4). In particular, a modest seamount chain east of the trench and along 144°E appears to play a major role in increasing the latitude of the Kuroshio east of Japan. In the ¼° model (Fig. 4c), the flow instabilities, abyssal currents, and abyssal eddy kinetic

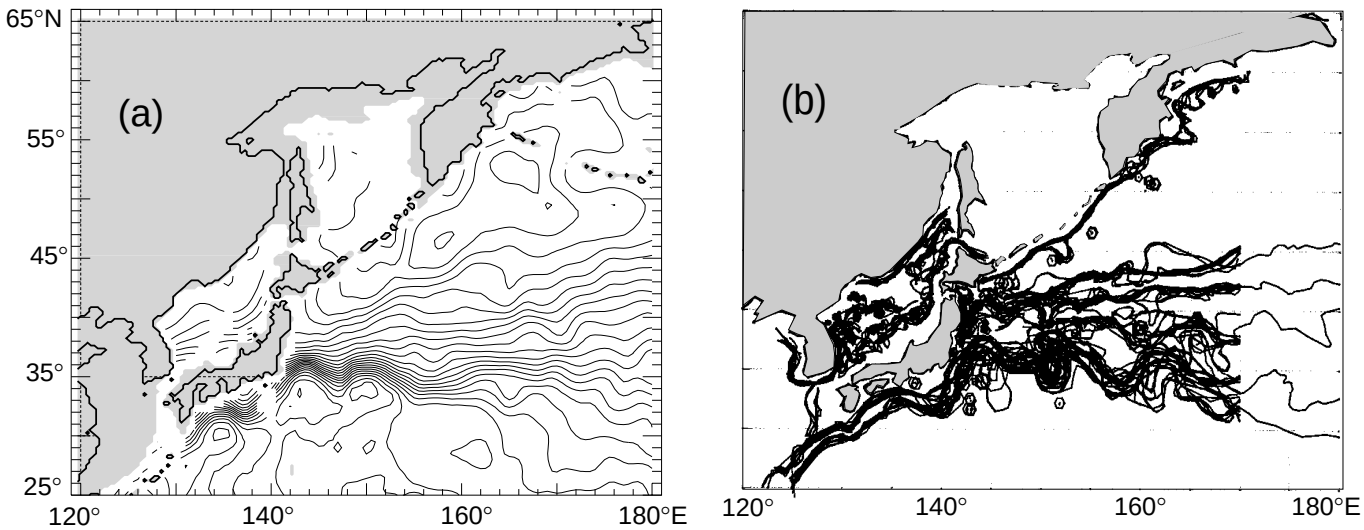

Figure 3. (a) Mean surface dynamic height relative to 1000 m from the US Navy's Generalized Digital Environmental Model (GDEM) oceanic climatology (Teague et al., 1990); contour interval is 5 cm. (From Hurlburt et al., 1996) (b) Composite of oceanic frontal analyses in the NW Pacific from satellite infrared measurements. It covers 10 April–19 July 1991 at ~3-day intervals. From 170° to 180°E, only one analysis is plotted, showing the five frontal boundaries plotted east of Japan. From north to south they are the northern and southern boundaries of the Oyashio/subarctic front, a transition front, and the northern and southern boundaries of the Kuroshio Extension. (Courtesy of Dale Ordish, Naval Oceanographic Office, Stennis Space Center, MS, USA). Adapted from Hurlburt et al. (1992).

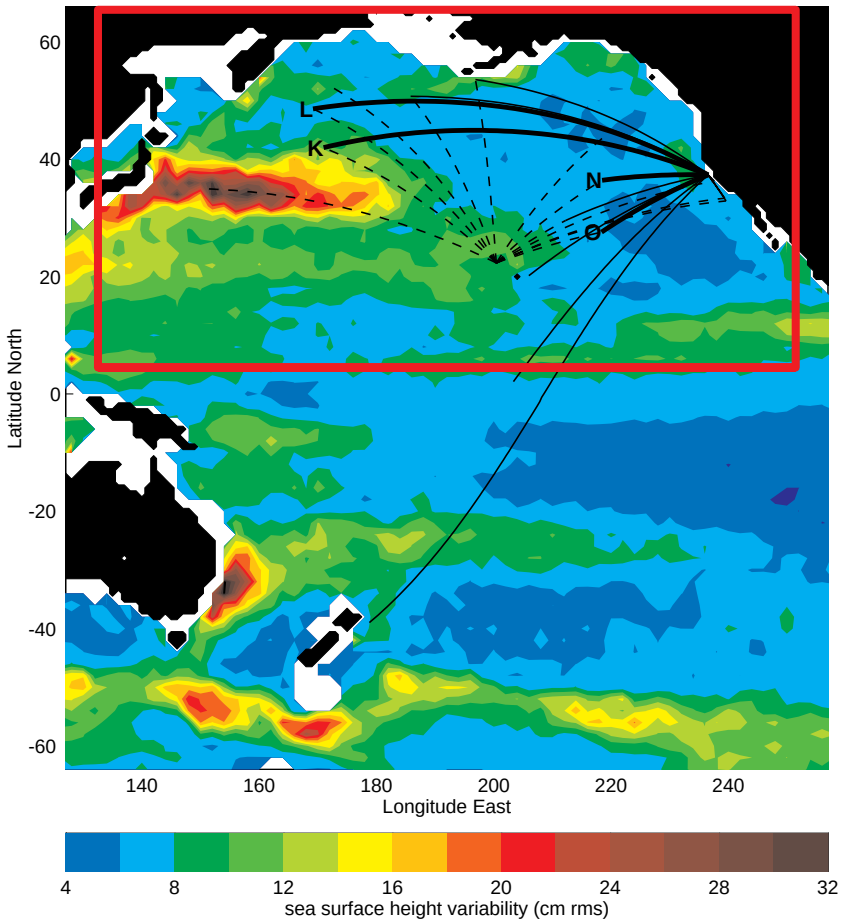

Menemenlis et al., page 7, Figure 1. *Sea surface height variability, in cm rms, measured by the TOPEX/POSEIDON altimeter for the period 21 November 1992 – 17 November 1995. The solid lines indicate the present coverage of the Acoustic Thermometry of Ocean Climate (ATOC) array using a single acoustic source near the California coast in operation since January 1996. The paths shown in dashed lines represent the increased coverage that will result from the installation of a second source near Hawaii in early 1997. The present study is of the region enclosed by the red rectangle and is based on a preliminary analysis of acoustic data from paths K, L, N, and O (bold lines).*

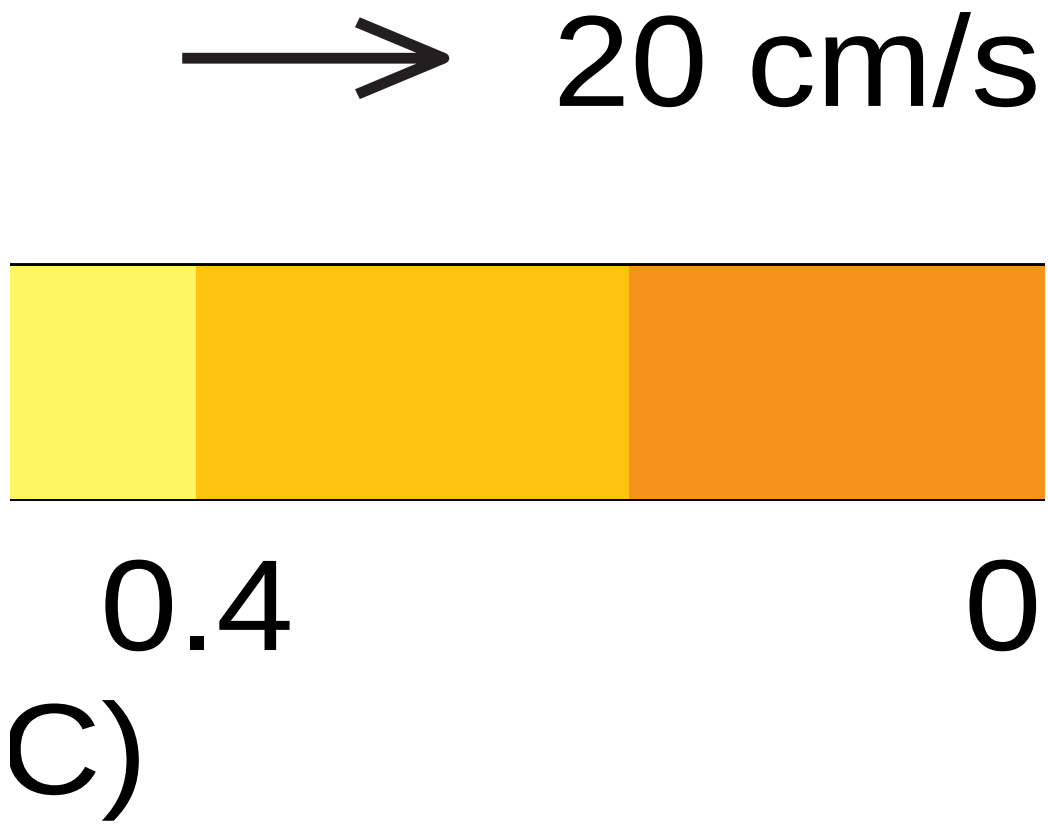

Menemenlis et al., page 7, Figure 5. *Temporal change of depth (0–1000 m) averaged potential temperature from 16 January to 16 July 1996. Also shown is the corresponding change in horizontal surface velocity below the Ekman layer. These estimates are consistent with the OGCM, the satellite altimetry, and the acoustic tomography.*

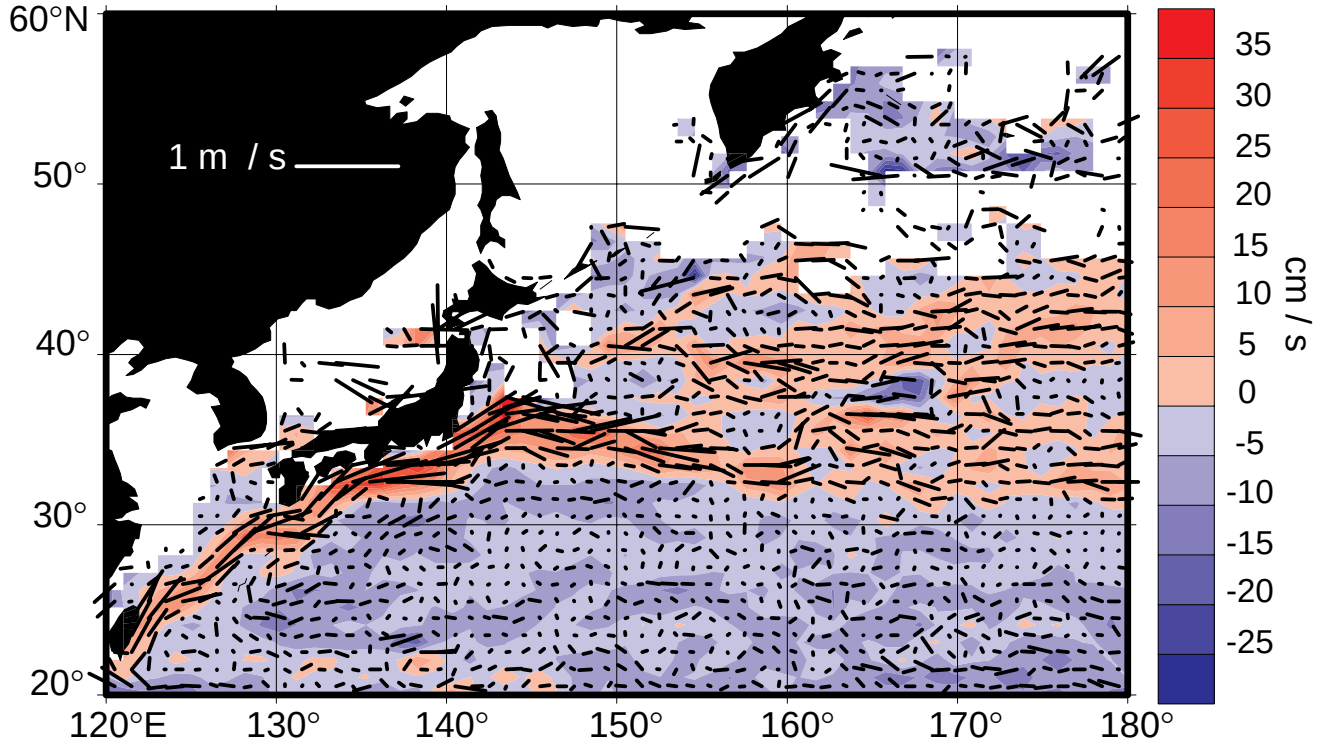

Maximenko et al., page 13, Figure 1. *Mean near-surface velocity vector field superimposed on the colour contour of their zonal component.*

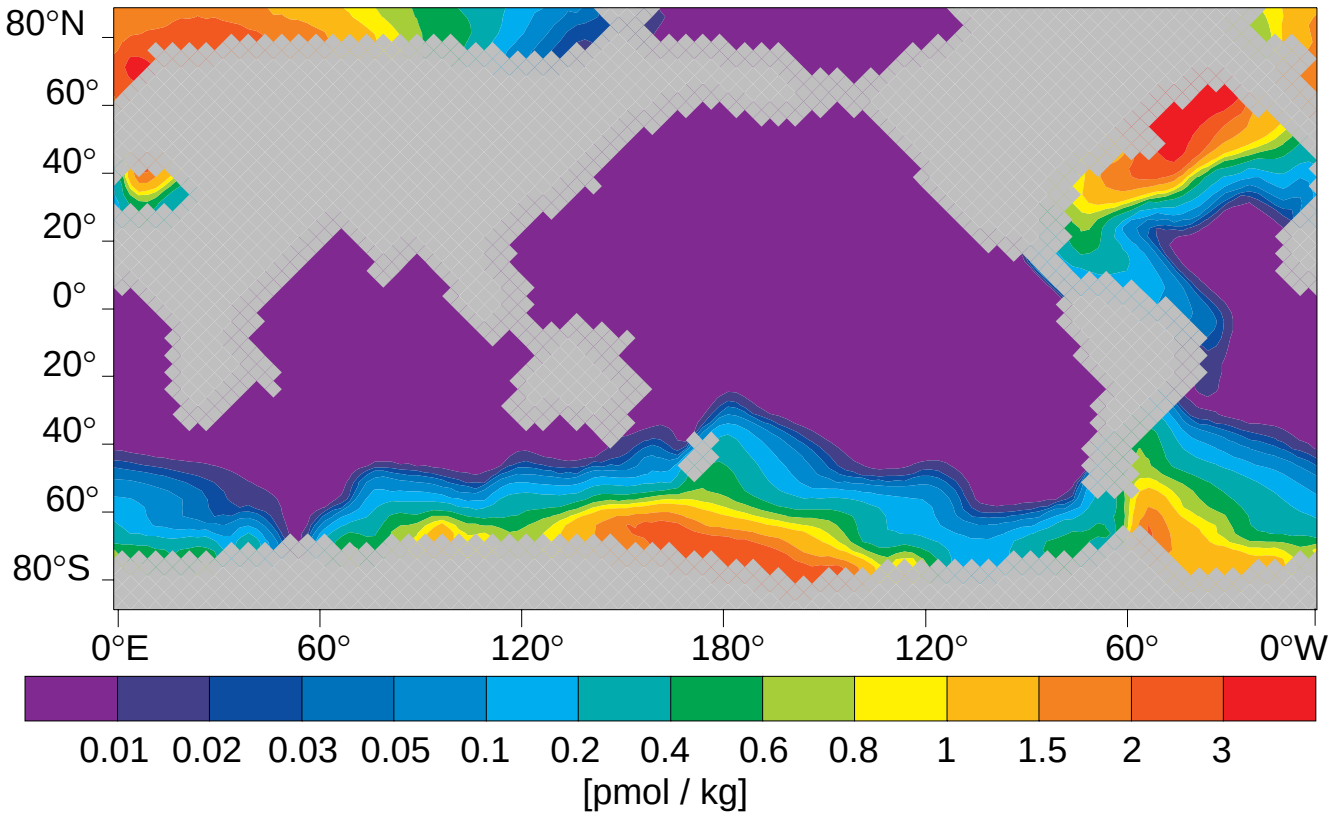

Heinze and Maier-Reimer, page 38, *Figure 1. CFC-11 for December 1991 in 2370 m depth as modelled with the velocity field of the LSG-OGCM.*

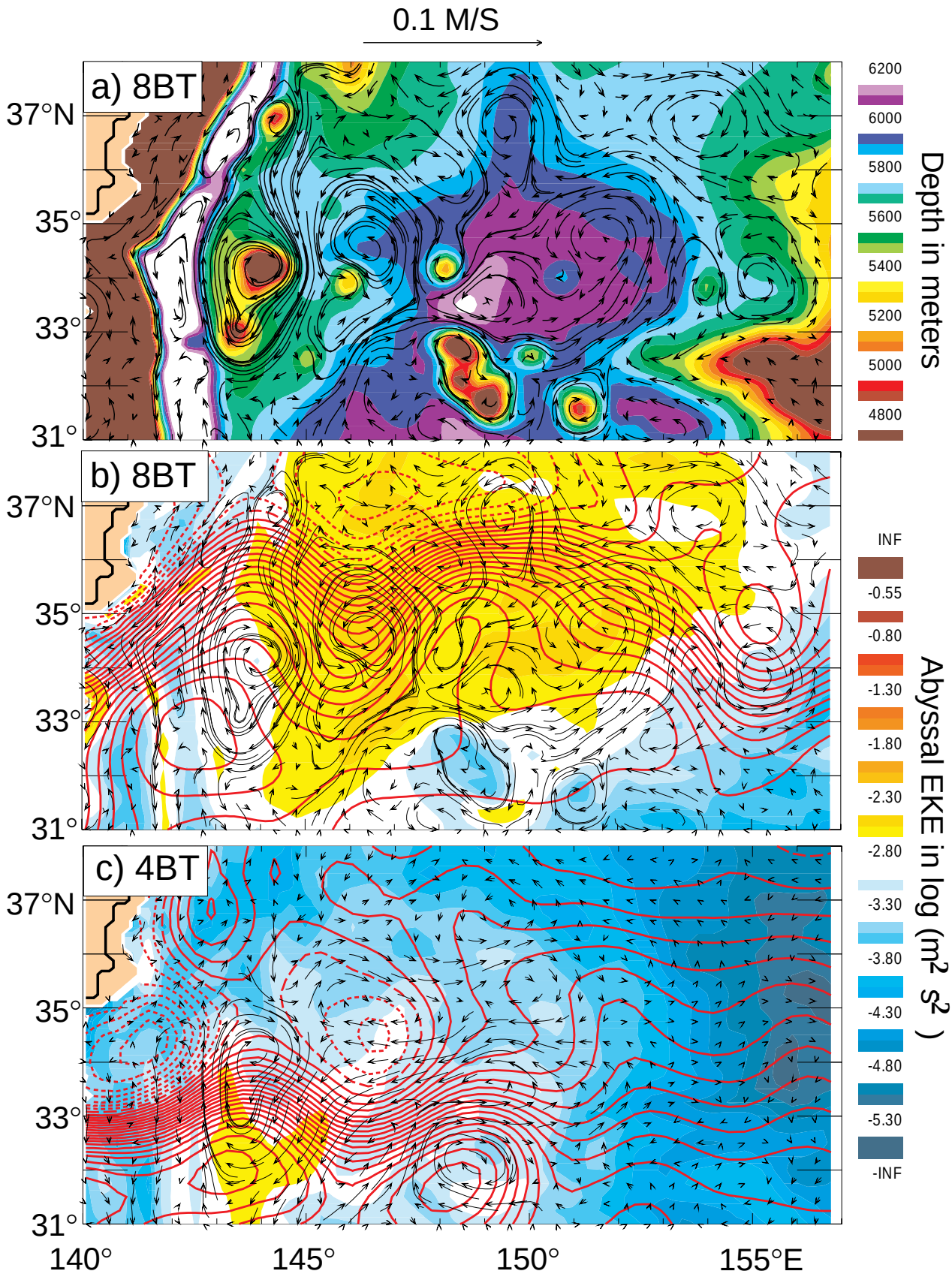

Hurlburt et al., page 19, Figure 4. *Results for the Kuroshio Extension region just east of Japan, which is seen in the NW corner of each plot. (a) Mean abyssal currents from simulation 8BT overlaying the bottom topography. (b,c) Mean abyssal currents (arrows) overlaying mean SSH (red contours with a 5 cm interval) and abyssal EKE (shades of color) for simulations (b) 8BT and (c) 4BT.*

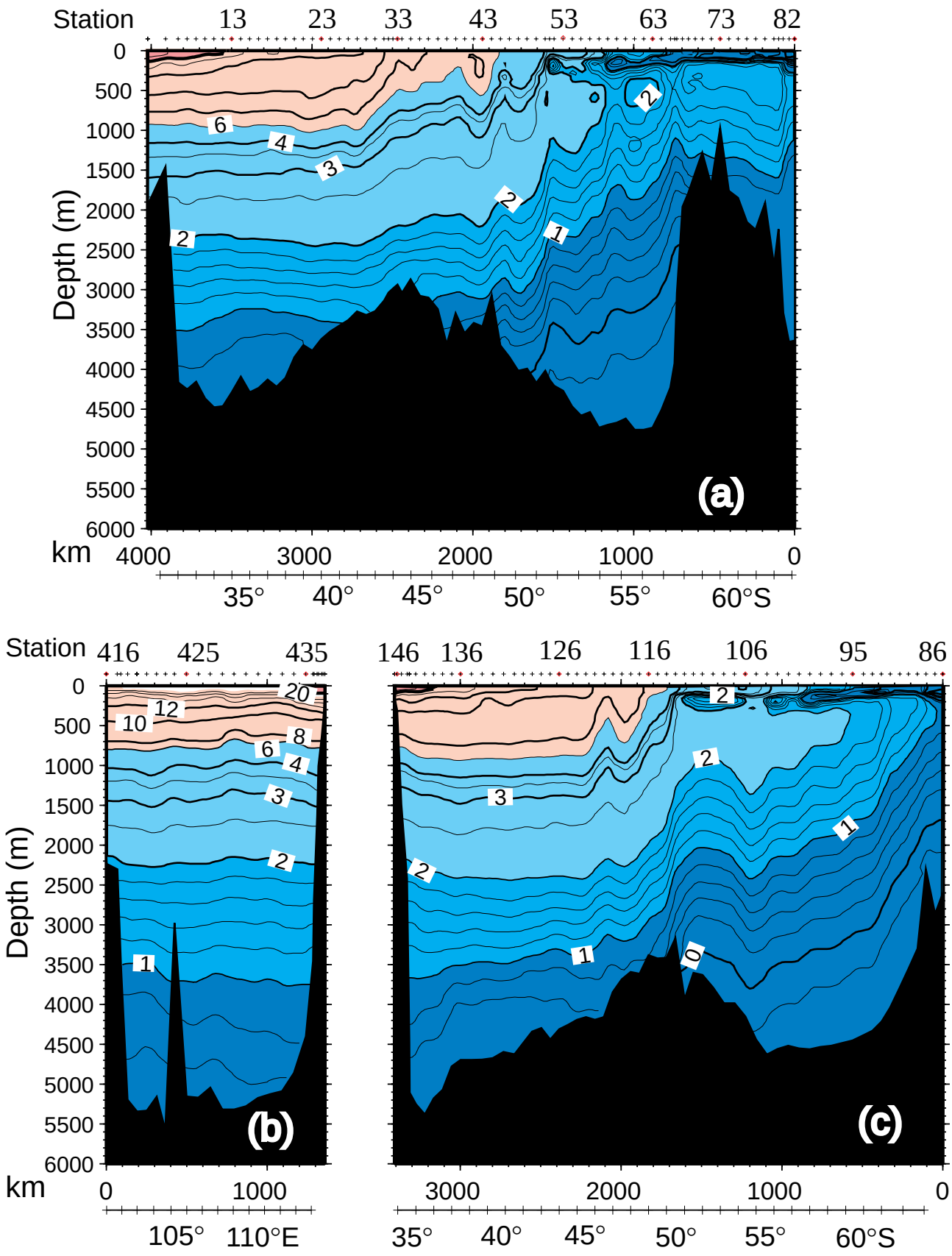

Hufford and McCartney, page 31, Figure 3. *Potential temperature cross sections: (a) WHP segment I8S; (b) a portion of WHP segment I8N5E; and (c) WHP segment I9S.*

energy (EKE) are much weaker and hence the upper ocean – topographic coupling via the flow instabilities is weaker and insufficient to produce a realistic Kuroshio pathway east of Japan. The mean abyssal currents in simulation 8BT are mostly consistent with current meter measurements from the Kuroshio Extension Regional Experiment (WOCE line PCM7) (Hallock and Teague, 1996), including a southward deep western boundary current on the west side of the trench.

In general, we are finding an increasingly wide spread importance of mesoscale flow instabilities in allowing bottom topography to steer upper ocean currents, as the horizontal resolution of the model is increased. This upper ocean – topographic coupling requires that mesoscale variability be very well resolved to obtain sufficient coupling. Thus, this topographic effect is missed at coarser resolution, and can lead to false conclusions about the role of topography, and unexplained errors in simulations of the mean pathways of ocean currents, such as the Gulf Stream and Kuroshio. For example, Hurlburt and Metzger (1996) find that $\frac{1}{16}^\circ$ resolution is required to obtain sufficient coupling to simulate the bifurcation of the Kuroshio at the Shatsky Rise and the pathway of the northern branch connecting to the subarctic front. Additional discussion of this modelling effort on the Kuroshio/Oyashio current system can be found in Hurlburt *et al*. (1996), including the Kuroshio meander south of Japan. A recent overview can be found in LeBlond and Endoh (1996).

Acknowledgements

This research was funded by the US Office of Naval Research under program elements 61153N and 62435N with the Kuroshio Extension Regional Experiment as the lead project. Computer time was provided in part under grants from the US Defense Department High Performance Computing initiative. Additional computer time was used at the US Naval Oceanographic Office, Stennis Space Center, MS, the University of Alaska, Fairbanks, Alaska and Fleet Numerical Oceanography Center, Monterey, CA. We thank Jan Dastugue for her work on Fig. 3.

References

Hallock, Z.R., and W.J. Teague, 1996: Evidence for a North Pacific Deep Western Boundary Current. J. Geophys. Res., 101, 6617-6624.

Hellerman, S., and M. Rosenstein, 1983: Normal monthly wind stress over the world ocean with error estimates. J. Phys. Oceanogr., 13, 1093-1104.

Hurlburt, H.E., and E.J. Metzger, 1996: Bifurcation of the Kuroshio Extension at the Shatsky Rise. J. Geophys. Res. (submitted)

Hurlburt, H.E. and J.D. Thompson, 1980: A numerical study of Loop Current intrusions and eddy-shedding. J. Phys. Oceanogr., 10, 1611-1651.

Hurlburt, H.E., A.J. Wallcraft, Z. Sirkes, and E.J. Metzger, 1992: Modeling of the Global and Pacific Oceans: On the path to eddy-resolving ocean prediction. Oceanography, 5, 9–18.

Hurlburt, H.E., A.J. Wallcraft, W.J. Schmitz Jr., P.J. Hogan, and E.J. Metzger, 1996: Dynamics of the Kuroshio/Oyashio current system using eddy-resolving models of the North Pacific Ocean. J. Geophys. Res., 101, 941–976.

LeBlond, P.H., and M. Endoh, ed., 1996: Modelling of the subarctic North Pacific circulation. PICES Scientific Report No. 5. Institute of Ocean Sciences, Sidney, B.C., Canada, 91pp.

Levitus, S., 1982: Climatological atlas of the world ocean. NOAA Prof. Pap. 13, US Govt. Print. Off., Washington, D.C., 173pp.

Munk, W.H., 1950: On the wind-driven ocean circulation. J. Meteorol., 7, 79–93.

Teague, W.J., M.J. Carron, and P.J. Hogan, 1990: A comparison between the Generalized Digital Environmental Model and Levitus climatologies. J. Geophys. Res., 95, 7167–7183.

Wallcraft, A.J., 1991: The Navy Layered Ocean Model users guide. NOARL Rep. 35, Nav. Oceanogr. and Atmos. Res. Lab., Stennis Space Center, MS, 21pp.

"OCEAN CIRCULATION AND CLIMATE"

The WOCE Conference
Halifax World Trade and Convention Centre
Halifax, Nova Scotia, Canada
Sunday, 24 May –Friday, 29 May 1998

Format: Morning sessions will be devoted to plenary talks by invited speakers. Topics of these talks will largely focus on progress that we have made towards achieving the original goals of WOCE but will also explore the remaining challenges. In order to permit the widest possible representation of WOCE research and to use this to stimulate interaction and discussion, afternoons will be devoted to poster sessions. Posters will be on display throughout the week but attention will be drawn on each afternoon to those that relate to the morning's plenary theme.

Provisional Timetable: A first announcement and call for initial expressions of interest in the conference will be issued early in 1997. It is expected that the main announcement and call for registrations will be in summer 1997 at which time a full list of plenary talks will be confirmed. The deadline for poster abstract submissions will be mid-February 1998 with confirmation of acceptance by mid-March 1998.

Scientific Organising Committee: Gerold Siedler (Chair), Trevor MacDougall (Vice-Chair), Nobuo Suginohara, Carl Wunsch, Bernard Barnier, Allyn Clarke (Representing the Local Organising Committee); John Gould and Andrea Frische (WOCE IPO).

Sponsors: The Conference will be co-Sponsored by WOCE's parent organisations – **WCRP, IOC, WMO and ICSU (SCOR) –** and will be co-hosted in Canada by **the Department of Fisheries and Oceans and by the Canadian Meteorology and Oceanography Society (CMOS).** Commercial sponsorship and support will be sought.

Further Information and enquiries: Please contact the WOCE IPO.

The North Pacific Intermediate Salinity Minima Along WHP P2

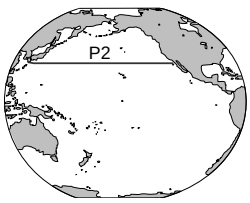

Ayako Nishina and Masao Fukasawa, Tokai University, Japan; Ichiro Yasuda, Hokkaido University, Japan; and Hiroyuki Yoritaka, Japan Marine Science and Technology Center, Japan, nishina@scc.u-tokai.ac.jp

In the sub-arctic North Pacific, fresher surface waters compared to those in other oceans, prevent subduction to deep layers, forcing the water to remain at mid depths. The North Pacific Intermediate Water (NPIW) is a well-known water mass in the North Pacific, characterized by its salinity minimum at the intermediate depths in the sub-tropical North Pacific (Reid, 1965). Reid defined the intermediate salinity minimum as the core of a water mass whose specific volume anomaly is 125 cl/ton (equivalent to potential density $26.8\,kg/m^3$). On the other hand, Hasunuma (1978) regarded NPIW not as a water mass but merely as the interface between deeper sub-polar water and shallower sub-tropical water in the western sub-tropical North Pacific. Hasunuma's conclusion is noteworthy because no dominant pycnostad is associated with the intermediate salinity minimum in most of the North Pacific. However in the western-most region of the North Pacific, the intermediate salinity minimum layer is so thick that a pycnostad can be observed being associated with the salinity minimum. Recent studies (Talley, 1993; Yasuda *et al*., 1996) may have re-defined NPIW in these western regions. They examined CTD data and suggested that NPIW is formed around the western Disturbed Area as a mixture of the sub-tropical water and the sub-polar water which originally comes from the Sea of Okhotsk.

Nishina *et al*. (1996) checked the characteristics of the intermediate salinity minimum water using CTD data collected during Kaiyo-maru P2 (30°N) and Pre-P2* (32.5°N) surveys. They found that the dissolved oxygen and salinity on the intermediate salinity minimum and the dominant zonal scale of fluctuations of these values in the area west of 160°W were remarkably different from those east of 160°W. They pointed out the possibility that the intermediate salinity minimum water is not NPIW east of 160°W. Fukasawa *et al*. (1996) showed that more than 15 Sv of water flows northward across 30°N in depths shallower than 800 m, but only 5 Sv of NPIW is estimated to be transported into the Sub-tropical Gyre through the Disturbed Area (Fukasawa, 1992). This large transport difference may suggest that the Sea of Okhotsk is not the only place where surface overturning takes place.

In this report, characteristics of intermediate salinity minimum water are re-examined using the whole P2 CTD data and the NOPACCS** CTD data (NOPACCS, 1995) to improve the hypothesis proposed by Nishina *et al*. (1996).

Data and analysis

WHP P2 line is located along 30°N but bends northward to run perpendicular to the coast in the Kuroshio and the California Current regions. There were two types of observation along P2. One was carried out on board Kaiyo-maru (Japan Fisheries Agency, 7 January–10 February 1994) and the other on board Shoyo (Hydrographic Department Maritime Safety Agency, 14 October–27 November 1993) and Bosei-maru (Tokai University, 20 January–3 February 1994). The former focused on water sampling for the chemical tracer analysis for 62 stations. The latter had CTD lowerings at 151 much closer spaced (about 65 km interval) stations. Since the quality control of P2 CTD data is not yet complete. We used CTD data after personal quality control of CTD and bottle data by the PIs.

CTD data analyzed here are from P2 and NOPACCS along 30°N and 175°E, respectively (Fig. 1). The coarse data set collected by Kaiyo-maru cruise will be referred to as P2K. The data set collected by the Bosei-maru cruise and Shoyo cruise will be collectively be referred to as P2S.

The computation of the neutral surface is started from

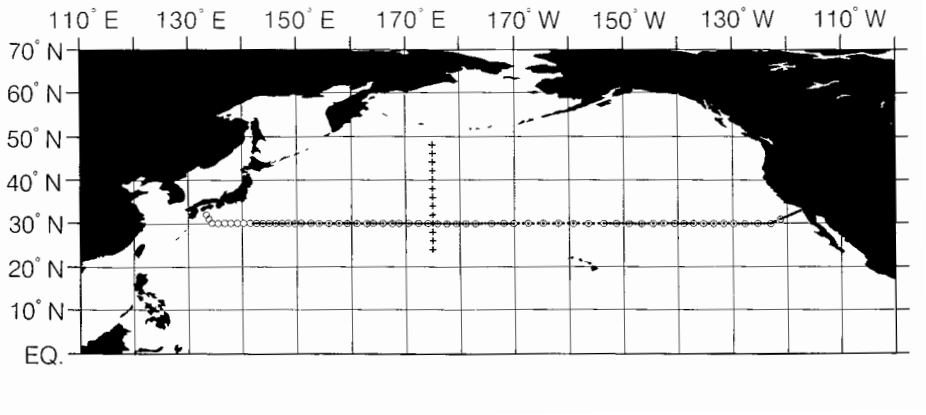

Figure 1. Location of CTD stations for P2 and NOPACCS along 30°N and 175°E, respectively. Circles denote Kaiyo-maru stations 7 January–10 February 1994. Dots denote Shoyo and Bosei-maru stations occupied 14 October–27 November 1993 and 20 January–3 February 1994. + denotes NOPACCS stations occupied during 10 August–25 September 1995.

*Pre-P2: The CTD line, planned under WOCE and occupied from 12 August to 16 September 1992 was along 32.5°N from 140°N to 158°W.

**NPOACCS (Northwest Pacific Carbon Cycle Study): The CTDs occupied by Hakurei-maru from 9 August to 1 October 1995 were along 175°E from 24°N to 48°N. Station intervals were 220 km.

the depth of the salinity minimum at 32°N using NOPACCS CTD data. Then it is computed zonally using P2 CTD data.

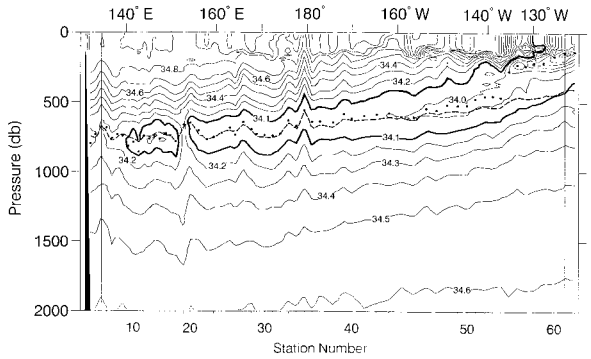

Figure 2. Salinity cross-section using Kaiyo-maru data. Dot denotes the intermediate salinity minimum at each station. The dashed line indicates the isopycnal of potential density of 26.8 (kg/m^3).

Results

Fig. 2 shows the salinity cross-section along P2K. The salinity minimum at depths shallower than 1000 m is denoted by a dot at each station. Of these salinity minima, those located east of 130°W are the Shallow Salinity Minima (Yuan and Talley, 1992) and those located west of 130°W are the intermediate salinity minima (ISM) regarded historically as North Pacific Intermediate Water (NPIW). ISM is a dominant structure common to most P2 stations however the values of salinity are low (below 34.0) between 145°E and 150°E and east of 160°W. The broken line in Fig. 2 indicates the potential density isopycnal $26.8\,kg/m^3$ of characteristic of NPIW. The broken line coincides with ISM west of the Date Line but east of the Date Line the ISM is mostly found at shallower depths. It seems that the salinity on the isopycnal surface gradually increases eastwards. This feature cannot be identified in standard depth hydrocasts or widely-spaced CTD observations. In fact, it is difficult to find any spatial density structure on ISM along 30°N even in a refined figure of Talley (1993).

Salinity, potential density and dissolved oxygen (only for P2K) on ISM along P2S and P2K are shown in Figs. 3 and 4, respectively. In both figures, steep salinity peaks

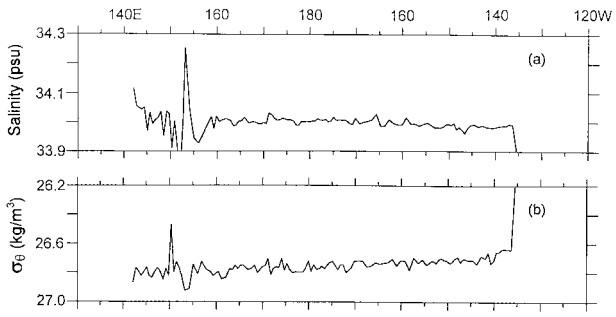

Figure 3. (a) Salinity and (b) potential density (kg/m^3) on the ISM layer defined using Shoyo/Bosei-maru data.

were found around 153°E (Figs. 3a and 4a). East of these peaks, salinity values of ISM are almost uniform although smaller amplitude mesoscale fluctuations are observed. The same pattern is also found in the potential density (Figs. 3b and 4b). The most interesting feature in Figs. 3a and 4a is that the salinity of ISM is lower east of 160°W than west of 160°W. Although dissolved oxygen data are available only for P2K (Fig. 4c), low oxygen ISM is observed between 160°W and 140°W with an oxygen front (0.5 ml/l in 400 km zonally) around 163°W. The potential density shows a tendency to decrease going east over the whole section (Figs. 3b and 4b).

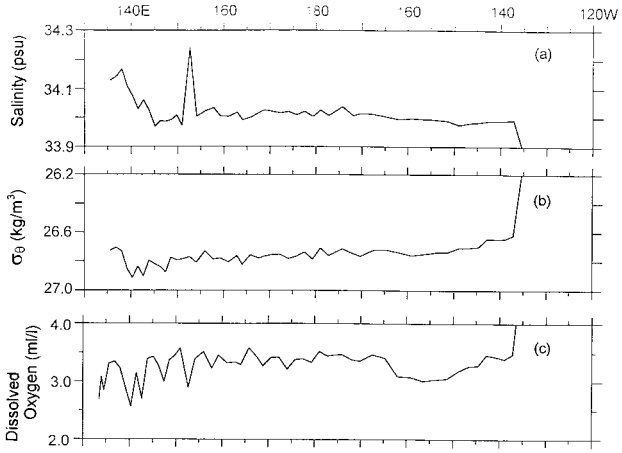

Figure 4. (a) Salinity, (b) potential density (kg/m^3) and (c) dissolved oxygen (ml/l) on the ISM layer defined using Kaiyo-maru data.

Fig. 5a shows salinity on ISM (solid line) and on a neutral surface (NS) (dotted line). The potential density on ISM and on NS are shown in Fig. 5b. The computation of NS was started from ISM at 32°N. In Fig. 5a, a discrepancy is seen between the salinity on ISM and that on NS north of 38°N and south of 28°N. The discrepancy becomes much larger as one goes northward beyond 42°N. Such tendency as seen in Fig. 5a is clearer in Fig. 5b.

ISM is safely regarded as NS within the region between 38°N and 30°N along the meridian of 175°E. This means that P2 is located near the southern boundary of a "real" NPIW and that there is a large possibility to observe ISM which do not coincide with NS originating from the "real" NPIW***.

Difference between the depths of ISM and NS is shown in Fig. 6 for P2K. NS was computed from the ISM located at 32°N, 175°E. In Fig. 6, one sees a clear tendency for NS to be deeper than ISM as it goes east. West of 160°E, the tendency mentioned above is weaker than east of 160°E. As a result the "real" NPIW, which is observed in NOPACCS data, is found within the region between 150°E and the Date Line in P2K. In the region east of 160°E, NS

***The term "real" NPIW means ISM where the density-salinity relation shown by Talley (1993) and Yasuda et *al.* (1996) in the Disturbed Area is observed.

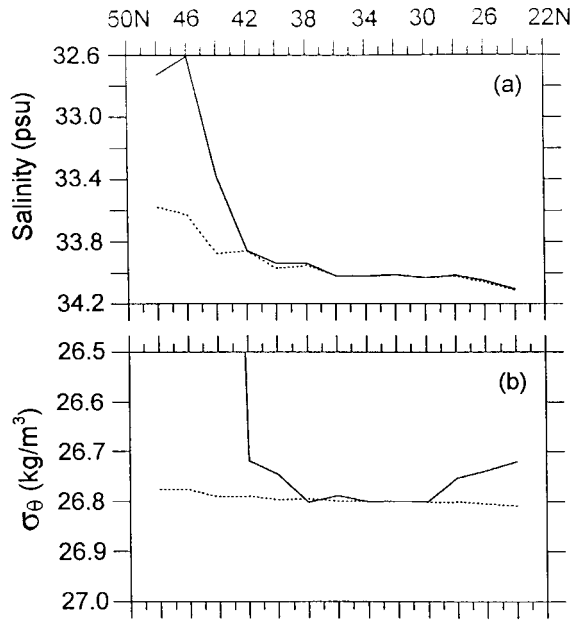

Figure 5. (a) Salinity and (b) potential density (kg/m^3) on the ISM layer (solid lines) and those on the neutral surface (dotted lines) defined using NOPACCS data.

goes significantly deeper. It is strongly suggested that ISM in this region is composed of some water mass other than NPIW based on the ISM property plots. Between the Date Line and 160°E, NS is deeper than ISM. This region almost coincides with that bounded by cores of southward flow in (Fukasawa, 1992).

Conclusion and remarks

We conclude that NPIW, which is suggested to be formed in the Disturbed Area by Talley (1993) and Yasuda *et al.* (1996), is confined to the region west of 160°W. Along 175E, NPIW is found only between 30°N and 38°N. East of 160°W, the intermediate salinity minimum seems to be embedded in a water mass other than NPIW at least along 30°N. We cannot yet identify the origin of that water. But, if sub-polar water with larger potential density (e.g.> $26.8\,kg/m^3$) intrudes into the eastern Pacific as Chen and Dewar (1993) suggest, it is possible that a thin and sharp intermediate salinity minimum, as observed in the eastern North Pacific, is formed at the vertical boundary between the lighter sub-tropical water and the heavier sub-polar water.

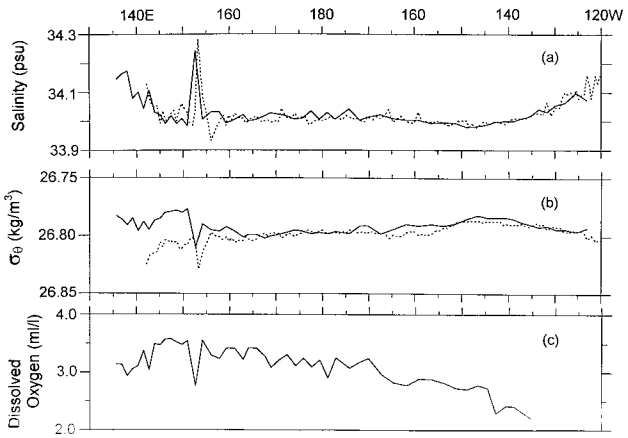

Figure 6. Depth difference between the ISM and the neutral surface computed using Kaiyo-maru data. The neutral surface computation was started from the NOPACCS ISM at 32°N, 175°E.

Acknowledgement

We would like to express our heartfelt thanks to all participants in P2 cruises for their cooperation. We are also indebted to Dr Kou Harada for his help during the NOPACCS cruise.

References

Chen, L.G., and W. Dewar, 1993: Intergyre Communication in a Three-Layer Model. J. Phys. Oceanogr., 23, 855–878.

Fukasawa, M., 1992: Large-Scale Ocean Circulation (in Japanese). Iwanami kagaku., 62,616–624.

Fukasawa, M., H. Yoritaka, and I. Yasuda, 1996: Heat and Mass Transport across 30°N in the North Pacific. In preparation.

Hasunuma, K., 1978: Formation of the Intermediate Salinity minimum in the North Western Pacific Ocean. Bull. Ocean Res. Inst. Univ. Tokyo, 9, 1–47.

Nishina, A., M. Fukasawa, K. Okuda, I. Yasuda, T. Bando, H. Yoritaka, and Y. Sugimori, 1996: Regional Characteristics of the North Pacific Intermediate Salinity Minimum (in Japanese with English abstract and figure caption). Journal of the School of Marine Science and Technology, Tokai Univ., 42, 1–11.

NOPACCS, 1995: Preliminary cruise report.

Reid, J.L., 1965: Intermediate waters of the Pacific Ocean. The Johns Hopkins Oceanographic Studies, 2, 85pp.

Talley, L.D., 1993: Distribution and Formation of North Pacific Intermediate Water. J. Phys. Oceanogr., 23, 517–537.

Yasuda, I., K. Okuda, and Y. Shimizu, 1996: Distribution and Modification of North Pacific Intermediate Water in the Kuroshio-Oyashio Interfrontal Zone. J. Phys. Oceanogr., 26, 448–465.

Can One Estimate the Oceanic Seasonal Baroclinic Heat Transport from Climatological Hydrography?

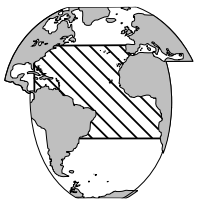

S. Wacongne and L. Crosnier, Labororatoire Physique des Océans (U.M.R.CNRS/IFREMER/UBO), Univ. Bretagne Occidentale, Brest, France.
Sophie.Wacogne@deneb.univ-brest.fr

Motivation

By "baroclinic heat transport" (BHT), we mean the contribution of the baroclinic geostrophic field to the heat transport, computed as in Hall and Bryden (1982). At each station pair, a geostrophic velocity v' is computed relative to a level insuring $\int v'\,dz = 0$, the potential temperature θ is split into its vertical average and the residual θ', and the BHT is obtained as $\rho c_p \int\int \theta' v'\,dx\,dz$, with $\rho c_p = 4.09 \times 10^6\ J\,m^{-3}\,K^{-1}$. Plotting θ', v' and their product as a function of longitude and depth, followed by the zonal accumulation of $\int \theta' v'\,dz$ as a function of longitude (not shown) clearly illustrates that the final integral depends essentially on the zonal structure of v' in the surface layer. The advantage of this decomposition is that the value obtained does not depend on any *a priori* choice of reference levels. It can therefore be viewed as an integral measure of the density field.

For the BHT to vary, the zonal structure of the upper density field (*i.e*. the zonal slope of the shallow isopycnals) must vary. This is likely to happen on a seasonal time scale at low latitudes where baroclinic waves are fast, less and less likely as one moves toward higher latitudes where baroclinic waves become increasingly slower. Except close to the equator then, the BHT computed from a single synoptic hydrographic section is usually considered as an estimate of the mean state, and changes between different occupations of the same section as estimates of interannual variability. Just how far from the equator one can stop worrying about the BHT varying seasonally and possibly aliassing estimates of interannual variability at one section, or estimates of the heat budget between two non synoptic sections, is unclear. The aim of this work is to investigate to which extent existing climatologies are able to resolve the BHT and whether or not they can be used to study its seasonal variability. Prior attempts are not very encouraging: Molinari *et al.* (1990) used Levitus's (1982) climatology to compute the annual cycle of BHT at 26.5°N in the Atlantic and found for the seasonal variation an amplitude of 0.5 PW ($1PW = 10^{15}\,W$), a surprisingly large value for a section at mid-latitude; the signal, however, varied by about as much from month to month. We have used the climatologies of temperature and salinity built by Levitus (1982), Levitus *et al*. (1994), Lozier *et al*. (1995), Reynaud *et al*. (1996) and will refer to them as LEV82, LEV94, LOC95 and REY96 respectively. Fields are monthly and seasonal in LEV82 and LEV94, seasonal in REY96 and annual in LOC95. The main originality of the 2 latest climatologies compared to the previous ones lies in that Lozier *et al*. average in density classes and that Reynaud *et al.* increase the vertical resolution and use influence radii that vary with topography.

In the era of WOCE high resolution "flux lines", it may seem preposterous to expect much from low resolution spatially and temporally smoothed climatological sections. Spatial smoothing, for instance, is expected to cause problems in regions of sharp unilateral gradients such as the western boundary. In the interior, however, smoothing sharp bilateral gradients such as those associated with geostrophic eddies or meanders matters less, since one side of the gradient cancels the other as one integrates through (see the cumulated BHTs from high resolution synoptic sections on Fig. 2b,d below). What matters is to capture the large scale interior gradients (and their seasonal changes). A smooth climatology may well be able to do that. Finally the exercise provides, if nothing else, a good way to assess and intercompare different climatologies.

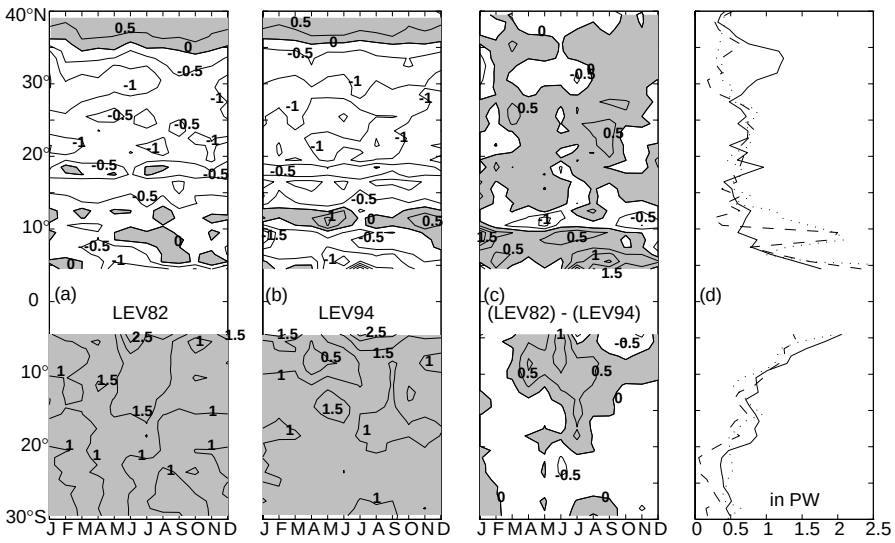

Figure 1. Seasonal cycle of baroclinic heat transport from LEV82 (a) and LEV94 (b). Seasonal cycle of their difference (c). Contour interval is 0.5 PW, positive contours are shaded. The largest value of the difference is plotted (in absolute value) as a dashed line on (d), along with the amplitude of the seasonal cycle from LEV82 (continuous line) and LEV94 (dotted line).

Results

Fig. 1, which displays as a function of latitude the annual cycle of BHT computed from LEV82 and LEV94 between 30°S and 40°N in the Atlantic, immediately illustrates the limitations of the approach: there is a lot of spottiness in the 4–25°N band from either climatologies (a-b), and there are considerable differences between the two, even in the more organized 4–30°S band (c). In many places, that difference reaches the amplitude of the seasonal cycle from either climatology (d). One has to conclude that the seasonal cycle is not resolved.

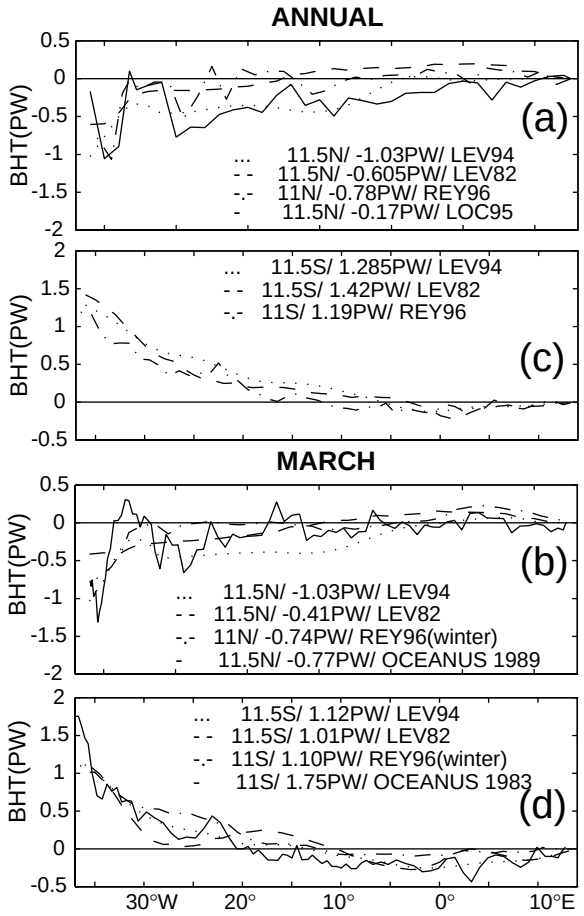

Figure 2. Baroclinic heat transport plotted cumulatively westwards at 11°N (a-b) tilted track (BHT) and 11°S (c-d) zonal track. Upper panels compare different climatologies of the annual mean, lower panels compare synoptic sections to climatologies for the month or the season of the cruise.

It is rather worrisome that different climatologies can lead to such different numbers for an integrated quantity like the BHT, and it seems worth investigating how that comes about, and how the results differ from those obtained from synoptic sections. Fig. 2 shows the BHT plotted cumulatively as a function of longitude at 11°N and 11°S, along the tracks of two synoptic sections occupied by RV Oceanus (11°N in March 1989, co-PIs D. Roemmich, M. Hall and T. Chereskin, and 11°S in March 1983, PI B. Warren). The 11°S section is zonal, the 11°N section bends perpendicular to the coast west of the Mid-Atlantic Ridge (Friedrichs and Hall, 1993); climatological temperatures and salinities were extracted accordingly. The accumulations were done from east to west on the ground that the curves were most likely to diverge near the western boundary. Panels on the left display the cumulative BHTs from the annual mean climatologies, panels on the right those computed from the synoptic sections and from LEV82, LEV94 and REY96 for the month or the season of the cruise. These 2 latitudes are a good example of a fairly hopeless case and a somewhat promising one.

We find the 11°N case (Fig. 2a-b) hopeless not only because the final BHT values are scattered (see the legend), but also because the accumulated curves are far apart, even when one only compares annual climatologies. That means that each of the climatologies sees fairly different zonal density gradients even in the interior of the section. The curve from the synoptic section is very noisy itself, reflecting the presence of a number of geostrophic eddies or meanders typical of that region of strong zonal flow. Compared to LEV82 and LEV94, less of this zonal structure is smoothed out in LOC95 and REY96, but both still end up with quite different numbers for the annual mean, -0.2 PW and -0.8 PW respectively. The annual climatology most resembling the synoptic section is REY96, but this is not systematically the case at other latitudes studied (not shown).

At 11°S (Fig. 2c) the final integrated values of BHT are fairly close and the curves from the various annual climatologies much less scattered than at 11°N. All exhibit southward BHT in the eastern third of the basin, northward BHT farther west, a pattern consistent with the known existence in that region of cyclonic surface geostrophic flow. Compared to the synoptic section (itself much less noisy than at 11°N), March LEV82, March LEV94 and winter REY96 yield a BHT too low by 0.6–0.7 PW but most of the difference takes place while integrating across the western boundary, as originally anticipated (Fig. 2d). This is an encouragement to look more closely at the seasonal cycle of BHT from LEV82 and LEV94 at least over the interior of the basin. Visualizing cumulated BHTs for each month reveals in both climatologies a similar tendency for less southward BHT (flatter isotherms) in the east in June to August, a signal that could indicate a not improbable seasonal modulation of the cyclonic gyre. There is still, however, a spectacular (almost 1 pW) difference in the net BHTs computed for July from both climatologies, caused by not so spectacular differences in the zonal temperature (and salinity) structures west of 25°W.

One could be tempted to simply discard LEV82 on the ground that LEV94, based on the same data and more, is best. This would be unwise because unrealistic anomalies in either temperature or salinity are present not only in LEV82 but also (and in fact in larger numbers) in LEV94 (only some were eliminated in a recent temperature release). As long as these anomalies are in the interior, they only cause "waves'' on the cumulated curves without affecting

the net integration (like a realistic eddy-induced anomaly would), but when they are near either boundary, they alter the final value, often dramatically (like a boundary current would), contributing to the spottiness of Fig. 1. Thus the sharp peak at 8.5°N in January (Fig. 1b and 1d) is spurious: it is caused by unrealistic salinities near 750 m at the eastern boundary.

Conclusions

This note illustrates why existing climatologies do not, in their present state, resolve the BHT and its seasonal cycle properly. It is necessary to understand better which differences in data bases or averaging techniques are responsible for the differences in the final data sets, and at least LEV82 and LEV94 need to be carefully scrutinised in order to eliminate, especially near the extremities of the sections, the unrealistic anomalies that passed quality control. The often very different results obtained from various climatologies are of concern for modelling purposes, because regional models often impose climatological fields in sponge layers, which amounts to imposing a climatological BHT there. A more complete discussion will be presented in a longer manuscript in preparation.

References

Friedrichs, M.A.M., and M.M. Hall, 1993: Deep circulation in the tropical North Atlantic. J. Mar. Res., 51, 697–736.

Hall, M.M., and H.L. Bryden, 1982: Direct estimates and mechanisms of ocean heat transport. Deep-Sea Res., 29, 339–359.

Levitus, S., 1982: Climatological atlas of the world ocean. NOAA Prof. Paper 13, US Govt. Printing Office, Washington, DC, 173pp.

Levitus, S., R. Burgett and T.P. Boyer, 1994: World ocean atlas 1994 CD-ROM sets. NODC Informal Report 13.

Lozier, M.S., W.B. Owens and R.G. Curry, 1995: The climatology of the North Atlantic. Progr. Oceanogr., 36, 1–44.

Molinari, R.L., E. Johns and J.F. Festa, 1990: The annual cycle of meridional heat flux in the Atlantic Ocean at 26.5°N. J. Phys. Oceanogr., 20, 476–482.

Reynaud, T., P. Legrand, H. Mercier and K. Speer, 1996: personal communication.

Deep Circulation Southwest of Australia

Gwyneth E. Hufford and Michael S. McCartney, Woods Hole Oceanographic Institution, USA.
gwyneth@gaff.whoi.edu

Deep water colder than θ = 1.0°C is found (Mantyla and Reid, 1995) in the subtropical/tropical Central Indian Basin (CIB), and all evidence points to its source as the South Australian Basin (SAB). The gap between Broken Ridge and Naturaliste Plateau (Fig. 1) is one passage for exchange between the SAB and the northern basins, allowing flow through the Perth and West Australian Basins, with leaks from the latter through the Ninety East Ridge into the CIB. Another pathway takes somewhat warmer deep water from the SAB directly into the CIB over the deep sills of the ridge connecting the Broken Ridge to the Southeast Indian Ridge, (see Talley and Baringer, 1995). The Australian-Antarctic Basin (AAB) is in turn the source of deep waters in the SAB, and the Southeast Indian Ridge separates the SAB and AAB with a sill depth of about 3500 m in the Antarctic Discordance Zone.

WHP sections I8S/I9S, December 1994 through mid-January 1995 provided two crossings of the Southern Ocean between the southern coast of Australia and the Adelie coast of Antarctica (Fig. 1). The I8S/I9S sections were designed to examine the interior gyral circulation of the AAB as well as the Deep Western Boundary Current (DWBC), Speer and Forbes (1994), flowing northwards along the eastern flank of the Kerguelen Plateau, and the Princess Elisabeth Trough (PET) separating the Plateau from Antarctica that allows exchange between the SAB and the Weddell Gyre. The sections in the SAB were designed to define the circulation carrying deep waters

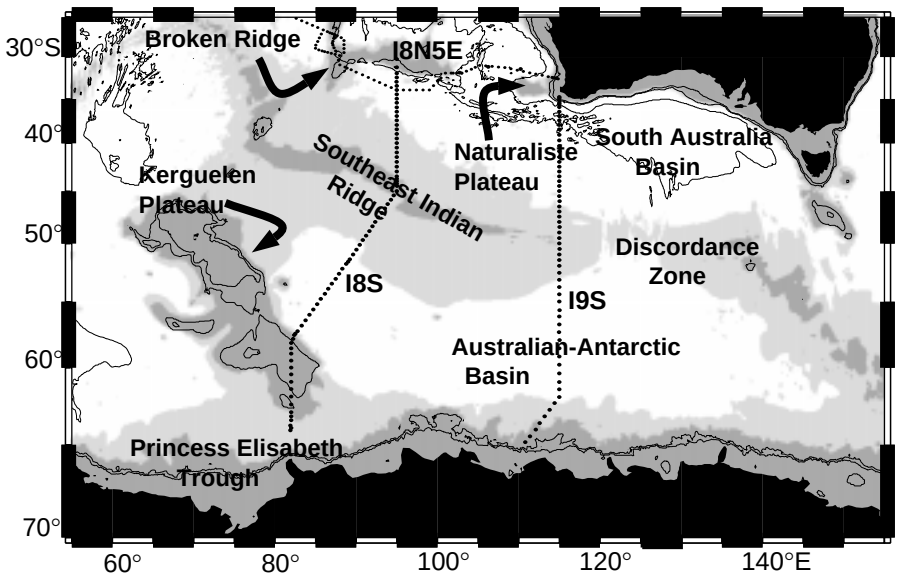

Figure 1. Bathymetric chart of South Australia and Australian-Antarctic Basins, depths less than 3000 m. are shaded dark grey, and less than 4000 m. light grey. Filled circles indicate the station positions of WHP segments I8S, I9S and I8N/5E (the last discussed by Talley and Baringer, 1995).

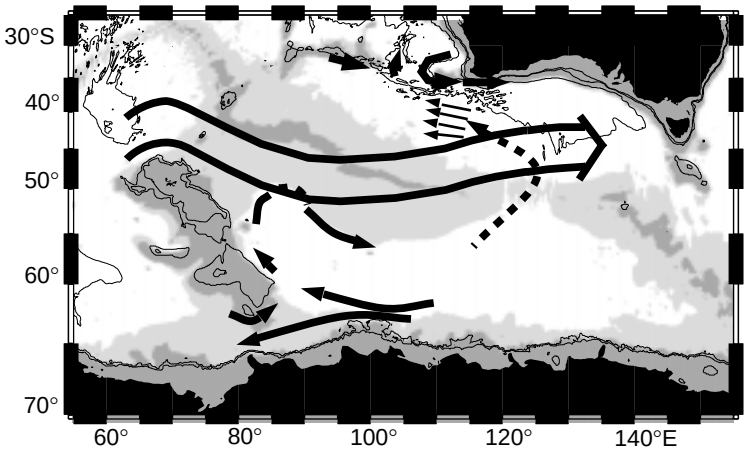

Figure 2. Summary circulation scheme based on preliminary I8S/I9S analysis.

towards the CIB. Fig. 2 gives a summary circulation scheme from our preliminary analysis. We produce a tentative, qualitative circulation scheme for some elements of the overall northward movement of cold deep water through the gyral flows in the SAB and AAB.

The origins of the DWBC off Kerguelen Plateau

I8S extended from Broken Ridge across the Southeast Indian Ridge, to Kerguelen Plateau and into the PET as far as the ice edge. The potential temperature contours are shown in Fig. 3a (page 24). A strong shear signature through stations 64-68 denotes the DWBC along the flank of Kerguelen Plateau, near where it was first reported by Speer and Forbes (1994) as having a transport of $6 \times 10^6 \, m^3 \, sec^{-1}$ following the contour of the Plateau. Stations 68–69 define a shear reversal as the section reaches the plateau top. Crossing the Plateau, isotherms descend well into the PET before rising steeply to the ice edge in the southern PET. That rise is the shear signature for westward flow through the PET similar to that reported by Speer and Forbes (1994) and Frew *et al.* (1995). They suggest that the westward flow precludes Weddell influence on the AAB by flow through the PET.

In the northern PET our section suggests eastward flow, which would bring Weddell Gyre waters into the AAB. The DWBC has a monotonic shear signature except for the reversal over the shallower part of the Plateau. The deep property scatter plots show onshore–offshore transitions across the DWBC and a vertical layering of the water masses. Fig. 4a shows one scatter plot example, θ-silica. I8S stations 55–69 span the DWBC and adjacent waters, with stations 65–67 lying in the core of the current. In the deep water the DWBC core stations are consistently slightly lower (order 2μmol/kg) in silica at a given temperature than offshore; we show this on Fig. 4a by two average curves. The only exception is station 67 on the inshore edge of the core, where the silica transitions to being higher than the waters in the rest of the core and offshore, for temperatures 0.1°C–0.3°C. Inshore of station 68, the silica levels systematically rise. High silica levels are found over the southern Kerguelen Plateau, and we indicate with a closed curve on the figure these warmer high silica waters. Most importantly, we find waters similar to those at stations 67–68 in the northern PET where the shear suggests eastward flow, and where the coldest water is 0.1°C. So we conclude that eastward flow of high silica waters from the Weddell through the PET occurs at temperatures above 0.1°C, and follows the Kerguelen Plateau contours to contribute to the northward flow of the DWBC. As we will see below, there seems to be no source internal to the AAB for these elevated silica values.

DWBC waters colder than 0.1˚C show lower silica than the waters offshore, Fig. 4b. Stations 67–68 have maximum differential and distinct silica minima near θ = -0.35°C. Low silica in the temperature range -0.3°C to -0.4°C is a general feature of deep waters near Antarctica. It stems from the plumes of dense, nutrient depleted water deep water formed near shelves that even after entrainment show nutrient minima far downstream, *e.g.* Carmack (1973). Waters this cold are not found in the eastward flow regime in the northern PET – and in any case, the interior waters of the Weddell have too high silica to be a plausible source of silica this low, *e.g.* Mantyla and Reid (1995, Fig. 2e). Our section in the PET does not extend far enough up the Antarctic continental slope to sample the westward flow regime. The part we did sample shows a more extreme silica minimum for the same temperature range as the DWBC, Fig. 4c. We attribute both these minima to the westward flow along the southern flank of the AAB, which was much better sampled in I9S, Fig. 2b. There, a more extreme silica minimum is found at the same temperature in the westward flow along the continental slope, most extreme in the south, less extreme in the north, Fig. 4c. Our second conclusion is the westward deep flow along the Antarctic continental slope, with ultimate origins in deep water formed in the Ross Sea and the Adelie coast, bifurcates in the southwestern AAB to supply both continued westward flow through the PET into the Weddell–Enderby Basin and a northward branch into the DWBC flow off the Kerguelen Plateau. This branch is the sole source for northward DWBC flow for θ<0.1°C, but for θ>0.1°C the northward branching waters converge with the eastward flow of Weddell waters from the northern PET as a combined source for DWBC flow.

Orsi and Bullister (1996) map CFC-11 on two surfaces close to our demarcation of 0.1°C. On both surfaces the CFC-11 picture mirrors the classical tracer fields, with the influence of the westward flow along the continental slope in the southern AAB (low silicate, phosphate and nitrate, and elevated oxygen) correlated with higher CFC-11, and feeding a northward extension in the DWBC and continued westward flow through the southern PET. Our eastward flow regime in the northern PET, and its northward extension as the inshore part of the DWBC (high silicate,

phosphate and nitrate, and low oxygen) show as lowered CFC-11. The overall circulation geometry leads to the westward flow regime providing isolated property extrema within the DWBC (low silicate, phosphate and nitrate, and elevated oxygen and CFC-11), with Weddell Waters from the PET to the west and AAB gyre interior waters to the east.

The bifurcation of the westward flow along the continental slope suggests a dividing streamline somewhere across the continental slope of the I9S section. North of this, the westward flow supplies the northward branch into the DWBC, south of it the waters continue westward through the PET to the Weddell. The dividing streamline may be at different positions along the I9S section for different temperatures. For a minimal mixing interpretation, producing the northern limit for the dividing streamline, we look along the I9S section for the θ-Si relation closest to the "Inner core" DWBC curve on Fig. 4c, yielding station 92, Fig. 4d. The transition from silica distinctly higher than that of the DWBC to silica distinctly lower is abrupt, across stations 91–93 suggesting division near station 92.

The I9S section, Fig. 3c shows that the southward rise of isotherms on the southern side of the AAB deep gyral flow steepens from station 93, suggesting an increasing westward flow at the sharp transition of θ-Si. On I8S southwestward from the AAB interior across the DWBC onto the Kerguelen Plateau, the same broad-scale rise of isotherms is seen, Fig. 3a. Thus the deep gyral flow in the AAB may include a recirculating interior pool of higher silica waters. The recent S4 section and Australian observations east of I9S should illuminate the eastern closure of this pool.

The interaction of the DWBC with the ACC

We now discuss the fate of these northern flowing waters east of Kerguelen as they encounter the Antarctic Circumpolar Current (ACC) entering the AAB from north of the Kerguelen Plateau. Park *et al*. (1993) extended a study of the ACC in the Crozet Basin to include the choke point between Kerguelen Plateau and Amsterdam Island. Their CTD and XBT data and satellite altimetry indicated the subtropical and subantarctic fronts (STF and SAF) compressed together between 44.5°S and 45.3°S, thus a narrow intervening subantarctic zone (SAZ); the (Polar Front (PF) was at 47.58°S. They calculated the bulk of the ACC transport ($100 \times 10^6 \, m^3 \, sec^{-1}$) concentrated in the STF–SAZ–SAF, with a $6 \times 10^6 \, m^3 \, sec^{-1}$ additional contribution in the PF. This transport feeds into the AAB along the southern flank of the Southeast Indian Ridge. Sections I8S and I9S cross this flow about 1600 km and 3400 km east of the Kerguelen–Amsterdam Passage. Along I8S the SAF lay between 42°S and 45°S with its southern edge directly over the Southeast Indian Ridge crest. I8S crossed the Polar Front (PF) twice at 51.5°S, 89°E and at 53°S, 87°E; both over 5° south of the mid-ocean ridge (the ambiguity was due to an eddy or meander embedded in the section). Along I9S the SAF lies between 46°S–49°S, north

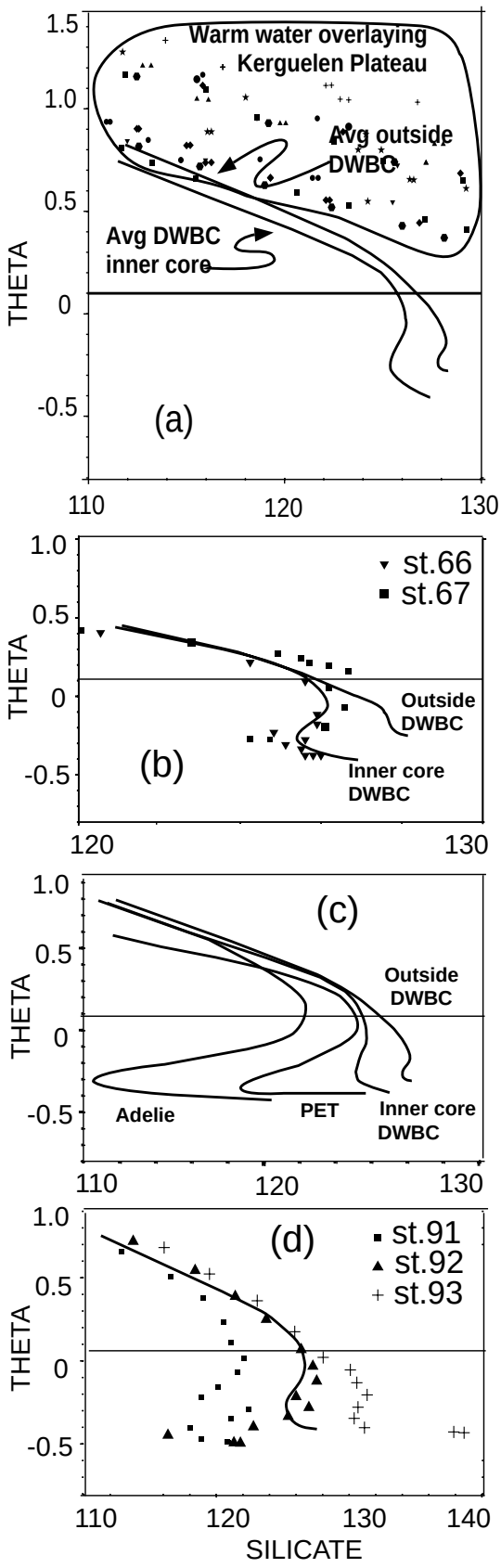

Figure 4. Theta-silica plots for WHP I8S and I9S section data through warmer core of DWBC and adjacent Kerguelen waters (a), colder core of DWBC (b), DWBC core and potential sources (c) and inner core of DWBC and Adelie Coastal Current (d).

of the Southeast Indian Ridge. The PF was at 51°S, much closer to the SAF and coinciding with the mid-ocean ridge crest. The bulk of the ACC transport thus has crossed the Southeast Indian Ridge, whose crest descends eastwards from above 3000 metres to below 2500 metres between the two sections.

The ACC brings deep water towards the Kerguelen-Amsterdam Passage at temperatures no colder than about 0.73°C, the coldest observation in the easternmost section by Park *et al*. (1993), near 3620 m, under the ACC axis. That section lies west of the sill of the passage, indicated in ETOPO5 digital bathymetry at 3140 m. In their section the coldest temperature at the sill depth is 0.87°C located at the base of the northern flank of the Kerguelen Plateau under the PF. We expect that the coldest deep water flowing eastward through this passage into the AAB falls in the range 0.7°C–0.9°C. In I8S (Fig. 3a), beneath the southern parts of the ACC (south of the Southeast Indian Ridge crest), deep water as cold as 0°C is associated with the deeper extension of the vertical shear signature of the ACC (north of station 50). The northward deep water transport of the DWBC evidently converges with and intrudes beneath the ACC as it flows into and along the northern AAB. In the process the DWBC must turn eastwards and descend some 1000–1500 m to get the waters between 0°C and 0.7°C on the slope of the Kerguelen Plateau down to their observed placement on the deep flank of the Southeast Indian Ridge. In I9S, Fig. 3c, along the southern flank of the Southeast Indian Ridge these same cold (<0.7°C) waters extend from 2400–4000 m, well above the Ridge crest to the north. The deep shear of the ACC, however, causes those isotherms to descend and intersect the Ridge south of the crest, except, marginally, 0.6°C and 0.7°C. Thus leakage of the DWBC waters across the Southeast Indian Ridge should occur mainly east of I9S, through the Discordance Zone, as anticipated by Mantyla and Reid (1983 and 1995). The intrusion of the DWBC waters beneath the ACC in the confluence region northeast of the Kerguelen Plateau sets the stage for this penetration of cold deep water across (under) the ACC being completed at the Discordance.

The flow of deep water from the Australian –Antarctic Basin to the South Australia Basin (SAB)

North of the Southeast Indian Ridge in the SAB, minimum temperatures are just above 0.5°C along I8S and just colder than that along I9S in the middle of the SAB. Examination of the I9S data show this bottom layer in the SAB is considerably warmer and lighter than the available pool of coldest water immediately south of the crest of the Southeast Indian Ridge. There are two extreme mixing alternatives for SAB bottom water evolution from the source waters from the south. One extreme is that the ridge dams up the cold dense waters below the (unknown) Discordance sill depth, so only waters warmer than sill depth flow over into the SAB. Perhaps that temperature is near 0.5°C, but in addition to not knowing the Discordance Zone sill structure, the local height of isotherms above the sills will reflect the exact placement of the ACC over the region, since the isotherms steeply slope across the ACC. The other extreme is that the coldest densest available waters leave the AAB through the Discordance Zone and strongly warm and lighten by entrainment of the overlying ACC waters. We favour something closer to the first scheme, because if there were substantial entrainment or mixing with the overlying warmer deep waters, it is hard to see how the SAB bottom water could end up only slightly altered from conditions on its isopycnals south of the ACC. The SAB bottom water does exhibit higher temperature and salinity and lower silica and oxygen than waters on the associated density surfaces south of the Ridge, but these anomalies are rather small.

A Deep Northern Boundary Current along the southern Australian continental slope

North of the ACC, the I9S data indicate a weak deep shear across SAB, with most of the "action" in a 200 km wide boundary against the continental slope of Australia. At thermocline levels a broader northward rise of isotherms indicates the Flinders Current (Bye, 1972) flowing westward and providing a partial recirculation gyre in the SAZ. The deeper shear signature is the same sign to around 3500 db, and isotherms reverse slope sharply below 3500 db. This shear reversal is not particularly strong, however, for the vertical density gradient is not large. If one imagines the Flinders Current to have a shallow reference level, then below that level the flow reverses to eastwards, reaches a maximum eastward speed near 3500 db (θ = 1.3°C), then declines below that core. The shear reversal allows the

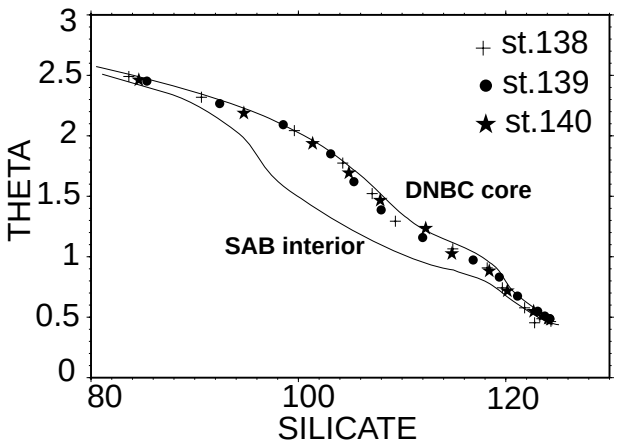

Figure 5. Theta-silica plots for WHP I9S section data in the South Australia Basin.

possibility that flow might reverse to westward near the bottom. One requires westward flow in the cold bottom layer between the Australian coast and about 45°S, for the pool of water colder than 0.5°C must be making its way from the Discordance Zone southeastward of the section to

pass between the Broken Ridge and Naturaliste Plateau, where coldest bottom waters have warmed to about 0.54–0.55°C, Fig. 3b. Whether this flow occurs at the bottom of this DNBC system or to its south, or both, will involve sorting out subtleties of the bottom water characteristics and reference level issues. For now we note that the bottom water south of the DNBC is very slightly colder than that in the DNBC stations, with the transition occurring through stations 137–138, the same station pair defining the sharpest deep shear reversal, and for which there is a transition from slightly lower to higher silica below 0.7°C, Fig. 5. Our first guess is that the principal westward bottom water flow occurs in the offshore part of the DNBC.

The DNBC otherwise appears to be an eastward flow regime. In Fig. 5 the DNBC is seen to have a distinctly elevated silica for $0.7°C \leq \theta \leq 2.5°C$, and we attribute this to origins in the southward flow near the Naturaliste Plateau described by Toole and Warren (1993) and Talley and Baringer (1995): this flow apparently turns the corner at the Plateau to flow eastwards through I9S. Defining the top of this eastward flow essentially defines a level of no motion for the DNBC above which the flow reverses to the westward flow of the Flinders Current. There is a pronounced oxygen minimum centred on $\theta = 2.5°C$ spanning the DNBC and extending southwards to station 132, and such waters are also found spanning the passage between Naturaliste Plateau and Broken Ridge, and it is tempting to assert eastward flow at this level in the DNBC across, transitioning to westward flow in the overlying Antarctic Intermediate Water. But since the gyral flow defined by the Flinders Current in the North and the SAF in the ACC to the south may penetrate to or into the oxygen minimum layer.

References

Bye, J.A.T., 1972: Oceanic circulation south of Australia, in Antarctic Oceanology II: The Australian-New Zealand Sector, Antarctic Res. Ser., Vol. 19, edited by D.E. Hayes, 95-100, AGU, Washington, DC.

Carmack, E.C., 1973: Silicate and potential temperature in the deep and bottom waters of the western Weddell Sea. Deep-Sea Res., 20, 927–932.

Frew, R.D., K.J. Heywood, and P.F. Dennis, 1995: Oxygen isotope study of water masses in the Princess Elizabeth (sic) Trough, Antarctica. Mar. Chemistry, 49, 141–153.

Mantyla, A.W., and J.L. Reid, 1983: Abyssal characteristics of the world ocean waters. Deep-Sea Res., 30, 8a, 805–833.

Mantyla, A.W., and J.L. Reid, 1995: On the origins of deep and bottom waters of the Indian Ocean. J. Geophys. Res., 100(C2), 2417–2439.

Orsi, A.H., and J.L. Bullister, 1996: Synthesis of WOCE chlorofluorocarbon data in the Pacific Ocean. US WOCE Report 1996, 11–3.

Park, Y.H., L. Gamberoni, and E. Charriaud, 1993: Frontal structure, water masses and circulation in he Crozet Basin. J. Geophys. Res., 98, 12,361–2,385.

Speer, K.G., and A. Forbes, 1994: A deep western boundary current in the South Indian Basin. Deep-Sea Res., 41(9), 1289–1303.

Talley, L., and M. Baringer, 1995: Preliminary results from a WHP section in the Central Indian Ocean. International WOCE Newsletter, 21, 35–38.

Toole, J.M., and B.A. Warren, 1993: A hydrographic section across the subtropical South Indian Ocean. Deep-Sea Res., Part I, 40(10), 1973–2019.

OOPC Ocean Climate Time Series Workshop
Baltimore, 18-20 March 1997
Cosponsored by GOOS GCOS SCOR/JGOFS WCRP

The term time series here refers primarily to observations at fixed sites, but also includes repeat sections and observations from drifters. Such data have provided invaluable, sometimes unique, information for monitoring and detecting climate change and for understanding variability over a range of time scales in the physics, chemistry and biology of the ocean. In recent time logistical and cost factors have provided severe constraints on the maintenance and implementation of time series stations, in many cases leading to the cessation of data collection. However, this period has also been the introduction of innovative, more cost effective techniques for data collection and communication from moored/fixed platforms, perhaps making time series stations once more an effective observational method.

It is timely then to organise a review of the contribution to ocean science from time series, in particular those recently established under the JGOFS, TOGA and WOCE research programmes, and to assess

(i) the viability and feasibility of maintaining the existing stations,

(ii) the possibility of re-occupying sites for which long records exist and for which new technology might offer more cost-effective systems, and

(iii) identifying, on the basis of research results from programs like WOCE, TOGA and JGOFS where there are sound cases for establishing new sites.

The workshop will provide guidance to GOOS and GCOS, through the Ocean Observations Panel for Climate (OOPC), as they seek to identify sites that should be maintained routinely as a long-term contribution to climate monitoring. The results and recommendations from the workshop will also take into consideration the research interests of JGOFS and the nascent CLIVAR programme.

The workshop is planned to take place at Johns Hopkins University in Baltimore with local arrangements kindly handled by SCOR. A full 3-day meeting is planned with 20-25 participants. This should allow the diversified group to discuss and develop useful recommendations and prioritisation transcending boundaries between individual programmes and disciplines.

Organizing committee

Art Alexiou, IOC
John Field, JGOFS (ex officio)
Elizabeth Gross, SCOR
Ed Harrison
Peter M. Haugan (chairman)
Neville Smith, OOPC (ex officio)
Gerold Wefer
Bob Weller
Walter Zenk

Inferring Ocean Transports from Surface Fluxes

W.G. Large and S.C. Doney, NCAR, Boulder, CO, USA. wily@ncar.ucar.edu

Introduction

From a climate perspective, a primary role of the ocean is to redistribute heat and freshwater in the meridional direction through the combined action of the wind-driven and thermohaline circulations. The first order balances are straightforward. Solar heat deposited in the tropics is transported poleward where it is lost as sensible and latent cooling. Rainfall in the mid-latitude storm tracks and tropical convergence zones is carried to the high evaporation regions of the subtropics. The critical scientific question is how to constrain the magnitude and variability of these transports?

Ocean transports are estimated in several ways. First, zonal sections of temperature and salinity across ocean basins can be used to compute the fluxes across particular latitudes (*e.g*. Hall and Bryden, 1982). Many such observations can be combined in an inverse model calculation to infer a consistent transport scheme for the ocean as a whole (*e.g*. Macdonald and Wunsch, 1996). Second, the meridional derivatives of the heat and freshwater transports are given by the zonal integral of the respective net surface fluxes (*e.g*. Wijffels *et al.*, 1992). Third, the ocean transports can be estimated from the meridional divergence of atmospheric heat and moisture transport (*e.g*. Trenberth and Solomon, 1994), which must balance the oceanic divergences. In the latter two methods, integration of the divergences to find the oceanic transports as a function of latitude can be made to start with a given northern boundary condition, such as zero transport at the North Pole. However, satisfying the southern boundary condition of zero transport at the Antarctic coast cannot, in general, by guaranteed. To do so usually requires subjective assumptions concerning errors in the data being analysed and this problem, as it pertains to surface flux inferences, will now be addressed.

Surface heat and freshwater fluxes

A major advance in the observational data base has come with the routine production of all the surface fluxes and flux parameters by the Numerical Weather Prediction centres such as the National Center for Environmental Prediction (NCEP). By combining NCEP reanalysis data (Kalnay *et al.*, 1996) with satellite derived cloud fraction and solar insolation (ISCCP, Bishop and Rossow, 1991), precipitation from satellite Microwave Sounding Unit data (MSU, Spencer, 1993), and a sea surface temperature climatology (Shea *et al.*, 1990), we have constructed global fields of the mean annual heat and freshwater fluxes. Further details on the flux calculations, including the bulk formulae used for the turbulent fluxes, are given in Large and Doney (1996), or Large *et al.* (1996). These global fields then are used to compute the meridional ocean heat and freshwater transports.

Considerable uncertainty exists for all of the heat and freshwater flux components. Nevertheless, we first compute transports from a set of uncorrected flux fields. On average, there is a net heating of the ocean of nearly $50\ \mathrm{Wm}^{-2}$, and precipitation exceeds evaporation by about 8%. Next, a set of corrected flux fields are used, where a global balance is nearly achieved for both heat and freshwater. In addition, transports are computed from the intermediate flux fields that result from the three individual corrections; absorption, drying and rainfall. Although other sets of corrections could be used to satisfy the southern boundary condition, these three are supported by observational evidence.

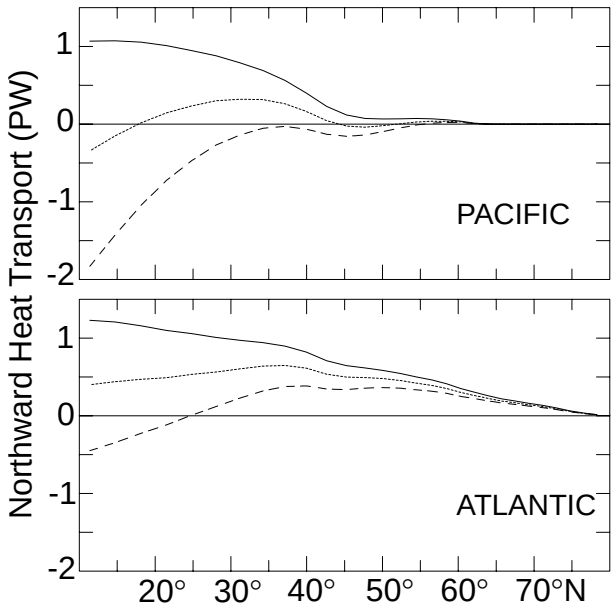

Figure 1. Annual mean northward heat transport by the North Pacific and North Atlantic, as inferred from surface flux fields: uncorrected (dashed), fully corrected (solid), drying correction only (dotted).

The absorption correction uniformly reduces the solar heating by 12.5% and is consistent with current radiative transfer models transmitting too much solar radiation (J. Kiehl, personal communication, 1996). The drying correction of reducing NCEP air humidity by a uniform factor of 0.94 brings the latent heat flux into good agreement with Kent and Taylor's (1995) annual cycle of latent heat flux for a portion of the North Atlantic and may reflect a tendency for ocean humidity observations to be too moist. However, it increases the evaporation so that the precipitation then has to be increased by about 10% in order

to achieve global balance in the freshwater flux. This rainfall correction brings the MSU precipitation into much better agreement with other precipitation climatologies (D. Shea, personal communication, 1996). Further discussion of these corrections and the resulting annual average global net heat and freshwater fluxes are given in Large and Doney (1996).

Meridional transports

Fig. 1 shows the northward heat transports inferred from the uncorrected (dashed) and fully corrected fluxes (solid). The latter are supported by the above rationale. However, a not unreasonable argument might be that data uncertainties are much larger in the southern hemisphere, so that the former are valid north of the equator. Since the transport differences between these two cases are systematic they accumulate as the integration proceeds from the north and are more than 1 PW at 24°N in both basins. Arguments could be combined to make the inferred transports fall anywhere within, and perhaps beyond, these two extremes. For example, opponents of the absorption correction might only apply the drying correction in the northern hemisphere and obtain the dotted curves of Fig. 1. An almost indistinguishable curve is obtained if only the absorption, but not the drying, correction is applied. In the Pacific, full correction gives a small net cooling north of 45°N, whereas the uncorrected fields indicate a substantial net warming.

The northward transports of freshwater is shown in Fig. 2. Here the uncorrected (dashed) and corrected (solid) have smaller differences, because the effects of the drying correction (dotted) are largely offset by the rainfall correction. Although there is global balance in the corrected fluxes, ocean general circulation model solutions indicate that the rainfall correction should not be uniformly applied. They support less rainfall in the tropical convergence zones (*i.e.* MSU level rainfall), and hence more rainfall, or less evaporation elsewhere. Again, arguments could be made for freshwater transports anywhere within the curves of Fig. 2, so there is a range of about 0.3 and 0.5 Sv at 15°N in the Pacific and Atlantic, respectively. We note that the surface flux inferred transports of Wijffels *et al.* (1992) fall within this range at all northern latitudes.

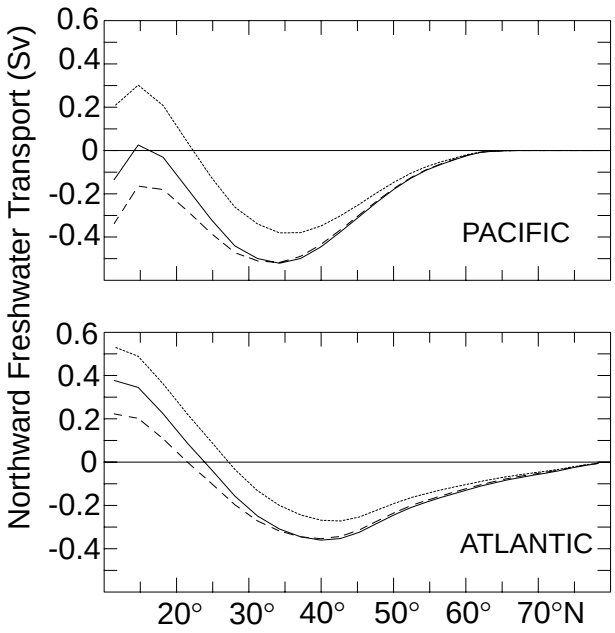

Figure 2. Annual mean northward freshwater transport by the North Pacific and North Atlantic, as inferred from surface flux fields: as Fig. 1.

Conclusion

The uncertainties in ocean transports inferred from surface flux estimates are uncomfortably large. Such estimates are of little use in constraining ocean transport values either from models or observations. Other methods must be used to obtain useful constraints. Regardless of the results, it is very likely that surface flux estimates could be made consistent, by applying reasonable corrections to the surface flux data. The transport related quantities that appear to be best known are: there is no meridional ocean transport either at the Antarctic coast, or at the north pole; and the globally averaged ocean surface heat and freshwater fluxes are near zero. Therefore, any estimate of ocean transports is more credible when these global constraints are satisfied.

References

Bishop, J.K.B., and W.B. Rossow, 1991: Spatial and temporal variability of global surface solar irradiance. J. Geophys. Res., 96, 16,839–16,858.

Hall, M.M., and H.L.Bryden, 1982: Direct estimates and mechanisms of ocean heat transport. Deep-Sea Res., 29, 339–359.

Kalnay, E., M. Kanamitsu, R. Kistler, W. Collins, D. Deaven, L. Gandin, M. Iredell, S. Saha, G. White, J. Woollen, Y. Zhu, M. Chelliah, W. Ebisuzaki, W. Higgins, J. Janowiak, K.C. Mo, C. Ropelewski, A. Leetmaa, R. Reynolds, and R. Jenne, 1996: The NCEP/NCAR reanalysis project. Bull. Amer. Meteor. Soc., 77, 437–471.

Kent, E.C., and P.K. Taylor, 1995: A comparison of sensible and latent heat flux estimations for the north Atlantic Ocean. J. Phys. Oceanogr., 25, 1530–1549.

Large, W.G., and S.C. Doney, 1996: Global surface forcing fluxes and parameters. US WOCE Implementation Report, No. 8, 48pp.

Large, W.G., G. Danabasoglu, S.C. Doney, and J.C. McWilliams, 1996: Sensitivity to surface forcing and boundary layer mixing in a global ocean model: Annual-mean climatology. J. Phys. Oceanogr., Submitted.

Macdonald, A.M., and C. Wunsch, 1996: An estimate of global ocean circulation and heat fluxes. Nature, 382, 436–439.

Shea, D.J., K.E. Trenberth, and R.W. Reynolds, 1990: A global monthly sea surface temperature climatology. NCAR Technical Note NCAR/TN-345, 167pp.

Spencer, R.W., 1993: Global oceanic precipitation from the MSU during 1979–91 and comparisons to other climatologies. J. Climate, 6, 1301–1326.

Trenberth, K.E., and A. Solomon, 1994: The global heat balance: Heat transports in the atmosphere and ocean. Climate Dyn., 10, 107–134.

Wijffels, S.E., R.W. Schmitt, H.L. Bryden, and A. Stigebrandt, 1992: Transport of freshwater by the oceans. J. Phys. Oceanogr., 22, 155–162.

Do Transient Tracers Really Help to Improve Ocean General Circulation Models?

Christoph Heinze and Ernst Maier-Reimer, Max-Planck-Institut für Meteorologie, Bundesstrasse 55, D-20146 Hamburg, Germany. heinze@dkrz.de

Introduction

In the early phase of WOCE, a vigorous discussion took place between physical oceanographic T-S-purists and lovers of "exotic" tracers about the value of tracers in general and transient tracers in particular for helping to understand and model the ocean velocity and thermohaline fields. Meanwhile the potential of tracers is widely acknowledged by the WOCE community, a fact that led to the publication of the tracers section in International WOCE Newsletter, No. 23, 1996.

In their inverse box model approach, Mémery and Wunsch (1990) found that the available bomb tritium data set only weakly constrained the flow field of the North Atlantic. In the conclusion of their paper, however, they expected that the use of transient tracers in prognostic three-dimensional global ocean models are an advantage since only the tracer distribution at the sea surface have to be prescribed. Tracer data in deeper layers are then used for comparison with the model instead of constraining the flow directly. Additionally, Mémery and Wunsch (1990), anticipated that CFC data are another promising alternative to bomb tritium because the delivery function for several CFCs is far less complicated than that for tritium.

Heinze *et al.* (submitted) simulated the distributions of bomb tritium and CFC-11 in the world ocean by use of an Ocean General Circulation Model (OGCM). They carried out sensitivity studies in order to find out whether the tracer source functions are sufficiently well known to permit the use of the internal oceanic tracer measurements as a firm model test. They found that discrepancies between observed and modelled tracer fields could not be removed by adjusting the less well defined parameters of the "known" transient tracer supply functions (*e.g.*, the air/sea gas exchange rate, the water vapour exchange rate, marine precipitation). It was impossible to obtain correct values for both, the oceanic tracer inventory and the structure of the modelled tracer distribution. Their conclusion was that the disagreement between tracer simulations and measurements could be removed only by an improvement of the model velocity field and that the tracer source functions – although being far from perfect – allow the use of bomb tritium and CFCs for a firm model test. In the following, another clear hint that in addition to temperature and salinity, tracer data provide oceanographers with further relevant information, is described.

The CFC simulation

The velocity field of the Hamburg Large Scale Geostrophic Ocean General Circulation Model (LSG-OGCM) (Maier-Reimer *et al.*, 1993) was used in a 22 layer configuration. For CFC-11, a tracer supply function following England *et al.* (1994) was applied. The tropospheric CFC-11 time series was taken from a compilation by Walker, Weiss, and Salameh (personal communication). A variable gas exchange coefficient according to Wanninkhof (1992) was determined as a function of the mean monthly wind speed over the ocean as simulated climatologically by the ECHAM-3 atmospheric model (Roeckner *et al.*, 1992).

The model simulation was started at 1930 (onset of CFC-11 emission) and integrated until 1991. An example of modelled CFC-11 distribution is shown in a map of the 2370 m level (Fig. 1, page 22). A comprehensive CFC-11 data base (a compilation from Scripps and Lamont-Doherty Earth Observatory, see Maier-Reimer, 1994) which also includes standard hydrographic data was available for comparison with model results.

Analysis of the errors "model–observation"

The goal of this small study presented here is to analyse the differences between model and observations in a more general way instead of identifying specific strengths and weaknesses of the model velocity field.

It is a common feature of prognostic global coarse resolution ocean models that the active tracers, temperature and salinity, cannot be reproduced simultaneously as described by the climatological Levitus data set (Toggweiler *et al.*, 1989; Maier-Reimer *et al.*, 1993). However, it is possible to adjust the model parameters such that the errors in temperature and salinity compensate each other with respect to density determining the flow field structure. The major deep water mass and deep water type characteristics varying only slowly are well known from hydrographic measurements, while the more variable surface and upper ocean values influenced by the seasonal cycling and individual weather systems are less well known and biased towards summer observations.

What are the errors of the model with respect to the observations? The individual deviations model-minus-observation from the combined CFC-11–salinity-temperature data set (20300 data points in the 0–3000 m depth range from the Atlantic and Pacific Oceans) were plotted against depth. For potential temperature, salinity, and density $\left(\sigma_{S,t,p}\right)$ the bulk of the data shows a decrease of the error in deep waters (Fig. 2). This means that though not every individual surface T-S-value can be reproduced by the coarse model, it is capable of blending the deep water characteristics almost correctly. The slightly too low temperatures and salinities combine to an approximately correct density.

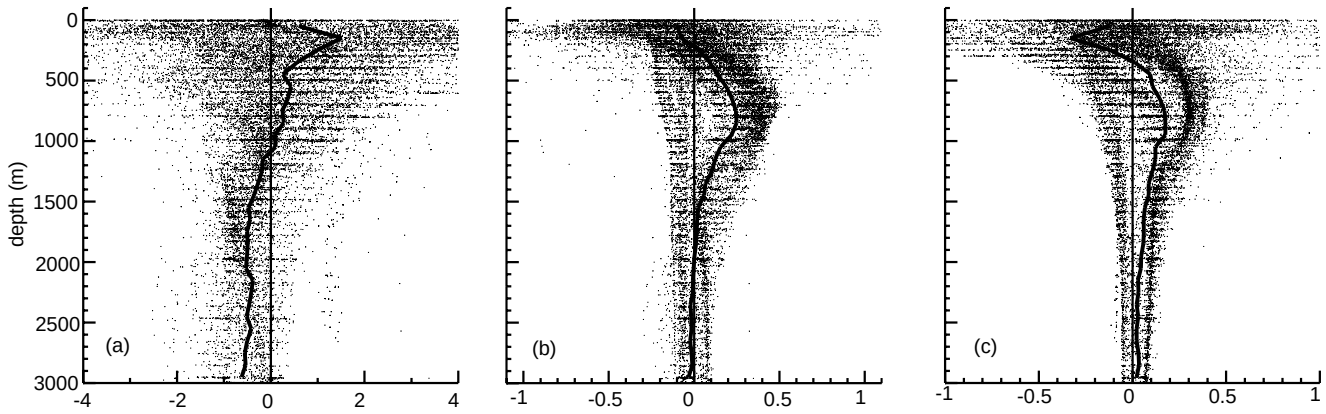

Figure 2. Absolute errors model–observation for the active tracers. (a) potential temperature [°C], (b) salinity [psu], and (c) density [$\sigma_{S,t,p}$] for the CFC-11 data base (depth range 0–3000 m, 20300 data points). The solid line indicates the mean error depth profile for 100 m increments.

The absolute CFC-11 error (Fig. 3a) also shows a general trend towards a decrease in accordance with depth. Deep water masses, however, are regimes of generally low CFC concentrations so that a look at the relative error is more revealing (how much dilution or concentration does the model show with respect to the real value?). The relative errors are minimal at the surface (where the "known" source is imprinted), increase strongly within the top 500 m, and grow even further in deep and bottom waters. The data with relative errors around 1.0 are data points in which the measurements indicate CFC-11 in the water, whereas the model predicts zero CFC-11 concentration. Although the model can reproduce the deep water density fairly well, for CFC-11 the quality of the simulation deteriorates in the deep ocean. The absolute CFC error depth profile (Fig. 3a) indicates, that the model deep water production rate is overestimated (deficit in the upper 1000 m and excess below). An attempt was also made to correlate the errors of the CFC simulation with errors in the active tracers but no globally significant correlation could be found.

A brief conclusion

The passive tracer simulation shows that additional information about the surface to deep water mass transformation is obtained from CFCs as compared with temperature and salinity. The model transports CFC-11 too quickly into the deep sea and, in parts, on pathways which do not coincide with the real world. Both deficiencies cannot be derived directly from temperature and salinity. The surface ocean history of CFC-11 is sufficiently well known to use the tracer as a valid tool for model testing. The CFC-11 input function is relative insensitive to scattering in the sea surface T and S values. The relative error of the modelled CFC concentration increases with depth, degree of dilution, and age of the respective water mass. This increase is concentrated within the upper 500 m of the water column. The model dynamics have to be improved primarily in this depth range. CFC data and other transient tracer data are useful for assimilation procedures in connection with three-dimensional OGCMs in order to improve the simulation of

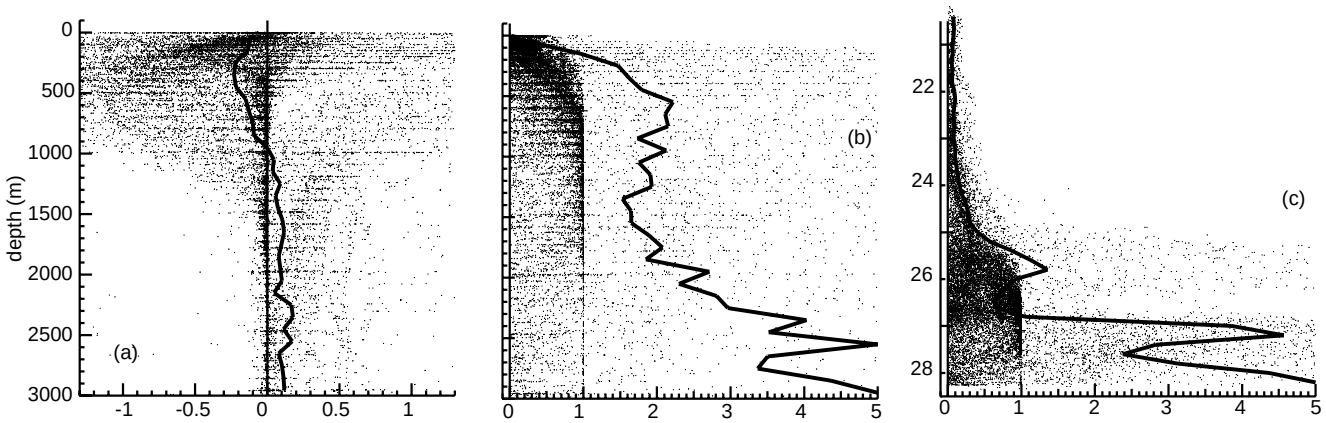

Figure 3. Errors model–observation for CFC-11. (a) Absolute errors [pmd/kg], (b) Relative errors with respect to the observations [$|(CFC_{model} - CFC_{obs})|/(CFC_{obs})$], (c) Relative errors versus modelled in situ density [$\sigma_{S,t,p}$]. The solid line indicates the mean error depth profile for 100 m increments.

water mass transformation processes, especially in the subsurface and intermediate water regime having a relatively fast turn over and, hence, is marked with measurable anthropogenic tracer signatures. The answer to the question raised in the title is: Yes, they do.

References

England, M.H., V. Garcon, and J.-F. Minster, 1994: Chlorofluorocarbon uptake in a world ocean model. 1. Sensitivity to the surface gas forcing. J. Geophys. Res., 99, C12, 25215–25233.

Heinze, C., P. Schlosser, and E. Maier-Reimer: Transient tracers in a global OGCM – source functions and simulated distributions. Submitted to the AGU volume based on papers presented at the Maurice Ewing Symposium on Applications of Trace Substance Measurements to Oceanographic Problems, October 1995, Biosphere 2 (Oracle, Arizona).

Maier-Reimer, E., 1994: CFC-Simulations. ATOC Occasional Notes (Acoustic Thermometry of Ocean Climate), 18, 1–4, June 1994.

Maier-Reimer, E., U. Mikolajewicz, and K. Hasselmann, 1993: Mean circulation of the Hamburg LSG OGCM and its sensitivity to the thermohaline surface forcing. J. Phys. Oceanogr., 23, 731–757.

Mémery, L., and C. Wunsch, 1990: Constraining the North Atlantic circulation with tritium data. J. Geophys. Res., 95, C4, 5239–5256.

Roeckner, E., K. Arpe, L. Bengtsson, S. Brinkop, L. Dümenil, M. Esch, E. Kirk, F. Lunkeit, M. Ponater, B. Rockel, R. Sausen, U. Schlese, S. Schubert, and M. Windelband, 1992: Simulation of the present-day climate with the ECHAM model: Impact of model physics and resolution. Max-Planck-Institut für Meteorologie, Report No. 93, 171pp., Hamburg.

Toggweiler, J.R., K. Dixon, and K. Bryan, 1989: Simulations of radiocarbon in a coarse-resolution world ocean model. 1. Steady state prebomb distributions. J. Geophys. Res., 94, C6, 8217–8242.

Wanninkhof, R., 1992: Relationship between wind speed and gas exchange over the ocean. J. Geophys. Res., 97, C5, 7373–7382.

The Comprehensive WOCE Data Information System

Katherine A. Bouton, WOCE Data Information Unit, University of Delaware. bouton@udel.edu

The WOCE Data Information Unit (DIU) maintains a WOCE data tracking system that collects and disseminates information about WOCE datasets. The DIU is evolving to meet the changing data information needs of WOCE. As WOCE moves to a synthesis and analysis phase, the WOCE data catalogue requirements are changing as well. The DIU has, therefore, begun the process of redesigning the data and information catalogue found on its OCEANIC Website to provide a comprehensive scheme which brings together the field programme and the data.

The first section of the WOCE data and information catalogue to receive this new all-in-one format is the sea-level section (see figure below for a sample). The extensive WOCE network of sea-level gauges provides data to monitor geostrophic currents and flows through straits as well as *in situ* data to use in conjunction with, and to validate, satellite altimetry data.

There are two components to the WOCE Data Assembly Centre (DAC) for sea-level data.

- a 'fast delivery' data centre, located at the University of Hawaii Sea Level Center (UHSLC) at Honolulu, assembles and distributes quality-controlled sea-level data from about 100 sites in near-real time, within 1–3 months after the data collection.
- a 'delayed mode' centre, located at the British Oceanographic Data Centre (BODC) at Bidston, responsible for the assembly, quality control, and distribution, of a sea-level data set (including that originally assembled in Hawaii) within 18–24 months after data collection. Bidston has a dataset of about 160 gauges.

Even though the World Wide Web (WWW) provides access* to each of these DACs individually, the distributed nature of the WOCE data system does not allow easy examination of sea-level information as a whole.

The DIU, therefore, created a comprehensive data information catalogue which allows a user to easily find data and information from both the UHSLC and Bidston datasets without having to traverse backwards and forwards across the Web from Hawaii to Bidston.

To do so, the DIU took the station listings, location information, and inventories of the data available online, from each of the two sea-level DACs and the Global Sea Level Observing System (GLOSS) CD-ROM. The DIU then compiled and organized the information into Atlantic, Indian, and Pacific Ocean tables. The DIU added links in each of these tables to station and location maps, and quality-assessment documentation found at the two DACS. To insure that the inventories and links to the data were accurate and up-to-date, the system automatically, on a weekly basis, examines each of the sites for new or changed information and alerts the DIU to these changes.

---

*WWW addresses for sites mentioned in this article are:

OCEANIC
http://www.cms.udel.edu/

WOCE DIU
http://www.cms.udel.edu/woce/

WOCE DIU Sea Level
http://www.cms.udel.edu/woce/data/sea_level/

UHSLC 'fast delivery' DAC
http://www.soest.hawaii.edu/kilonsky/uhslc.html

BODC 'delayed mode' DAC
http://www.nbi.ac.uk/bodc/dmsldac.html

Permanent Service for Mean Sea Level
http://www.nbi.ac.uk/psmsl/psmsl.info.html

Global Sea-level Observing System (GLOSS)
http://www.nbi.ac.uk/psmsl/gloss.info.html

A WOCE data user can now, from one location, use the comprehensive WOCE DIU data catalogue to:

- view the entire sea-level programme.
- see all available data from the programme.
- read a detailed description of the quality of the data
- directly download any of the online hourly, daily, monthly, or yearly data from Hawaii or Bidston as required.

A sample page (Fig. 1) from the WOCE DIU WWW site is seen below. The WWW page uses tables and Javascript, so to view the clickable buttons, a Javascript capable browser such as Netscape 3.xx or Microsoft Internet Explorer 3.xx is required.

The sea-level table includes the following information:

Station name

The table is sorted alphabetically by station name in each ocean basin.

GLOSS No. and Location Map

Bidston classifies their data using the international numbering system of the IOC's Global Sea-level Observing System (GLOSS). The entries in this column are the GLOSS station numbers. A clickable button will appear in this column if a detailed site map is available. A more general location map can be reached as a clickable button from the detailed site map. These maps were taken from the GLOSS Station Handbook, Version 3.0 – July 1996, BODC, UK.

UHSLC No. and Location Map

Hawaii classifies their data using their own numbering system. The entries in this column are the UHSLC station numbers. A clickable button will appear in this column if a location map is available directly from Hawaii.

Location

The latitude and longitude of the station is given in dd°mm'.

Observation Period

The times for which gauges are known to have been in operation, are given according to Bidston. The data for these observation dates are not necessarily at either centre and, in any case, will only have on-line links here post-1985. The centres may provide earlier data, either electronically, or upon written request.

On-line UHSLC Fast Data

This column contains direct ftp links, when available, to Hawaii for the hourly, daily and monthly data files for the period 1985–present. "N" indicates that no online data are available. A blank column indicates that these data are not presently collected as WOCE data by Hawaii.

UHSLC Quality Assessment

This column links directly to Hawaii's quality assessment reports which list site and detailed information on any data problems encountered. Note that at the end of each year the year's accumulated fast delivery data is replaced in the file by the quality controlled (qc'd) "research quality" data. This "research quality" data is updated annually by UH/NODC as part of another programme.

On-line Bidston Delayed Data

This column contains direct links to BODC's yearly data files for the period 1985-present. "N" indicates that no online data are available. A blank column indicates this station's data are not collected by Bidston. "Banked" means the data are collected by Bidston, but not available on-line. "Received" means the data are indicated as having been collected by Bidston in the Bidston inventory, but for which there is no further information available. PSMSL means that only monthly mean sea-level data are available through the Permanent Service for Mean Sea Level. The links "banked" and "received" take one to the Bidston inventory where more detail is available. The PSMSL link is to the PSMSL WWW home page.

Bidston Quality Assessment

This column contains the Bidston quality-assessment reports which list site and detailed information on any data problems encountered as part of the GLOSS system.

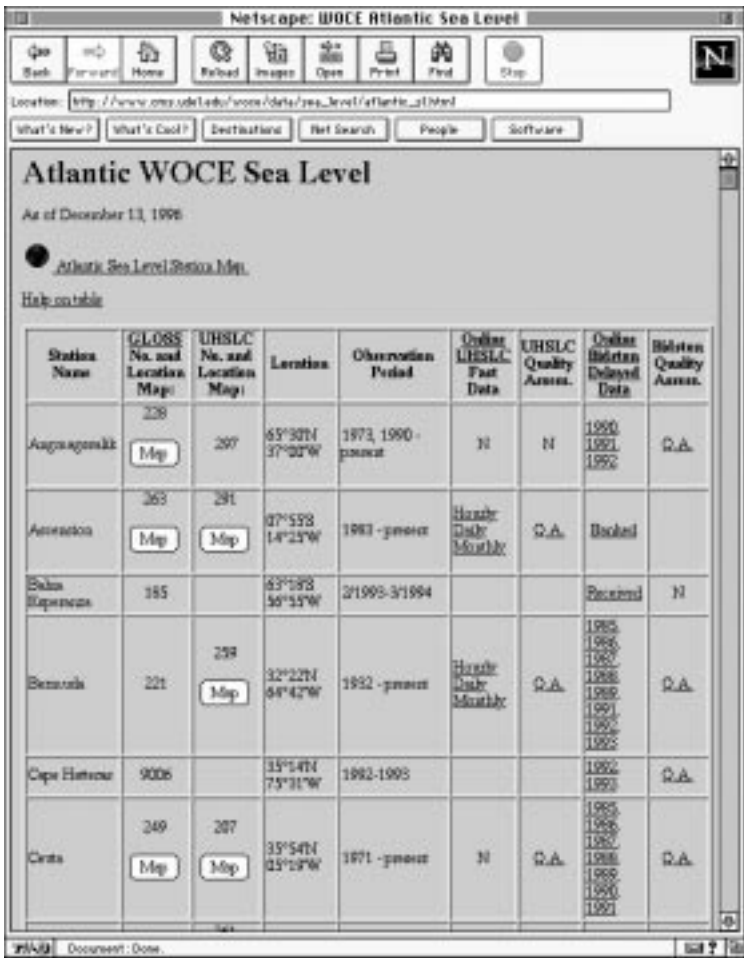

Figure 1. A sample of the comprehensive WOCE DIU Sea Level Data and Information WWW page.

An International Survey of the North Atlantic, 1996–1998

N. Penny Holliday, WOCE IPO, Southampton Oceanography Centre, UK. penny.holliday@soc.soton.ac.uk

The comprehensive survey of the North Atlantic from 1996 through 1998 is the final major international effort of the WOCE observational phase. A wide variety of physical, chemical and biological observations will be made. Several sections have already been occupied in 1996, and a brief outline of those and the plans for 1997 and 1998 is provided here (Fig. 1). More details of these activities and other parts of the WOCE field programme can be found at the Data Information Unit (http://www.cms.udel.edu/woce/).

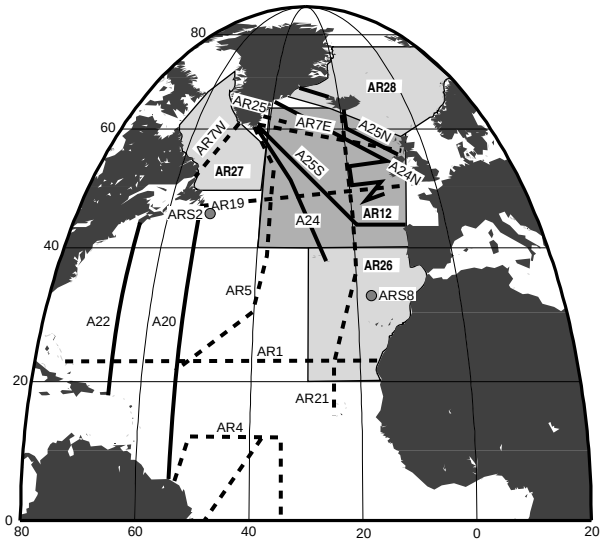

Figure 1. North Atlantic Hydrographic Programme 1996–1998. Hydrographic One-Time Survey sections (solid lines), Repeated Sections (dashed lines), Study Areas (shaded) and Time Series Stations (dots).

Hydrography

Five sections will be completed to WOCE One-Time standards with full depth CTDs and tracers measurements. Around 15 repeat sections will be carried out over the 3 year period (Table 1).

Four study areas are being intensively sampled by a variety of measurement techniques. The original AR12 area has been expanded northwards to Iceland to include the UK Vivaldi programme of SeaSoar sections between a grid of widely spaced CTDs (Pollard and Leach, Sept–Nov 1996). AR12 encompasses the French co-ordinated ARCANE project which is mainly 40–50°N and east of 14°E. Also contributing to ARCANE are Portugal, USA, and Spain, and the measurements comprise hydrography, moorings, floats, acoustic tomography, drifting buoys and current meter moorings. In addition, AR12 is being visited twice by Germany (Zenk, Müller) in May–June 1997 and 1998 for Iceland Basin circulation and water mass transformation studies.

AR26 is subject to the European Union project, CANIGO, coordinated by Spain and including 11 other countries (Aug 1996–1998). CANIGO is a multidisciplinary project encompassing hydrography, moorings, drifters, acoustic tomography, satellite data, and modelling. The Eastern Boundary Current system is being investigated by Germany (Knoll and Müller) with two cruises (Dec 1996–Jan 1997 and Sept 1997).

AR27 is a new designator covering the Labrador Sea and Newfoundland shelf. Canada (Lazier and Clarke) occupied a series of sections in Oct–Nov 1996 and plan to revisit them in Spring 1997. Germany (Send, Schott, Fischer) are investigating the convective processes in the Labrador Sea with moorings, CTDs and acoustic tomography in 1996 and 1997.

Existing time series stations will continue; Canada makes weekly occupations of ARS2, and Germany makes monthly occupations of ESTOC (ARS8). The XBT network will continue in its present form as long as funding for probes can be found. This includes the high density sections of AX3 (Germany) and AX7 (USA).

Subsurface Floats and Drifting Buoys

Approximately 360 profiling ALACE floats will be deployed during 1996–1997 mainly by the USA, but also by Canada and UK. In addition over 270 RAFOS floats and 61 MARVOR floats are being distributed throughout the North Atlantic by France, Germany, USA, Spain and UK. France is deploying 40 subsurface drifters as part of ARCANE over the 1996–1998 period, and Canada and USA released 18 drifters in the Labrador Sea in Oct–Nov 1996.

Table 1. Hydrographic Sections

A20, A22	USA	Joyce, Pickart	Jul–Aug 1997
A20N	Russia	Sokov	Apr–Jun 1997
A24	USA	McCartney, Talley	Nov–Dec 1996, May–Jul 1997
A25	UK	Bryden and Bacon	Aug–Sept 1997
AR1	USA	Molinari	1998
AR4	France	ETAMBOT II	Apr–May 1996
AR7E	Germany	Meincke, Sy	Aug–Sept 1996, Aug–Sept 1997
AR7E/AR5N	Russia	Sokov	Apr–Jun 1997
AR7W	Canada	Lazier	May–Jun 1996, Oct 1996
AR19	Germany	Koltermann	Jun 1996, Jun–Jul 1997
AR21	UK	Smythe-Wright	1998
AR25	Germany	Kaese	Aug 1996, 1997/98
AR25/AR27	Germany	Schott, Rhein	Jul–Aug 1996, Jul–Aug 1997, 1998
AR28	Nordic		1997–1998

Moorings

ACM8 was redeployed by UK (Dickson) in Aug 1996 and is coordinated with 3 other Denmark Strait moorings set by Germany (Meincke) and Finland (Malki). The UK hopes to lay a profiling CTD in the Irminger Sea, Aug–Sept 1997. Germany is maintaining additional moorings in the Labrador Sea (1997–99), the west and east sides of the Mid Atlantic Ridge (1996–98) and in the Eastern Boundary Current (with Spain, 1997–99).

WOCE Hydrographic Program Office

UCSD/SIO, 0214
9500 Gilman Dr.
La Jolla, CA 92093-0214
fax: (619) 534-7383
e-mail: whpo@ucsd.edu (1/97)
www: http://whpo.ucsd.edu (2/97)

James H. Swift, Director
Tel: (619) 534-3387
e-mail: jswift@ucsd.edu

Stephen C. Diggs, Data Manager
Tel: (619) 534-1108
e-mail: sdiggs@ucsd.edu

The WOCE Hydrographic Program Office (WHPO) is moving from the Woods Hole Oceanographic Institution to the UCSD Scripps Institution of Oceanography beginning January 1997. The Woods Hole and Scripps staff are working together to ensure that the transition is smooth and completed by April 1997. Jim Swift is the Director of the Scripps WHPO, and Lynne Talley is assisting. The WHPO is pleased to announce that Mr Stephen Diggs has accepted the position as Data Manager. Steve will be the person with whom most data communications and exchanges take place, and who oversees all data functions. The WHPO will also hire a Publications Assistant to produce WHP Data Reports and help manage cruise and data information.

The primary function of the WHPO remains assembly of all CTD, hydrographic, and tracer data and essential related documentation from the WOCE Hydrographic Program. The SIO WHPO will not change existing WHP formats and guidelines. The WHPO prefers that data providers send in all data in WOCE formats. But the WHPO will accept data in any unambiguous, readable format. The WHPO will do its best to transfer data to WHP format, tell data providers what it did, and provide data and documentation back to data providers in WHP format. All submitted files will be maintained at the WHPO as originally received, partly as protection against errors made by the WHPO and partly as an emergency back-up should data providers suffer a catastrophic loss at their facility.

The WHPO prefers to have all WHP data as soon as possible, including preliminary versions. The WHPO will want a so-called "final" version when available, but there is no need for data providers to wait until all the problems have been worked out. The data providers and the WHPO need to be certain they can read each other's files, and the WHPO will help check to see that formats and units and basic documentation are clear.

Another important WHPO function is to make WHP data available to those who wish to work with those data, following WOCE guidelines for data availability but with unconditional respect for investigator proprietary rights to data. This means, for example, that should some of the data from an expedition be cleared by the data provider(s) for unconditional public release, but other data still are regarded as proprietary by other data providers, the public files will be stripped of the proprietary data.

The WHPO will provide a modern on-line data and information service. The address of this service will be http://whpo.ucsd.edu. The service will begin in primitive form (public data only) by 1 February 1997. Full services will be added incrementally during 1997. Public data will be freely available but access to proprietary data will require a password issued to each data provider by the WHPO. This will provide an easy way for data providers to permit colleagues to have access to the latest versions of their data. The WHPO will also provide data on media (diskettes, CD-ROM, tape) following the same rules.

The WHPO also plans to assemble in WHP format as many ocean tracer data as possible – including those from pre-WOCE and non-WOCE cruises – to broaden the data available to the community. Placing all data in a single format simplifies and broadens access to data. Proprietary non-WOCE data will be accorded the same password protection as proprietary WOCE data.

The WHPO will continue to publish WHPO Data Reports, will continue investigator support such as the WHPO Data Manual and WHP Methods Manual, and will support WOCE workshops and other related activities. The Director and the Data Manager will do their best to meet as many data providers as possible. For example one or both plan to attend the South Atlantic and Southern Ocean workshops this year.

The WHPO looks forward to working with data providers – and to receiving all of their data!

Note on Copyright

WOCE is a component of the World Climate Research Programme (WCRP), which was established by WMO and ICSU, and is carried out in association with IOC and SCOR. The scientific planning and development of WOCE is under the guidance of the Scientific Steering Group for WOCE, assisted by the WOCE International Project Office.

The WOCE Newsletter is edited at the WOCE IPO at the Southampton Oceanography Centre, Empress Dock, Southampton SO14 3ZH (Tel: 44-1703-596789, Fax: 44-1703-596204, e-mail: woceipo@soc.soton.ac.uk).

We hope that colleagues will see this Newsletter as a means of reporting work in progress related to the Goals of WOCE as described in the Scientific Plan. The SSG will use it also to report progress of working groups, experiment design and models.

The editor will be pleased to send copies of the Newsletter to institutes and research scientists with an interest in WOCE or related research.

Printed by the Design and Print Centre of the University of Southampton